Cooperative Adaptive Cruise Control Vehicles on Highways
Modelling and Traffic Flow Characteristics

Xiao, L.

DOI
10.4233/uuid:fb938e90-bda7-47bd-ac90-7b1f9887c027

Publication date
2020

Document Version
Final published version

Citation (APA)
Xiao, L. (2020). *Cooperative Adaptive Cruise Control Vehicles on Highways: Modelling and Traffic Flow Characteristics*. [Dissertation (TU Delft), Delft University of Technology]. TRAIL Research School. https://doi.org/10.4233/uuid:fb938e90-bda7-47bd-ac90-7b1f9887c027

Important note
To cite this publication, please use the final published version (if applicable).
Please check the document version above.

Cooperative Adaptive Cruise Control Vehicles on Highways: Modelling and Traffic Flow Characteristics

Lin Xiao

Delft University of Technology, 2020

Cover illustration by Lin Xiao

Cooperative Adaptive Cruise Control Vehicles on Highways: Modelling and Traffic Flow Characteristics

Dissertation

for the purpose of obtaining the degree of doctor
at Delft University of Technology
by the authority of the Rector Magnificus, Prof.dr.ir. T.H.J.J. van der Hagen,
chair of the Board for Doctorates
to be defended publicly on
Thursday 3 December 2020 at 15:00 o'clock
by

Lin XIAO
Master of Engineering in Transportation Planning and Management, Tongji University, China
born in Xiamen, China

This dissertation has been approved by the
promotor: Prof. dr. ir. B. van Arem
copromotor: Dr. ir. M. Wang

Composition of the doctoral committee:

Rector Magnificus	chairman
Prof. dr. ir. B. van Arem	Delft University of Technology, promotor
Dr. M. Wang	Delft University of Technology, copromotor

Independent members:

Dr. S. E. Shladover	University of California – Berkeley
Prof. S. Ahn	University of Wisconsin – Madison
Prof. dr. ir. S.P. Hoogendoorn	Delft University of Technology
Prof. Dr. M.H. Martens	Eindhoven University of Technology
Dr. ir. R. Happee	Delft University of Technology
Prof. dr. ir. J.W.C. van Lint	Delft University of Technology, reserve member

Use of Cooperative Adaptive Cruise Control to Form High-Performance Vehicle Streams

This research has been funded by an FHWA Exploratory Advanced Research Program Grant No. DTFH61-13-H-00013 and was conducted in cooperation with California PATH at the University of California, Berkeley.

TRAIL Thesis Series no. T2020/19, the Netherlands Research School TRAIL

TRAIL

P.O. Box 5017

2600 GA Delft

The Netherlands

E-mail: info@rsTRAIL.nl

ISBN: 978-90-5584-280-3

Printed in the Netherlands

Dedicated to
My parents, my husband and my daughter

Preface

Before I started my PhD research, I would say PhD means several years of hard work on an interesting topic. Now PhD means much more than that to me when I look back to my PhD journey. In April 2014, I joined the Transport and Planning department at TU Delft and started my PhD research in a collaborative project with the California PATH, in which I had the opportunity to work with leading researchers in the field of vehicle automation. I was excited, motivated and ambitious to start my work, but it does not go smoothly in the beginning – one and half a year spent on model calibration which was planned for three months only. It was a stressful time for me that I stared at those moving dots in simulations for 10 hours a day. Fortunately, the pressures and struggles made me increase my productivity, actively search for resources and helps and improve my problem-solving skills. All the changes largely contribute to my success of this thesis. Now I would say PhD is an adventure which provides challenges and difficulties to stimulate a self-development. At the end of this adventure, I would like to take this opportunity to thank all the people who have been with me during this journey.

I would like to express my deepest appreciation to my supervision team. The completion of the thesis would not have been possible without their effort and support. I want to first express my deepest gratitude to my promotor Bart van Arem for guiding me the research direction and coaching me towards an independent researcher by his openly shared knowledge, experience and wisdom. His kind mental support at those hard time is greatly appreciated. I was strongly motivated by his enthusiastic encouragements and deeply touched when he shared my worries.

I am greatly indebted to my co-promotor Meng Wang for the inspired guidance and constructive criticism. He provided invaluable insights into my research and greatly helped me to improve my structure of thinking. I am grateful for his patience to extensively review and revise each version of my manuscripts. Handling his comment is never an easy task but doing that largely expand my vision. I am also grateful for his solid support and the opportunities he created to promote my work.

I would like to express my special appreciation to Wouter Schakel for his contribution to the chapters of vehicle behaviour modelling. Thanks for providing me insightful comments on the simulation modelling and coaching me in the model implementation. I would also like to thank Raymond Hoogendoorn for being my supervisor in the first year of my PhD. His encouragements and openness helped me to build up confidence at my work.

I am lucky to have the opportunity to collaborate with the excellent researchers in the PATH in my PhD project. Their visions and expertise greatly helped me shape my research in the early stage. Deep admirations and appreciations to Steve Shladover and Xiao-Yun Lu for their boundless enthusiasm for research and continuous contributions to academia. Many thanks to Hao Liu for the helpful research and technical discussions.

All of these would have not been possible if Yusen Chen and Serge Hoogendoorn did not introduce me to Bart back in 2013. Many thanks to the recommendations and opening this life-

changing opportunity. Special thanks to Yusen for the enormous help and advice he has offered both at TU Delft and TNO.

I would like to express my gratitude to Steve Shladover, Sue Ahn, Riender Happee, Marieke Marten, Serge Hoogendoorn and Hans van Lint for being my doctoral committee members and for their valuable comments to improve the quality of this research.

I would also like to thank my colleagues from the Transport and Planning department for creating such a friendly, pleasant and supportive environment. I enjoyed our research discussions and daily conversations in all official or unofficial events. My sincere appreciations to Silvia, Xavier, Mo and Mehdi for the friendships, trusts and supports over these years. The time of my PhD would not have been so enjoyable and meaningful without their accompanies. Thanks also go to the best officemates Paul, Hamid, Na, Yao, Hari and Raeed for the creative activities, coffee breaks and sharing. Many thanks to Yu, Freddy, Yufei, Kai, Jeroen for fruitful research discussions, and to Qu, Fei, Nicola, Haneen, Nadjla, Bernat, Pengling, Ding, Vincent, Yongqiu, Gonçalo, Meiqi and Solmaz for the great time we had in different events. Xiao, my best friend, thanks for making the great decision – choosing TU Delft to be my colleague again.

Special thanks to Dehlaila for arranging all the administrative work and helping me out under many unexpected situations. Thanks to Edwin for his timely technical support on the remote computation. Sincere appreciation to Conchita at the TRAIL research school for supporting me in my doctoral education program and helping me prepare for my defence.

I would like to extend my sincere thanks to my colleagues at TNO for their supports at the final stage of my PhD study. Particular thanks to Gerdien for translating the thesis summary into Dutch. Her coaching and support during my TNO onboarding period are sincerely appreciated. Thanks to Fieke for helping me to plan dedicated time on the thesis.

Thanks also go to the people I met during these years who become a friend for life. Thanks to Yaqing&Lan for their continuous support and countless dinner invitations; Thanks to Yuling&Michael for their shared happiness and difficulties; Thanks to Xavier&Montse for their friendships beyond a culture gap; Thanks to my best neighbour Bin&Yuguang for their generous help and creative food recipes. Thanks to Natalie&Ying for sharing the difficulties in raising a child; Thanks to Xin (Tian), Hongqin, Xiangming, Zhiwei, Xin (Li), Ming, Feifei, Xiaochen, Jinhu and Xueming for the enormous fun we had in trips and board games.

I would like to express my most sincere gratitude to my parents. It is very difficult to have the only child being far away, but they still strongly encouraged me to go aboard to peruse my doctoral education. Their endless love and unstinting support encourage me to overcome all difficulties in living abroad. 我要感谢我的父母，因为这一切都源于他们对我无止境的爱和支持。你们是我最强力的后盾，让我拥有直面困难的勇气。你们也是我最安心的避风港，是我永远的依赖。

Jin, my lovely daughter, although you are only two years old, you already can show your understanding and support when I have to work on the thesis during weekends. Your smile, love and trust give me great strength to accomplish the thesis. Finally, my beloved Zhen, my gratitude for the love and support for over 13 years. On the way to this thesis, he believes in me and strongly encouraged me to fight against the struggles I was locked in. He always stands behind me whenever I need and take care of me and our family without notices. Together with Jin, you make my life full of joy and happiness.

Lin Xiao

November 2020

Content

List of Figures

List of Tables

1 Introduction

1.1 Background

Traffic congestion presents a serious challenge to the road traffic system due to the substantial travel time delay. In the Netherlands, Rotterdam, Utrecht, the Hague, Eindhoven and Nijmegen are the five most congested cities. Drivers in these cities lost more than 50 hours in congestion in 2019 (INRIX, 2020a). Congestion costed nearly seven billion pounds in 2019 in the United Kingdom (INRIX, 2020c) and 88 billion dollars in the United States (INRIX, 2020b). In addition to that, traffic congestion increases collision risk and air pollution. Thus, congestion has detrimental effects on economy and society. Unfortunately, it is not always feasible or desirable to expand the traffic infrastructure to accommodate the increasing traffic demand due to limited public funding and resources. Therefore, improving traffic efficiency of the road traffic system is important in order to deal with the congestion.

In order to improve traffic efficiency, Intelligent Transportation Systems (ITS) offer advanced applications of information and communication technologies for a well-integrated system combining infrastructures, vehicles and users. Features such as road loop detectors, floating car data and online trip planners provide a large amount of trip and traffic information; and via real-time communication technologies, ITS enable to react in time to expected or unexpected events and provides better coordination between the traffic demand and supply in order to minimize congestion. Depending on the information technologies and strategies applied, ITS includes many systems, e.g. traveller information systems, advanced traffic management systems and driving automation systems.

A driving automation system is a system that performs part or the entire dynamic driving task on a sustained basis, whereas the dynamic driving task refers to the operational manoeuvres such as steering, braking, accelerating and monitoring, and tactical strategies such as lane change decision-making or response to events such as traffic congestion and roadworks. Driving automation systems have been shown to have an influence on several indicators of traffic flow efficiency such as capacity, capacity drop and traffic stability (Hoogendoorn et al.,

2014). The SAE Recommended Practice describes six levels of driving automation depending on the specific role played by the human driver and the automation system (SAE international standard J3016),

- Level 0 No Automation. All the dynamic driving tasks are performed only by human drivers.
- Level 1 Driver Assistance Automation. The execution of either steering or acceleration/deceleration is conducted by an assistance system and the human drivers perform all the remaining aspects of the dynamic driving task.
- Level 2 Partial Automation. The system executes both the steering and acceleration /deceleration manoeuvres while the drivers monitor the driving environment via object and event detection, recognition, classification and response preparation (OEDR).
- Level 3 Conditional Automation. The system performs all aspects of the dynamic driving task with the expectation that the human driver will respond to a request to intervene due to system failures or when the condition is out of the system operational design domain.
- Level 4 Highly Automation. Within a prescribed operational design domain, all aspects of the dynamic driving task could be performed without any expectation that a user will respond to a request to intervene.
- Level 5 Fully Automation. A full-time performance of all dynamic driving task under all driver-manageable on-road driving situations.

Current driving automation systems such as adaptive cruise control (ACC) and lane keeping systems are examples of Level 1 Automation, in which the automation system only partially controls vehicles' longitudinal or lateral behaviour and drivers are required to monitor and resume vehicle control in emergency situations.

Adaptive cruise control (ACC) has been implemented in production vehicles. It enables a vehicle to follow its predecessor automatically using the detected vehicle position, speed or acceleration obtained from a radar sensor. The potential impacts of ACC when used on a wide scale on traffic operations in terms of capacity and traffic stability have been extensively discussed. It has been shown that ACC vehicles are found to result in an increased lane capacity if a short following gap is used (Minderhoud & Bovy, 1999; VanderWerf et al., 2001). However, drivers using ACC tend to choose a larger time gap than the time gap under manual driving (Nowakowski et al., 2011). Therefore ACC generally leads to in a small capacity increase or even a decreased flow throughput (van Arem et al., 1996; VanderWerf et al., 2002). Moreover, although the smooth response of ACC is reported to attenuate the traffic disturbance (Ioannou & Stefanovic, 2005), its performance is overestimated if one overlooks the delays in information transmission and actuator response. In fact, ACC vehicles can result in unstable traffic flow (Yi & Horowitz, 2006) and the overshoot in car-following response of ACC vehicles has been demonstrated in a platoon field test (Milanés & Shladover, 2014). Overall, in their present form, ACC vehicles are not likely to increase roadway capacity and can instead result in worse traffic performance due to traffic instability.

As an extension of ACC, cooperative adaptive cruise control (CACC) aims to improve traffic flow throughput and attenuating traffic flow disturbance with the help of vehicle information from downstream traffic (Shladover et al., 2015). Via on-board vehicle-vehicle (V2V) communication, a CACC vehicle receives information from multiple preceding vehicles and reacts to the change of the preceding vehicle behaviour earlier than an ACC vehicle, which offsets the communication and actuator delays and generates string-stable performance among

the CACC vehicles. The string stability performance of CACC platoons has been shown both in analytical studies (Talebpour & Mahmassani, 2016) and in field test (Milanés & Shladover, 2014). Thanks to the early response of CACC vehicles, the following gap between them can be made much smaller than the gap between two manually driven vehicles, up to 0.5 seconds (VanderWerf et al., 2002). In this regard, CACC vehicles offer potential for roadway capacity growth.

1.2 Problem statement

Growing attention has been paid to CACC vehicles in terms of its real-world deployment in traffic. Several road experiments with a string of CACC vehicles have been conducted so that the CACC following performance, e.g. acceleration/speed response, can be examined (Bu et al., 2010; Milanés et al., 2014; Raboy et al., 2017; Vugts, 2009). However, the impacts of CACC on traffic flow when applied at a large scale have not been fully explored. The traffic impact will largely affect the CACC deployment and a lack of understanding of the CACC effects will raise challenges to public authorities and road operators to react to the mixed traffic of CACC vehicles and conventional vehicles. Public authorities may not be able to formulate appropriate traffic policies if the benefits and risks of deploying CACC are unknown; meanwhile, road operators may not be able to address the traffic problems and develop effective traffic management strategies without the understanding of the key features of mixed CACC traffic flow.

Existing CACC impact studies generally focus on CACC's capability to increase roadway capacity. The capacity increment highly depends on the market penetration rate (MPR) of CACC vehicles and a trend of small capacity gains at low MPRs and large increases at high MPRs is revealed (Shladover et al., 2012; Talebpour & Mahmassani, 2016; van Arem et al., 2006; VanderWerf et al., 2002). Unfortunately, these studies only pay attention to the capacity in the free-flow scenario at a homogeneous section or a single bottleneck due to merging, weaving or lane drop. There is little discussion about the impacts of CACC vehicles on traffic congestion, e.g. queue discharge rate and capacity drop. In dense traffic, CACC may have to be switched off when the driving condition is out of the CACC operational design domain. Thus CACC may have different effects on queue discharge rate, compared to that on free-flow capacity concluded in existing studies.

Given the difficulty of carrying out CACC impact analysis with real vehicles at a large scale, traffic simulation is often selected to conduct CACC impact evaluations. It allows experiments with different assumptions on CACC operations and different CACC MPRs. Most CACC studies based on traffic simulation pay attention to vehicle behaviour under CACC. The CACC car-following response is either simplified as the CACC control algorithms which ignore the mechanical driveline dynamics and rolling and the (reduced) aerodynamic resistance (Makridis et al., 2017; Shladover et al., 2012; Talebpour & Mahmassani, 2016; Tientrakool et al., 2011; van Arem et al., 2006; VanderWerf et al., 2002; Zhao & Sun, 2013) or modelled against vehicle trajectories obtained from a real-vehicle experiment (Milanés & Shladover, 2014). Unfortunately, few studies pay attention to (1) the multiple driving modes of CACC, particularly the approaching mode that serves as the transition between the speed control mode and the gap control mode (Milanés & Shladover, 2015). (2) the degraded operation of CACC to ACC when a qualified leader is absent; and (3) the take-over of control by drivers to drive the CACC vehicles manually when the traffic condition is out of the ACC or CACC operational design domain (Varotto et al., 2015). Therefore, there is an open scientific challenge to model the vehicle behaviour in a realistic way, including the behaviour under multiple CACC modes, ACC modes, manually driving mode and the authority transitions among them. A car-following

model of CACC vehicles which does not capture these features will not represent realistic and plausible vehicle behaviour in simulations. Simulation experiments based on that cannot reliably estimate CACC impacts on traffic flows.

Given that the benefit of CACC is expected to be marginal at low CACC market penetration rates, a dedicated lane for CACC vehicles has been considered as a solution to promote the adoption of CACC(Chen et al., 2016). It is found that the effectiveness of a CACC lane is highly related to the CACC MPR. A CACC lane in combination with low CACC MPRs can lead to a degraded flow performance (van Arem et al., 2006). Deploying a CACC lane should wait until the CACC MPR reaches the medium level (30-60%) in order for a sufficient number of CACC vehicles to use the dedicated lane (Liu et al., 2018b; Talebpour et al., 2017). However, these studies do not explicitly model the specific lane change behaviour of the eligible or ineligible users when a dedicated lane appears. They either assume mandatory lane changes to dedicated lanes or use a general lane change model for the eligible users of CACC lanes. The former method results in overestimating clustering effects on the CACC lane and the latter method underestimates the attractions of CACC lane to eligible users, both of which lead to an unrealistic traffic impact analysis. This might affect the decision-making by policymakers, traffic system planner or road operators regarding the deployment of CACC lanes. In addition to that, most studies evaluated the effects of CACC lanes either in long segments without entries and exits or at road bottlenecks such as on-ramp and lane drop sections. Realistic traffic disturbances and the resulting formation and dissolution dynamics of CACC vehicle string are rarely completely taken into consideration. Frequent lane changes and vehicle join/exit string manoeuvres can offset CACC benefits with small following gaps. Therefore, the impacts of CACC might be overestimated if traffic disturbances from on/off ramps are not modelled and the vehicle join and leave manoeuvres are assumed to be instantaneous.

1.3 Research objectives

The objectives of the thesis are threefold: (1) to develop realistic behavioural models for CACC vehicles; (2) to apply the models in traffic simulations to understand the impact of CACC on traffic capacity and to gain new insights into the flow characteristics of mixed manual and CACC traffic; (3) to evaluate the traffic flow performance of converting an existing high-occupancy-vehicle lane to a dedicated CACC lane on a highway corridor.

To achieve the research objectives, the following research questions are to be pursued:

1. *How to reproduce realistic behaviour of CACC vehicles in a microscopic simulation?*

Research question 1 is aimed at the enhanced capability of microscopic simulations to model CACC vehicles in a realistic way. By answering this question, realistic vehicle behaviour, e.g. a full-speed range operation and driver take-over under specific situations, can be taken into account and mimicked in simulations, contributing to the realistic impact assessments in various simulation scenarios. To answer this question, a multi-regime conceptual model which integrated the CACC system control and driver control in parallel is proposed. This will address the lack of realism of simplified CACC models in literature.

2. *What are the characteristics of traffic flows with different CACC vehicle market penetration rate?*

This research question is designed for the flow characteristics of the mixed traffic with CACC vehicles and conventional vehicles. The relations between fundamental diagram, capacity and capacity drop with different CACC MPRs can be revealed in the answers to this question. This provides new insights into the CACC impacts in a broad scope including both free-flow and

congested-flow scenarios. To answer this question, the proposed CACC car-following model is integrated with a lane change model and a systematic simulation experiment of a typical merging bottleneck is conducted.

3. *How to model the lane change behaviour with the presence of a dedicated lane?*

This research question is proposed to improve the simulation capability for a dedicated lane scenario. Modelling the specific lane changes of eligible and ineligible users to the dedicated lane can produce more plausible vehicle behaviour in the simulation and reproduce the key flow features when a dedicated lane is presented. This leads to more realistic and reliable conclusions regarding the traffic impacts of a dedicated lane. This research question can be answered by an enhanced lane change model capturing the speed incentive from dedicated lanes and the constant lane preference in the lane change decision.

4. *What are the effects of converting an HOV lane to a CACC lane in a realistic highway corridor?*

The flow operation and mobility indicator (e.g. travel time) after converting an HOV lane to a CACC lane at different MPRs will be examined to answer this research question. They will unravel the proper timing to deploy a CACC lane in mixed traffic flow, and also demonstrate the combined benefit of CACC vehicles with a CACC lane referring to the flow operation with an HOV lane. To achieve reliable results, the realistic CACC car-following model from question 1 and enhanced lane change model from question 3 are integrated and a realistic highway corridor with multiple exchanges and a reserved HOV lane is selected. A simulation experiment with varying CACC MPR is conducted.

1.4 Research scope

There are various developed CACC systems for various applications in different traffic scenarios and their traffic impacts are largely diverse from different aspects. This thesis does not intend to discuss all the possible CACC systems and their impacts, and thus the research scope is narrowed down as follows.

Firstly, this thesis focuses on the CACC application on highway traffic. The highway environment is a structured scenario with fewer types of traffic participants and disturbances compared to urban traffic scenarios, being a more promising scenario to implement the CACC system in the near future.

Second, this thesis focuses on CACC operations taking the driver-system control transitions into account. The included driver-system intervention is based on the limitations of current Level One automation that human drivers are requested to monitor the traffic conditions and override the CACC system when traffic conditions are out of the CACC operational design domains. For example, drivers override the CACC system in safety-critical situations or when preparing for lane changes.

Finally, this thesis concentrates on the CACC impacts on traffic efficiency, particularly on roadway capacity and traffic congestion. Since CACC directly influence inter-vehicle gaps, vehicle throughput will show the most straightforward consequence of introducing CACC vehicles, and thus this thesis discusses the CACC impacts from the aspect of traffic efficiency instead of other aspects such as traffic safety and environmental issues.

1.5 Contributions

This research makes contributions to the modelling of CACC vehicle behaviour, theories of mixed traffic flow, as well as the practical relevance to society. In this section, the scientific and practical contributions are highlighted as below.

1.5.1 Scientific contributions

A new realistic and full-speed-range CACC car-following model for microscopic traffic simulations is developed (Chapter 2). Reproducing realistic CACC vehicle behaviour and assuring full-speed range operation in a wide range of traffic scenarios are two essential requirements for car-following models in simulation. To achieve both, the integration of realistic vehicle behaviour, CACC operational design domain and fall-back performance is necessary. The developed CACC car-following model has three important features: (1) the vehicle following response is empirically underpinned; (2) the operational design domains of CACC and ACC degrading from CACC are limited; (3) the authority transition from CACC to the human driver is modelled including a fall-back capability. This model is a multi-regime model due to the multiple controllers in the car-following response, and it can be adequately used in microscopic simulations to generate plausible vehicle behaviour in a full-speed range.

New insights into the impacts of CACC market penetration rates on roadway capacities are provided (Chapter 3). It is shown that an increasing number of CACC vehicles can increase free-flow capacity; however, the capacity at a merging bottleneck is substantially lower than the capacity of a homogenous pipeline section due to CACC deactivations caused by merging traffic. The increasing CACC MPRs can also increase queue discharge rates at merging bottlenecks but the capacity drop at a merging bottleneck persists at all CACC MPR levels. Moreover, it is found that the scatters in the fundamental diagram and hence the heterogeneity in traffic states, particularly in the congested flow, increase with CACC MPR. This is attributed to the multiple system operations and driving modes resulting in increased heterogeneity of vehicle behaviour.

*An enhanced lane change model for a continuous-access dedicated lane scenario is developed and calibrated (Chapter 4).*The lane change model with relaxation and synchronization (LMRS) is a lane change decision model based on multiple lane change incentives, determining four types of lane change behaviour taking headway relaxation and speed synchronization into account (Schakel et al., 2012). Based on the lane change model with relaxation and synchronization (LMRS), the proposed model introduces the additional lane change incentives, i.e. speed incentive and lane preference, as a result of the presence of dedicated lanes and generates plausible lane change behaviour for eligible and ineligible lane users respectively. The model was systematically calibrated using loop detector data to reproduce macroscopic traffic performance in a U.S. highway corridor with a high occupancy vehicle lane.

Effectiveness of converting an HOV lane to a CACC lane on improving traffic flow performance and CACC operation at a corridor level is revealed (Chapter 5). The impacts of CACC lanes highly depend on the CACC MPRs. At low MPRs, converting an HOV lane to a CACC lane results in more severe congestion due to insufficient lane capacity for conventional vehicles. At higher CACC MPR, the CACC lane is shown to substantially alleviate or prevent congestion. From the aspect of CACC operation, a CACC lane can indeed increase the time usage of the CACC system and its operation in CACC strings. In addition, the results show that a CACC lane can provide less travel time and higher travel time reliability for CACC vehicles, compared to conventional vehicles in general purpose lanes.

1.5.2 Practical contributions

Besides the scientific contributions, the results of this thesis also provide contributions to society and practice. It is beneficial for policymakers, traffic system planner, traffic infrastructure designer, road operators and vehicle users.

The integration of a realistic CACC car-following model and enhanced lane change model provides an effective simulation tool to evaluate CACC impacts in various scenarios. This simulation tool can reproduce realistic CACC vehicle behaviour including the multiple driving modes and authority transition, which is useful for policymakers and road operators to examine the consequences of introducing CACC vehicles in mixed traffic before promoting CACC to the market.

The estimated roadway capacities at different CACC MPRs are fundamental and important for traffic planning and traffic management. Given that the capacity increase is strongly related to CACC MPRs, road operators may consider proactive management strategies to adapt the flow characteristics at different CACC MPRs to improve traffic efficiency. Meanwhile, due to the different capacity increase on homogeneous sections and at bottlenecks, traffic planners may need to redesign the road network with the new capacity properties of each node and link.

The effects of CACC deactivation in capacity drop have important implications to traffic management and road infrastructure design. Since the deactivation of CACC is the main cause of throughput reduction, road operators could encourage a higher level of vehicle coordination and cooperation to reduce the number of driver take-overs from CACC.

To vehicle users, the combined benefits of using CACC vehicles and CACC lanes are clarified. CACC lanes not only offer a high possibility for CACC vehicles to form a vehicle string, but also provide more reliable travel time than general purpose lanes. However, road operators should be cautious when deploying CACC lanes. Deploying CACC lanes at low CACC MPRs might deteriorate overall traffic performance by placing high demand of conventional vehicles in general purpose lanes.

1.6 Thesis outline

The chapters of this thesis are based on scientific articles which have been published. Part of the texts have been modified for clear chapter positioning and logical connections between chapters. Nevertheless, some repetition in part of the chapters takes place because of the self-contained composition of each chapter. Figure 1.1 illustrates the structure of chapters in this thesis.

The research starts in Chapter 2 with modelling the longitudinal behaviour of CACC vehicles, focusing on the essential behavioural differences compared to manually driven vehicles. Chapter 2 proposes a conceptual model for the car-following response of a CACC vehicle. Two parallel control loops are integrated into the conceptual model, consisting of a CACC system control loop and a human driver control loop. Both loops follow a basic multiple regime control process, which represents the relationship between control inputs and actual vehicle response including the internal drivetrain dynamics and external resistance. The CACC car-following model is able to reproduce realistic CACC following behaviour as well as manually driving response when the traffic situation is out of the CACC design domain. The collision-free property is assured in a full-speed range, being verified by a serious simulation test in five typical traffic scenarios. The proposed model is therefore considered as an effective and reliable car-following model for CACC vehicles in application to microscopic simulations.

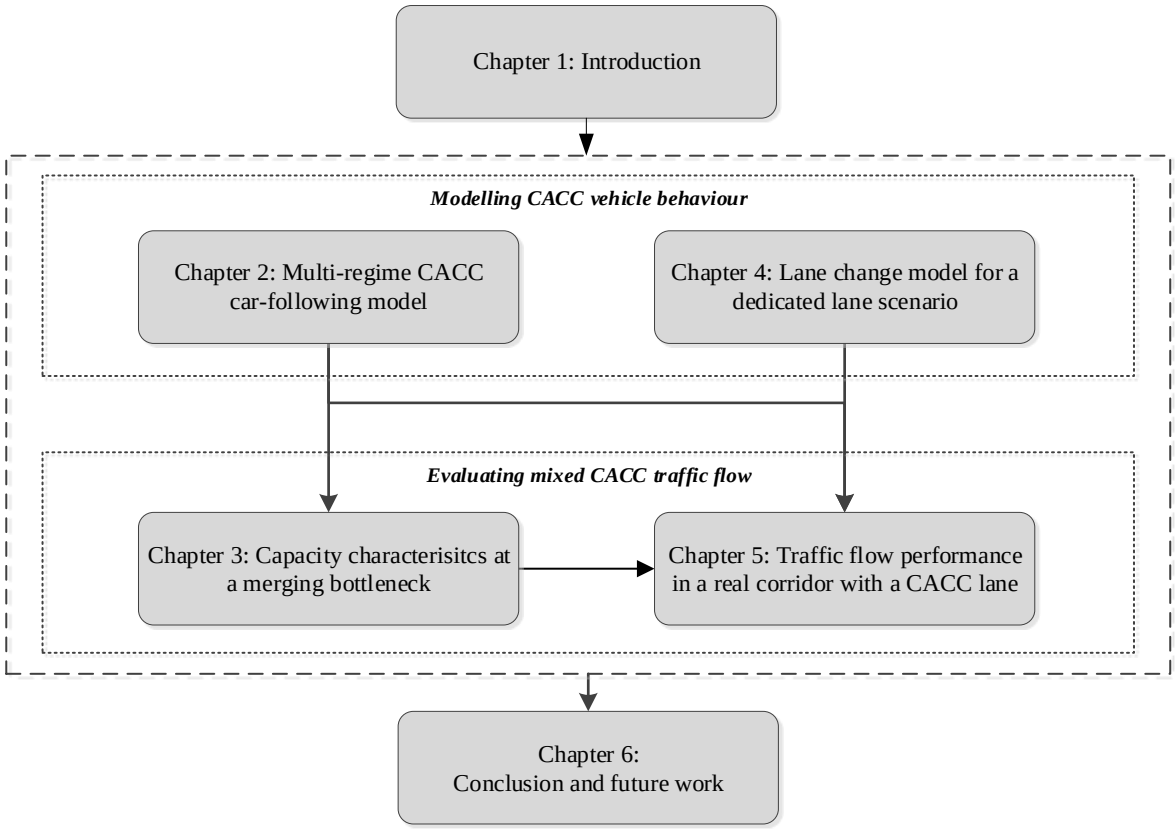

Figure 1.1 Thesis outline.

In Chapter 3, based on the aforementioned CACC car-following model and a lane change model with synchronization and relaxation (LMRS) under manually driving, we focus on the capacity characteristics of traffic flows regarding CACC MPRs. In particular, we pay attention to both pre-queue capacity and queue-discharge rate at a merging bottleneck of a four-lane highway, revealing the different CACC impacts on free flow and congested flow. It is concluded that increasing CACC MPRs can increase roadway capacities and the throughputs during congestion. The capacity drop, as the difference between these two throughputs, pertains at all CACC MPRs and is correlated to the authority transitions from CACC to manual driving.

According to the capacity analysis in Chapter 3, the CACC benefits on traffic flows at low MPRs are not substantial due to the low time usage of the CACC system. To increase CACC usage, a CACC dedicated lane clustering these vehicles in one lane, is considered as an optional lane-management strategy. Assessing the effectiveness of a CACC lane before its practical application is important, and two challenges are raised. One challenge is to model the adaptive lane change behaviour in the presence of a dedicated lane and the other is how to evaluate realistic and reliable impacts of CACC lanes. Chapter 4 and Chapter 5 respond to these challenges from the modelling and evaluation aspect respectively.

In Chapter 4, the lane change model from Chapter 3 is extended for a dedicated lane scenario. The lane change incentive is modified for eligible and ineligible users of dedicated lanes and the model is carefully calibrated using detector data from the SR-99 corridor in California where an existing HOV lane is in operation. The extended and calibrated lane change model is able to generate similar congestion pattern along the corridor as shown in the empirical data, as well as section-based fundamental diagrams and lane-based flow distribution, with plausible lane change behaviour.

Integrating the extended lane change model in Chapter 4 with the CACC car-following model in Chapter 2, the CACC vehicle behaviour in a dedicated lane scenario can be modelled and simulated. In Chapter 5, simulations at 0-50% CACC MPRs are conducted to explore the effectiveness of a CACC lane on improving mixed CACC flow performance. Macroscopic congestion patterns are investigated regarding CACC MPRs, and the flow operation in CACC lanes and the friction effects of the CACC lane are described and observed, showing the combined effects of CACC lane and CACC MPRs. Additionally, travel time reliability of CACC and general purpose (GP) lanes are estimated and compared; and the benefits of CACC lanes in CACC operation are presented.

Chapter 6 summaries the main findings regarding the impacts of CACC on mixed traffic flows. Those impacts answer the main research question and provide useful implications for policymakers, road operators and vehicle users for their decision-making.

2 Multi-regime CACC car-following model

To investigate the impacts of CACC vehicles in microscopic traffic simulations, modelling the representative behaviour of these vehicles and their interaction with surrounding traffic is fundamental and essential. Existing studies have modelled the CACC car-following response either in an unrealistic way, without properly considering the vehicle driveline dynamics, aerodynamic drag and rolling resistance, or in a manner that is only applicable to a limited scenario because models are not collision-free for a full-speed range. This chapter proposes a model for the longitudinal response of CACC vehicles, integrating an empirical CACC car-following model with a manually driving car-following model. The supplementary manual-control loop captures realistic vehicle behaviour when traffic conditions are out of the CACC operational design domain, and it extends the empirical model into a full-speed range without rear-end collisions. The collision-free property of the proposed conceptual model is verified through a systematic simulation experiment that five typical safety-critical scenarios are simulated.

The chapter is organized as follows. Section 2.1 gives an overview of existing CACC car-following models and identifies the scientific gaps. Section 2.2 illustrates the conceptual model with dual control loops, formulates the car-following models in different driving modes and proposes two switching conditions between CACC control and manual driving. To verify the model's collision-free property, section 2.3 designs five typical scenarios with critical safety issues; the resulting vehicle-following performance and model capability are provided in section 2.4.

This chapter is an edited version of the following paper:

Xiao, L., M. Wang and B. van Arem. (2017). Realistic Car-Following Models for Microscopic Simulation of Adaptive and Cooperative Adaptive Cruise Control Vehicles. *Transportation Research Record: Journal of the Transportation Research Board, vol. 2623*, pp. 1-9

Abstract—Adaptive Cruise Control (ACC) and Cooperative Adaptive Cruise Control (CACC) are important vehicle technologies toward vehicle automation and their impacts on traffic system are generally evaluated via microscopic traffic simulations. A successful simulation requires realistic vehicle behaviour and a minimal number of vehicle collisions. However, most existing ACC/CACC simulation studies use simplified models that are not based on real vehicle response and rarely discuss collision avoidance in the simulation. This study aims to develop a realistic and collision-free car-following model for ACC/CACC vehicles. We propose a multi-regime model combining a realistic ACC/CACC system with driver intervention for vehicle longitudinal motions. This model assumes that human drivers resume vehicle control either according to his/her assessment or after a collision warning requests the driver to take over. The proposed model is tested in a wide range of scenarios to explore the model performance and collision-possibilities. The testing scenarios include three regular scenarios of stop and go, approaching and cut-out manoeuvres, as well as two extreme safety-concerned manoeuvres of hard brake and cut-in. The simulation results show that the proposed model is collision-free in the full-speed-range operation with leader accelerations within -1 to 1 m/s^2 and in approaching and cut-out scenarios, indicating that the proposed ACC/CACC car-following model is capable of producing realistic vehicle response without causing vehicle collisions in the regular scenarios for vehicle string operations.

2.1 Introduction

Technologies of automated vehicle control have drawn great interests since the automated highway system (AHS) was introduced in the 1930s (Shladover, 1995). Adaptive Cruise Control (ACC) is one of the emerging technologies for driving assistance systems and it is designed to enhance driving comfort by automatically responding to a preceding vehicle. Cooperative Adaptive Cruise Control (CACC), an extension of the ACC with Vehicle-to-Vehicle (V2V) communication, is favoured by road operators since it has the possibility of vehicle coordination and cooperation, which provides a potential opportunity to enhance traffic efficiency.

Studying the potential impacts of ACC/CACC vehicles on traffic efficiency is of great importance and necessity, since the penetration rate of ACC and CACC vehicles is expected to increase in the near future. An early study showed that ACC and CACC vehicles have the potential to increase the lane capacity at 100% market penetration rates (MPR) (VanderWerf et al., 2001). Unfortunately, the conclusion for ACC vehicles does not hold in a simulation if a realistic distribution of the desired time gap is considered (Shladover et al., 2012). The impact of CACC vehicles on lane capacity is still significant in moderate and high MPR scenarios (Shladover et al., 2012; van Arem et al., 2006; VanderWerf et al., 2002). Regarding flow stability, CACC vehicles are effective in smoothing traffic flow and damping shock waves (Schakel et al., 2010; van Arem et al., 2006; Wang et al., 2016b; Wilmink et al., 2007), whereas ACC vehicles may, on the contrary, deteriorate traffic stability with amplified disturbances (Milanés & Shladover, 2014; Ploeg et al., 2011).

Existing traffic impact analyses of ACC/CACC vehicles are generally based on microscopic traffic simulations. To represent ACC/CACC vehicle behaviour in traffic simulations, default human-driver car-following models need to be replaced by ACC/CACC car-following models. According to the accuracy of simulated car-following models, the literature on simulating ACC/CACC vehicles can be categorized into four groups. The first group of studies (Deng, 2016; Wilmink et al., 2007) used the desired speeds or accelerations from ACC/CACC controllers as the actual speeds or accelerations in the simulation. It can be easily implemented, but the predicted vehicle response may not be realistic since the model ignores driveline

dynamics, rolling and aerodynamic resistance. Studies of the second group (Jia & Ngoduy, 2016; van Arem et al., 2006; VanderWerf et al., 2001) applied a first-order lag between the controller command (i.e. the desired speed/acceleration) and the actual vehicle speed/acceleration to represent the driveline dynamics and the inertia of vehicle mass. The response of mechanical drivetrain is included in the simulations, whereas the effects of external factors still cannot be captured. A full vehicle dynamic model, which includes vehicle controllers and both internal and external influential factors, was adopted in the third group (Swaroop et al., 2001). Although the vehicle dynamic is reasonably simulated, the detailed vehicle model consumes large computation time and it is barely feasible for the large-scale traffic simulations. The last group of studies modelled the realized speeds/accelerations of ACC/CACC vehicles as the car-following response using data collected during field tests (Milanés & Shladover, 2014). Empirical car-following models based on measured vehicle response are expected to outperform the aforementioned groups in the aspects of model validity as well as implementation simplicity. Empirical car-following models were, therefore, selected as our basic simulation models.

Empirical ACC and CACC models need to be developed to fulfil the requirements of large-scale traffic simulations. The first requirement is the full-speed-range operation of ACC/CACC vehicles. Empirical car-following models have been calibrated only within a speed range from 25.5 to 29.5 m/s (Milanés & Shladover, 2014); however, simulated ACC/CACC vehicles can easily operate at a lower speed especially when traffic congestion occurs. Secondly, vehicles collide in simulations may lead to an unexpected simulation stop or deleted vehicles. The collision-free property is often considered as an important characteristic of a car-following model to ensure proper performance of a traffic simulator. Unfortunately, the collision-free property cannot be guaranteed in simulations since the empirical car-following models are not designed to represent collision situations, which are rare events in practice. In emergency situations, drivers often override system control to avoid collisions (Klunder et al., 2009; Pauwelussen & Feenstra, 2010) and the car-following models need to explicitly incorporate that collision avoidance behaviour (van Arem et al., 1997). Existing studies pay insufficient attention to the integrated ACC/CACC car-following model with driver take-overs, and resulting collision properties have seldom been investigated. In our research project collaborating with California Partners for Advanced Transportation Technology, the empirical ACC and CACC models from Milanés & Shladover (2014) are used in two simulation frameworks for CACC impact assessments. By comparing simulation outputs in the same scenario from these two studies, underlying effects of simulators on CACC simulation results could be minimized. The parallel study (Liu et al., 2018b) proposed a CACC vehicle simulation framework integrating the manual driving for lane-change-related manoeuvres and depicting the transitions among the CACC string leader mode, the string follower mode and the ACC mode.

This paper aims for a simulation framework of realistic CACC vehicle behaviour, in which CACC is operated in a full-speed range and the collision-free requirement is satisfied. To reproduce realistic vehicle behaviour, the empirical ACC and CACC models are selected as the basis models for vehicle following responses near equilibrium states; the vehicle behaviour under the multiple driving modes of ACC and CACC are included; and the driver-system interaction for lateral manoeuvres and that in safety-critical situations are taken into account. The authority transition from the ACC/CACC system to a human driver in safety-critical situations is also considered as a fallback manoeuvre by a driver to avoid collisions, meeting the collision-free requirement of simulations. The model properties and validity of the proposed framework, especially the collision avoidance in safety-critical conditions, were tested and assessed in a wide range of simulation scenarios. This study fills, for the first time, the gap

between ACC/CACC empirical car-following models in limited scenarios and its extension and applications in various traffic scenarios.

The remaining of the paper is divided into four parts. The first part introduces a conceptual car-following model for ACC/CACC simulations with model specifications. The second part builds a simulation experiment to evaluate collision avoidance in five scenarios that ACC/CACC vehicles may encounter in a simulation. The third part presents the simulation results and explores the relationship between collision and vehicle string disturbance. Conclusion and future work are discussed in the last part.

2.2 Model formulation

This section proposes a schematic control structure of simulated ACC/CACC vehicles and formulates the models for their longitudinal behaviour.

2.2.1 Conceptual model and underlying assumptions

A multi-regime model for ACC/CACC longitudinal vehicle response is proposed with two parallel control loops: a human driver control loop and a system control loop. Each loop represents the sequential procedures for corresponding vehicle control within a simulated time step and both loops are based on a three-stage control structure from (Milanés et al., 2014).

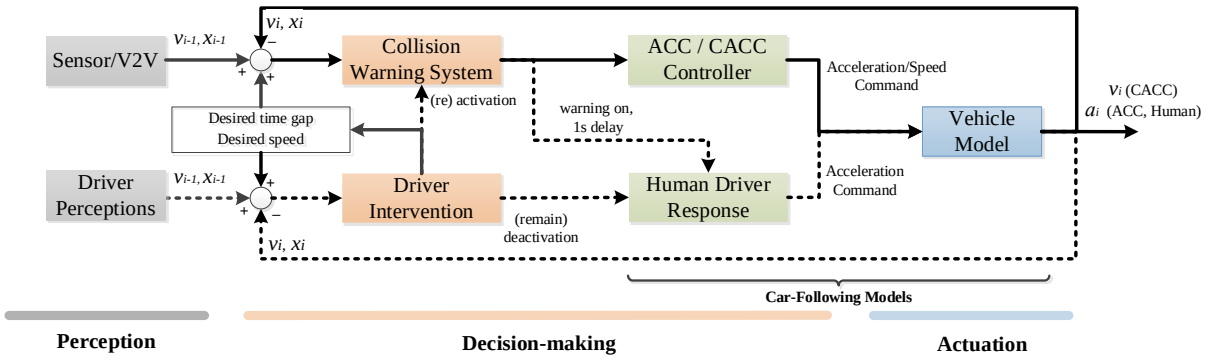

Figure 2.1 Conceptual longitudinal models for ACC/CACC vehicles in simulations.

Figure 2.1 illustrates the multi-regime framework of double loop control, where v_i, x_i and a_i refer to the speed, location and acceleration of vehicle *i*. At each time step, the model inputs are speed and position of preceding vehicle *i*-1 and subject vehicle *i* at a previous time step, as well as the desired time gap and the cruise speed set by human drivers. These inputs are processed either by ACC/CACC or human driver response models and eventually the actual kinematic data becomes model outputs and provides feedback information for next time step.

In the system control loop, the first perception stage obtains vehicle kinematic data through radar sensors/V2V communication and provides required inputs to the decision-making stage. In the second stage, the ACC/CACC controllers receive and process the inputs after the collision warning system does not issue a warning. A speed or acceleration command is delivered to the lower-level vehicle system in the third phase. The lower-level vehicle system, which is related to throttle and brake actuations, operates vehicles to meet commands. The final outputs are actual acceleration, speed and location. Depending on the ACC/CACC controller algorithms, relevant kinematic information is collected and used as input for decision-making of the next time step.

The human driver control loop performs similar control processes. The driver firstly perceives the leader's speed and location and determines the activation/deactivation of automation or retains vehicle control in the last time step. If the driver take-over is initiated, the human driver response model overrules the ACC/CACC controller and generates a desired acceleration to the vehicle model in the third phase.

The proposed car-following model reflects the relations between actual vehicle speed/acceleration and vehicle's relative speed and gap error in the previous time step. It can be generally formulated as equation (2.1) and replaces the combination of the decision-making phase and actuation phase.

$$a_{i,k} = f\left(x_{i-1,k-1}, x_{i,k-1}, v_{i-1,k-1}, v_{i,k-1}\right) \tag{2.1}$$

where subscript of *i* and *k* represent vehicle sequence and time step respectively.

The driver intervention and the collision warning system determine when to switch between the two control loops. They correspond to two types of authority transition: discretionary overrides and mandatory overrides (Klunder et al., 2009; Pauwelussen & Feenstra, 2010). The discretionary override is initiated by drivers, for drivers actively interacting with the automation system. The mandatory override is activated as long as a collision warning is given in a safety-critical situation. Regarding automation activation, we assume the switch is only effective from the driver control loop to system control loop, and the automation system cannot switch on by itself.

2.2.2 ACC/CACC Car-following models

ACC/CACC controllers based on feedback control generally include three sub-controllers for three different motion purposes (Milanés & Shladover, 2015). The cruising controller is designed for maintaining a user-set desired speed if a preceding vehicle is absent. Gap regulation controller works for car-following situations and it aims to keep a constant time gap with its predecessor. When an ACC/CACC vehicle approaches its leader with a high relative speed, the gap-closing controller performs a transition from cruising controller to gap regulation controller. In the text below, models for three operation modes are formulated respectively.

2.2.2.1 Cruising Model

Cruising models for ACC and CACC vehicles are the same since additional V2V information does not play a role in vehicle cruising operation. The vehicle acceleration is modelled as a feedback control law which keeps the vehicle travelling at the desired speed. The general formula is shown as

$$a_{i,k} = k \cdot (v_{set} - v_{i,k-1}) \tag{2.2}$$

where the control gain *k* is a parameter to determine the feedback rate of speed error for acceleration, and v_{set} is the desired cruising speed. This value was generally set as 0.3-0.4 s^{-1} in the literature (Schakel et al., 2010; Shladover et al., 2012; van Arem et al., 2006; VanderWerf et al., 2001) and 0.4 s^{-1} is selected in this study.

2.2.2.2 Car-following Models

The Milanés ACC and CACC car-following models from Milanés and Shladover (2014) are selected as the basic simulation models. The responses of ACC followers were modelled as a second-order transfer function and it is described by

$$a_{i,k} = k_1 \cdot e_{i,k} + k_2 \cdot (v_{i-1,k-1} - v_{i,k-1}) \tag{2.3}$$

where $e_{i,k}$ is the gap error of vehicle i at time step k. Equation (2.3) shows that the vehicle acceleration depends on a gap error and a speed difference with the preceding vehicle, where their feedback gain k_1 and k_2 are 0.23 s^{-2} and 0.07 s^{-1} respectively.

For CACC vehicles, the car-following behaviour is represented by a first-order model. Vehicle's speed is calculated by the speed in previous time step $v_{i,k-1}$, the gap error $e_{i,k-1}$ in previous time and its derivative, according to

$$v_{i,k} = v_{i,k-1} + k_p \cdot e_{i,k-1} + k_d \cdot \dot{e}_{i,k-1} \tag{2.4}$$

where k_p and k_d are 0.45 s^{-2} and 0.25 s^{-1}.

Model Revision In original formulas, the gap error is determined by the inter-vehicle spacing, desired time gap and subject vehicle speed. The inter-vehicle spacing was expressed as the position difference of two consecutive vehicles, where the vehicle length was assumed as zero. A distance variable d_0 is introduced here to include the vehicle length in the gap error term, which is formulated as

$$e_{i,k} = x_{i-1,k-1} - x_{i,k-1} - d_0 - t_{des} \cdot v_{i,k-1} \tag{2.5}$$

where t_{des} is the desired time gap.

We re-build the original simulation scenario in (Milanés & Shladover, 2014) and ran the simulation by the revised models with a 5-meter vehicle length assumption. The results showed the model revision does not change the car-following response of ACC/CACC vehicles.

Dynamic Spacing Margin According to equation (2.5), the desired gap between vehicles at standstill is zero, if d_0 equals to the vehicle length. To prevent rear-end collisions, we formulate d_0 as a function of vehicle speed which gives additional clearance at low speeds (Swaroop et al., 1994; VanderWerf et al., 2001). A preliminary full-speed-range simulation test on equation (2.3) and (2.4) suggests that ACC and CACC vehicles require different spacing margin. ACC vehicles should have a 2-meter additional clearance under the speed of 10 m/s while CACC vehicles request only one meter of spacing margin at speeds below 2 m/s. In this regard, we assume a maximum 2-meter spacing margin for ACC vehicles and the transitional speed range begins at 15 m/s where the margin gradually increases from zero. The d_0 is assumed to be inversely proportional to vehicle speed with boundaries of 5 and 7 m and is formulated as

$$d_0 = \begin{cases} 5 & v \geq 15 \text{ m/s} \\ \dfrac{75}{v} & 10.8 \leq v < 15 \text{ m/s} \\ 7 & v < 10.8 \text{ m/s} \end{cases} \tag{2.6}$$

For CACC vehicles, we assume a one-meter margin at speeds of 2 m/s (where the desired gap is 1.2 m) and a transitional speed range starts at 10 m/s. By a linear function, the dynamic d_0 policy for CACC vehicles is expressed as

$$d_0 = \begin{cases} 5 & v \geq 10 \text{ m/s} \\ -0.125v + 6.25 & v < 10 \text{ m/s} \end{cases} \tag{2.7}$$

A larger spacing margin was given to the ACC model than CACC model, for a reason that ACC vehicles need more spacing to compensate the gap variation by an overshoot. The inverse

proportional function and linear function of d_0 were determined through our preliminary simulation tests to avoid rear-end collisions.

A combination of a constant time gap (CTG) policy and a dynamic spacing margin ensures a realistic ACC/CACC car-following response without collisions at low-speed operations. Maintaining a constant time gap most likely represents the driving behaviour at highways. Therefore, the CTG policy is widely accepted by commercial ACC/CACC systems and becomes the dominating gap-regulation discipline in the field test (Milanés & Shladover, 2014) and our study for reproducing realistic vehicle response. A minimum spacing between two vehicles at standstill is often required in addition to the CTG policy to give some safety margin, which is lacking in the original model. We, therefore, proposed a dynamic spacing margin to avoid collisions only in a simulation use. The dynamic spacing margin can extend the safety margin with smooth vehicle performance, without altering the validity of the original model in the field test speed range.

2.2.2.3 Approaching Models

The vehicle response under gap-closing controller has not been modelled previously in Milanés and Shladover (2014). We tuned the parameters of the original car-following models for approaching. The approaching model is operated once the vehicle gap is twice larger than the desired gap and it falls into the detection range of forward-looking sensors. For a smooth transition, the approaching model is switched to the car-following model when the gap and speed errors are smaller than 0.2 m and 0.1 m/s simultaneously.

Reducing the speed difference and shortening the gap are the control objectives in the approaching model. To achieve safe approaching, we increase the feedback gain on speed error and reduce the feedback gain on gap error. After tuning, k_1 and k_2 are 0.04 s^{-2} and 0.8 s^{-1} in equation (2.4), k_p and k_d are 0.01 s^{-2} and 1.6 s^{-1} in equation (2.5). This approaching model in combination with the driver intervention is able to guarantee collision-free when an ACC/CACC vehicle approaches a standstill vehicle, as we will show with simulations.

2.2.3 Collision warning system and human take-over

The multi-regime nature of ACC/CACC operations requires modelling transitions between different driving modes, in particular, the take-over by human drivers. We assume that the system-initiated override is performed based on a collision warning and the driver-initiated override is activated in a particular condition.

2.2.3.1 Forward collision warning

A safety-critical situation can be identified by either kinematic approach or perceptual approach. The kinematic approach triggers the collision warning if the spacing is equal or smaller than an estimated safety spacing; while, the perceptual approach is based on drivers' perception of critical situations and it often uses Time-to-Collision (TTC) or its variations as indicators.

The indicator and suggested criteria in the Kiefer study (Kiefer et al., 2005) are chosen to trigger the critical situation warning. Kiefer proposed a probability indicator based on a "hardness of braking" index, which is a function of inverse TTC and subject vehicle speed. This indicator can be used for modelling and estimating the drivers' hard brake response to a variety of safety-critical conditions and here is used to evoke the collision warning. This approach is simple and computationally efficient.

2.2.3.2 Human driver car-following models and switching assumptions

The Intelligent Driver Model from Treiber et al. (2000) is a collision-free car-following model for human-driven vehicles and its modified version IDM+ in Schakel et al. (2010) has been successfully applied in an open-source traffic simulator. Thus, IDM+ was chosen to act as the car-following model in the loop of human control.

Driver-initiated deactivation depends on the driver's subjective evaluation of the situation. Before a vehicle leaves a string, the driver may overrule the system to implement manoeuvres that ACC/CACC controllers are incapable of, e.g. open a safe gap at the front or adapt the speed with the leader in an adjacent lane. Moreover, the driver may take over control when the vehicle approaches a traffic jam, which has been observed in an ACC field operational test in the Netherlands (Viti et al., 2008). In this case, we assume a driver-initiated overrule is performed when an ACC/CACC vehicle approaches a low-speed vehicle with a relative speed over 15 m/s, as well as the gap with the low-speed leader is less than drivers' perception range (150 m).

System-initiated overrule is evoked by the collision warning and the switch from ACC/CACC car-following model to IDM+ has a time delay considering the drivers' reaction time. Different from driver-initiated overrule, the driver is assumed not being prepared to the warning and thus the driver response is subject to a delay. The delay includes the time that drivers re-pay attention to driving tasks, the action of braking and the response of vehicle mechanism. In total, a delay of 1 s between alarm onset and vehicle actual braking is assumed. This assumption is in accordance with the observations of a driving simulator experiment in which participants have to react to a red stop sign by overriding ACC (De Winter et al., 2016). A larger delay of 3.85 s is observed in the experiment of Varotto et al., 2015 that participants are required to resume ACC control after a message of sensor failure. The underlying reason for the large difference between two experiments might be that the red stop sign implies a more urgent safety-critical situation than the displayed sensor failure message does. In addition to that, driver state and distraction are also found largerly influence the delay (Zhang et al., 2019).

2.3 Simulation experimental design for model verification

The multi-regime model is an approximate imitation of ACC and CACC vehicles in the real world and it should be verified to the degree needed for particular applications. We designed and conducted a series of simulation experiments to scrutinize potential collision avoidance characteristics and the following response.

2.3.1 Experiment design and general simulation setups

The experiment is to examine the impacts of several typical string disturbance on the vehicle following response and the collisions avoidance. Five representative traffic scenarios are selected: Stop and Go Scenario, Hard Brake Scenario, Cut-In Scenario, Cut-Out Scenario and Approaching Scenario.

The simulated scenarios were established and programmed in MATLAB. The vehicle speed, acceleration and location are used to represent vehicle kinematic motions and they were calculated and updated every 0.05 s. The simulation starts when a vehicle string travels at a constant speed and vehicles following their preceding vehicles in equilibrium status. The ACC vehicles maintain a 1.1 s time gap while the CACC vehicles maintain a 0.6 s time gap. Simulated disturbances are introduced at 10 s and simulations end when the string return to the equilibrium status again. In each simulation, there is only one single string and the simulated vehicle string is assumed homogeneous (vehicle length 5 m). The length of ACC vehicle string

is restricted to four vehicles, due to the string instability of ACC vehicles found in the field test (Milanés & Shladover, 2014). The length of CACC vehicle string is assumed as ten vehicles, for implementation constraints in reality and model consistency from the original model.

2.3.2 Scenario A: stop and go

Stop and go Scenario aims to examine the full-speed-range string operation, as opposed to the limited speed range that the original car-following models were calibrated and validated. The simulated vehicle string initially travels at 32 m/s and the leader starts to decelerate at second 10 to a full stop using decelerations of 1/80 g, 1/40 g, 1/20 g and 1/10 g respectively. After a stop of 10 s, the leader accelerates to 32 m/s by a positive value of previous decelerations and remains the 32 m/s till the end.

2.3.3 Scenario B: hard brake

In hard brake Scenario, the string leader applies large decelerations comparing to the comfortable decelerations in Scenario A. The deceleration values and duration, together, define the string disturbances introduced in simulations and we tested that within different speed ranges. We select the mean value of the original speed range as the first tested initial speed and then sequentially set it towards lower values on a 4 m/s speed interval. The tested decelerations are from 2 m/s^2 to 6 m/s^2 and the time for decelerating is tested on a scale of 1-5 s.

2.3.4 Scenario C: cut-in

Cut-in Scenario is set up for determining collision impacts of a cut-in vehicle on ACC/CACC vehicle string. The cut-in manoeuvre inevitably leads to a sudden drop of the gap to the direct following vehicle, which creates a critical situation. The disturbance is simulated as a vehicle cut-in at the second place of the string with a relative speed. The cut-in vehicle remains the cut-in speed and the vehicles behind respond to this new leader. We assume both ACC/CACC string vehicles maintain a 1.1 s time gap and the cut-in vehicle emerges at the place that left a 0.6 s time gap to its direct follower (Milanés & Shladover, 2015). If a 5-meter gap between the cut-in vehicle and its leader is taken into account, only the simulations with initial operational speeds higher than 20 m/s satisfy the aforementioned assumptions.

2.3.5 Scenario D: cut-out

Cut-out Scenario simulates a potential safety-critical process of ACC/CACC vehicles leaving the string. A driver-initiated override and a comfortable deceleration to open a gap are assumed for the leaving vehicles and the remaining vehicles have to decelerate as well to respond which may raise the collision risk. A maximum number of three vehicles is designed to leave the string. The second vehicle in the string is always considered as the leaving vehicle for its extensive influence. The other leaving vehicles are chosen by a balanced-distributed sequence pattern or a concentrated distribution. All leaving vehicles are assumed to start opening gaps simultaneously at second 10 and the remaining vehicles will catch up their leader after the leaving manoeuvre.

2.3.6 Scenario E: approaching

A vehicle string detects and approaches a leading vehicle at downstream is simulated in the Approaching Scenario. Relative speeds of the approaching is an influencing variable since it does not only determine the activation of driver-initiated overrule, but also raises high collision risks. For relative speeds below 15 m/s, the detection range was 120 m by ACC vehicle sensors and otherwise 150 m by human perception. For CACC vehicles, the detection range is assumed as the range of V2V communication, which is 300 m. At 10 s, a vehicle was set up at downstream of a string and cruised at a constant speed. Tested relative speeds were set from 0 m/s up to initial vehicle speed, covering the approaching situations of standstill leaders, low-speed leaders and leaders with same speeds.

Table 2.1 lists the details of the tested variables in each scenario. To verify the vehicle behaviour, vehicle response and string performance are evaluated by a qualitative analysis of vehicle speeds, accelerations and gaps. The collision is strictly defined as the distance gap between two vehicles equals to or is smaller than zero.

Table 2.1 Parameter setups for simulated disturbances

Reference	**Scenario A Stop and Go**	**Scenario B Hard Brake**	**Scenario C Cut-in**	**Scenario D Cut-out**	**Scenario E Approaching**
Speed Range (m/s) [25.5 29.5]	Speed Range (m/s) [0 32]	Initial Speed (m/s) 30, 25, 20, 15, 10, 5	Initial Speed (m/s) 32, 28, 24, 20	Initial Speed (m/s) 30, 25, 20, 15, 10, 5	Speed Range (m/s) 30, 25, 20, 15, 10, 5
Acceleration ±1/80g, ±1/40g, ±1/20g, ±1/10g	Acceleration ±1/80g, ±1/40g, ±1/20g, ±1/10g	Acceleration (m/s^2) -2, -4, -6	$\Delta v = v_i - v_{i-1}$ (m/s) 0, 2, 4, 6, 8, 10	Opening Gap (s) 1.2, 1.4, 1.6, 1.8	$\Delta v = v_i - v_{i-1}$ (m/s) 0, 5, 10,15, 20, 25, 30
		Deceleration Time (s) 1, 1.5, 2, 2.5, 3, 3.5, 4, 4.5 5		Leaving Position ACC, [2,3] CACC, [2,3],[2,6], [2,5,8], [2,3,4]	Detection Range (m) ACC 120 ($\Delta v < 15$ m/s) 150 ($\Delta v \geq 15$ m/s) CACC 300

2.4 Results and discussion

Collision properties and prevented potential collision by human take-over are the results that are relevant for the verification of the conceptual model. Results of the collision avoidance are presented in the following section, followed by illustrated string performance by kinematical parameters and model capability.

2.4.1 Collision property and human take-over

The simulation results showed that the tested disturbance does not lead to rear-end collisions in full-speed range scenario, approaching scenario and cut-out scenario. It verifies the collision-

free property during normal string operation and provides strong evidence to support the model applicability in traffic simulation. Nevertheless, high collision risk still can be identified, particularly in the low-speed range operation and approaching situations. The potential collisions are eventually avoided by driver take-over on time. The collision-free property for such a linear ACC is guaranteed in a way that could be applied for a non-linear ACC. Table 2.2 and Table 2.3 list the timing at which drivers override ACC systems in the Scenario A and Scenario E, respectively. The override timing indicates how soon a vehicle encounter a safety-critical situation after an introduced disturbance. This time lag between a disturbance and the resulting driver intervention implies the collision risk of a disturbance. For vehicles in a string, it could be used to compare the collision risks at different string positions.

Table 2.2 Override timing for each ACC vehicle drivers in Scenario A

Acceleration	Second ACC	Third ACC	Fourth ACC
±1/80g	—	—	—
±1/40g	—	—	—
±1/20g	74.5	75	76.3
±1/10g	40.65	41.75	35.2

NOTE: — = data are not available, indicating that drivers do not override the system.

In the stop and go scenario, collision-critical situations were found at leader decelerations of 1/20 g and 1/10 g. It is noticed that those overrides happened at speeds below 10 m/s, where we introduced a 2-meter spacing margin. The results implied that our proposed spacing margin and driver intervention work successfully in preventing collision for a full-speed-range string operation.

Table 2.3 Override timing for each ACC vehicle drivers in Scenario E

String speed (m/s) / Relative speed (m/s)	Second ACC	Third ACC	Fourth ACC
15 / Δv = 10	-	13.55	14.9
10 / Δv = 10	-	12.9	14.45
10 / Δv = 0	-	-	25.35
30 / Δv = 30	10.05	12.75	14.4
30 / Δv = 25	10.05	13.7	15.2
30 / Δv = 20	10.05	-	17.9
30 / Δv = 15	10.05	-	-
25 / Δv = 25	10.05	14.5	15.9
25 / Δv = 20	10.05	18.6	18.4
25 / Δv = 15	10.05	-	-
20 / Δv = 20	10.05	17	18.25
20 / Δv = 15	10.05	20.4	21.35
15 / Δv = 15	10.05	18.75	20.1

In approaching scenarios, collision warning is rarely triggered by the approaching vehicle when the relative speed is no larger than 10 m/s. Once the relative speed reaches beyond 10 m/s, the approaching vehicle is overridden by either system-initiated requests or driver-initiated requests at once (at 10.05 s), and resulting human hard brake may activate the warnings for the other following vehicles. High relative speed approaching is an extreme safety-critical situation. Especially for a standstill leader, 120 m detection range is insufficient for ACC vehicles to decelerate to a full stop before collisions. Override timing shows the collision warning system and driver override are effective in preventing collisions.

Interestingly, if more than one collision warning were given, ACC vehicles at the front of the string generally received the warning and switched to human driver control earlier than the vehicles at the string tail. This reflects a phenomenon that the severe disturbance propagated from downstream to upstream within an ACC string. In addition, it is worth mentioning that no critical situation was detected by CACC vehicles in both scenarios. The V2V communication reduces the speed difference within vehicle string and the disturbances do not amplify toward upstream.

No collision and warning were observed in any cut-out simulation with various operational speeds, opening gaps and leaving vehicle sequence. Particularly in CACC model tests, high collision probability was expected due to long-lasting decelerations during gap-openings. Owing to the fast and smoothing response of CACC controllers, the disturbances by gap opening were damped out and no collision occurs. In general, simulation results suggested that opening gaps by a comfortable deceleration does not cause a collision, regardless of operational speeds and settings of time gaps. The number of leaving vehicles and vehicle sequences also do not affect the collision results.

2.4.2 Vehicle string performance

For illustrating the vehicle-following performance, we present nine plots of time-varied speeds, accelerations and preceding gaps for ACC and CACC models respectively. To be specific, results come from the full stop test with decelerations of -0.5 m/s^2 in the *Scenario A*, approaching a 20 m/s leader with a 10 m/s relative speed in *Scenario E* and the second vehicle cut-out at 1.8 s gap in *Scenario D* were selected.

Figure 2.2 shows the dynamic response plots of ACC vehicle string in those three scenarios. In (a), the string leader and the following vehicles decelerated till a full stop with a substantially amplified deceleration rate shown in (d). A deceleration of 0.5 m/s^2 leads to driver take-overs for all the following vehicles and the fourth vehicle reached a deceleration up to 1 m/s^2. This result is in accordance with Milanés and Shladover (2014) and it is explained as accumulated vehicle response delay when relying solely on on-board sensors. It is noticed that during the period of 50-75 s in subplot (d), we observed the deceleration variation by the extra spacing margin setups. ACC vehicles decelerate slightly harder than the string leader in order to create an extra spacing.

Subplot (b), (e) and (h) show a continuous deceleration and smooth approaching trajectories with the proposed model parameters for approaching. The third and fourth vehicles responded to the deceleration of the second vehicle and lead to a speed variation which may cause discomfort to drivers.

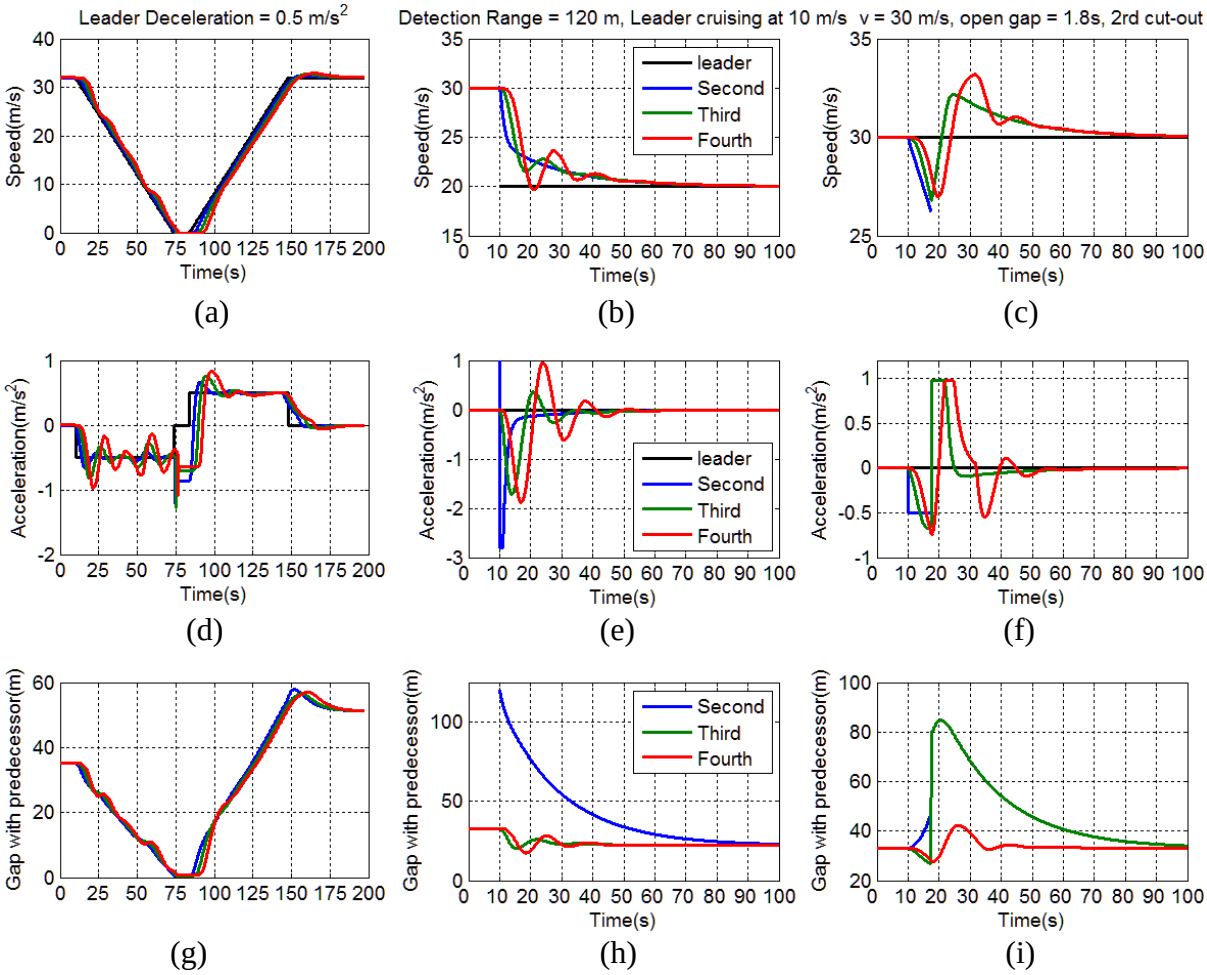

Figure 2.2 Simulated ACC vehicle speeds (a-c), accelerations (d-f) and distance gaps (g-i) in Scenario A, E and D.

For the cut-out scenario, the second vehicle changed lane after it had opened a 1.8 s gap at second 18. The results point out that following vehicles behind the cut-out vehicle reacted properly to the comfortable deceleration during the gap-opening, and they smoothly caught up the new leader and back to car-following status soon after the cut-out vehicle left.

Compared to ACC, string operation of CACC vehicles is smoother and more efficient. Figure 2.3 shows the vehicle dynamic response in selected scenarios. As it is observed, CACC vehicles do not lead to amplified disturbance thanks to the V2V communication. Vehicles at the tails experienced similar accelerations to the leader even with a 10-vehicle string length. The smooth speeds and accelerations in approaching scenario suggest a reasonable vehicle trajectory toward a low-speed vehicle and the 300 m gap was effectively reduced within 100 s. These performance plots show that the conceptual CACC model functions properly in generating plausible vehicle behaviour.

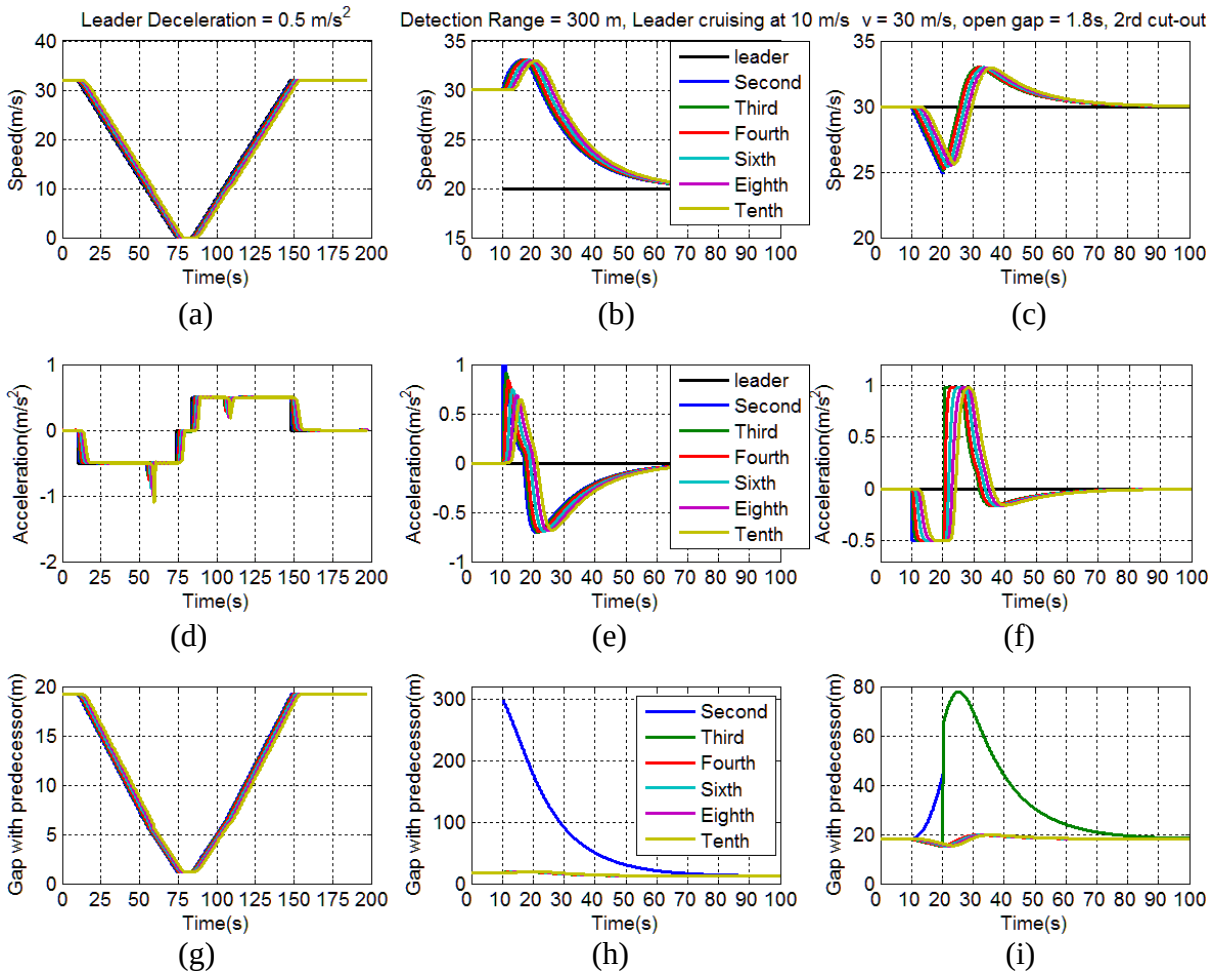

Figure 2.3 Simulated CACC vehicle speeds (a-c), accelerations (d-f) and distance gaps (g-i) in Scenario A, E and D.

2.4.3 Model capability in hard brake and vehicle cut-in

Table 2.4 summarizes the maximum deceleration time (MDT) of an ACC/CACC string leader that a collision-free string operation still can be achieved with. The number in each cell is the MDT correspond to leader's deceleration in the second row and the initial string speed in the first column. A strong correlation was found between MDT and leader decelerations. The smaller decelerations, the larger acceptable deceleration time. This suggests the proposed car-following models can accept either a long-last but soft brake or a short but strong deceleration as a disturbance that do not cause collisions. In addition, the effect of an initial ACC vehicle speed on MDT is substantial while the effect of a CACC vehicle speed is insignificant. At decelerations of -4 and -6 m/s^2, the MDTs of ACC leaders in high-speed range doubled the MDTs at low speeds.

Table 2.4 MDT for collision-free ACC/CACC strings in hard brake scenario

Initial String Speed (m/s)	Leader Deceleration MDT(s)					
	At -2 m/s^2		At -4 m/s^2		At -6 m/s^2	
	ACC	CACC	ACC	CACC	ACC	CACC
30	5	5	3.5	2.5	2	1.5
25	5	5	3	2.5	2	1
20	5	5	2.5	2	1.5	1
15	4	5	1.5	2	1	1
10	4	5	1.5	2	1	1

Results of *Cut-in Scenario* showed that the maximum safety speed difference for a low-speed cut-in vehicle is 6 m/s, 6 m/s, 8 m/s and 10 m/s for string speed at 20 m/s, 24 m/s, 28 m/s and 32 m/s. The results are the same for the ACC and CACC models, suggesting that impacts of a cut-in vehicle on ACC/CACC vehicles with equal time gaps are similar. All maximum speed differences are larger than zero implies that a vehicle cut in with the same speed does not lead to collisions.

Large cut-in speed differences rarely occur in a simulation. An assumption is often made in a simulation that if the speed difference between cut-in vehicle and target leader is considerable, the corresponding lane-change gap is strongly rejected and the lane-change manoeuvre is canceled. For this reason, cut-in vehicles normally do not evoke extreme collision situations in a simulation.

2.5 Conclusions and future work

The purpose of this study was to build a bridge between ACC/CACC empirical car-following models and their applications in microscopic traffic simulations. The empirical ACC/CACC car-following models presented in Milanés and Shladover (2014) are ideal for a traffic simulation owing to its well-calibrated vehicle response. Unfortunately, these models are incapable of achieving a collision-free operation in the full-speed range, which is an essential requirement for effective and efficient simulation. We propose multi-regime car-following models for ACC and CACC systems, extending the empirical ACC/CACC models with human interventions. The simulation results suggest that no collisions occur in representative traffic situations.

We conducted systematic simulation experiments to test model collision avoidance properties. Meanwhile, this paper has verified the capability of the proposed multi-regime model with human interventions to avoid collisions. We concluded that the proposed models are collision-free under the typical traffic situations and most safety-critical scenarios in simulations. It should be noted that our proposed model was only verified in simulation. An analytical proof of the collision-free property needs to be investigated further. Another research limitation comes from the same model parameter setting within a vehicle string in the simulation experiments. The impacts of different vehicle lengths, acceleration capabilities and desired time gaps within a string can be found by a sensitive analysis in subsequent simulations. Future research efforts aim to implement this model into an advanced and sophisticated traffic simulation model to discover the traffic impacts of ACC/CACC vehicles.

3 Effects of CACC on traffic flow characteristics

The previous chapter shows that the proposed car-following model realistically reproduces the complex behaviour of CACC vehicles, laying the foundation for a reliable CACC vehicle simulation. But to measure precise CACC impacts on traffic flow, more influencing factors, such as road configurations and vehicle market penetration rates (MPRs), should be taken into account. By incorporating the Lane change Model with Relaxation and Synchronization (LMRS), this chapter builds up a multi-lane freeway simulation with a merging bottleneck and investigates the performance of mixed CACC traffic flow. Focusing on fundamental diagrams and roadway capacity, the mixed-flow characteristics are revealed, providing new insights into traffic operations with different percentages of CACC vehicles. Section 3.1 offers an overview of CACC impact studies, followed by a detailed description of CACC vehicle behaviour and the modelling assumptions in Section 3.2. Section 3.3 designs a simulation experiment with a typical highway and widely varying CACC MPRs in order to explore the effects of CACC MPRs in a merging bottleneck scenario. The results are provided in Section 3.4, where fundamental diagrams, theoretical capacity, merging capacity and capacity drops are analysed. In Section 3.5, the relation between capacity characteristics and CACC MPRs is further discussed, and conclusions are drawn in Section 3.6.

This chapter is an edited version of the following paper:

Xiao, L., M. Wang, W. Schakel and B. van Arem. (2018). Unravelling effects of cooperative adaptive cruise control deactivation on traffic flow characteristics at merging bottlenecks. *Transportation Research Part C: Emerging Technologies, vol. 96*, pp. 380-397

Abstract—Cooperative Adaptive Cruise Control (CACC) systems have the potential to increase roadway capacity and mitigate traffic congestion thanks to the short following distance enabled by inter-vehicle communication. However, due to limitations in acceleration and deceleration capabilities of CACC systems, deactivation and switch to ACC or human-driven mode will take place when conditions are outside the operational design domain. Given the lack of elaborate models on this interaction, existing CACC traffic flow models have not yet been able to reproduce realistic CACC vehicle behaviour and pay little attention to the influence of system deactivation on traffic flow at bottlenecks. This study aims to gain insights into the influence of CACC on highway operations at merging bottlenecks by using a realistic CACC model that captures driver-system interactions and string length limits. We conduct systematic traffic simulations for various CACC market penetration rates (MPR) to derive free-flow capacity and queue discharge rate of the merging section and compare these to the capacity of a homogeneous pipeline section. The results show that an increased CACC MPR can indeed increase the roadway capacity. However, the resulting capacity in the merging bottleneck is much lower than the pipeline capacity and capacity drop persists in bottleneck scenarios at all CACC MPR levels. It is also found that CACC increases flow heterogeneity due to the switch among different operation modes. A microscopic investigation of the CACC operational mode and trajectories reveals a close relation between CACC deactivation, traffic congestion and flow heterogeneity.

3.1 Introduction

Connected and automated vehicles (CAVs) have received considerable attention in recent years, since they are seen as a promising solution to mitigate traffic congestion, a source of enormous loss to the economy and society. One concept entails CAVs travelling in very close distance to substantially increase roadway capacity (Ioannou, 1997). To realize that, Cooperative Adaptive Cruise Control (CACC) is often employed, which enables CAVs to maintain a constant time gap with the predecessor automatically. Thanks to the use of Vehicle-to-Vehicle (V2V) communication, CACC vehicles are able to anticipate traffic further downstream and respond faster and earlier so that disturbances can be damped out even when a small time gap is used (Shladover et al., 2015).

Many studies have shown that introducing CACC vehicles in traffic changes the characteristics of traffic flow, such as roadway capacity (Arnaout & Arnaout, 2014; Shladover et al., 2012; van Arem et al., 2006; VanderWerf et al., 2002; Zhao & Sun, 2013) and flow stability (Calvert et al., 2011; Schakel et al., 2010; Talebpour & Mahmassani, 2016). In particular, roadway capacity attracts the most attention since it presents the great potential of CACC in mitigating traffic congestion. In this study, our scope is limited to the traffic flow characteristics in the presence of CACC vehicles with a focus on roadway capacity.

Existing studies on roadway capacity involving CACC are often carried out via an analytical approach or traffic simulations. Using an analytical approach, roadway capacity is inversely related to the averaged time headway. The individual time headway is determined by the inter-vehicle spacing, vehicle length, and travelling speed. The averaged time headway also depends on the proportions of each vehicle type. In this regard, the CAV spacing control and the mixture of vehicle classes are the determining factors to the capacity in analytical studies. For the spacing control, it is found that the constant time gap control is a more attractive option than the constant spacing control regarding string stability (Swaroop et al., 1994), so it is widely accepted in commercial CACC systems and assumed in most of the capacity studies. The chosen time gap for CACC should consider vehicle braking capability as a constraint (Kanaris et al., 1997; Michael et al., 1998) and the capacity estimation should consider the headway/time

gap stochasticity (Ghiasi et al., 2017). Regarding vehicle classes, it is found that the roadway capacity is sensitive to the ratios of vehicle classes in mixed traffic, due to various time gap settings for each vehicle class. Introducing 10% new vehicles with large desired time gap could lead to a capacity reduction of 15% at a highway segment and of 40% at a merging section (Hall & Li, 1999; Michael et al., 1998). Besides that, Chen et al. (2017) shows that roadway capacity increases with the CAV penetration rate and platoon size, and a mixed-used lane for both CAVs and conventional vehicles can realize higher capacity than a strict segregation between these two types of vehicles. In addition, Tientrakool et al. (2011) examined the capacity change in terms of vehicle connectivity. The result shows that using radar sensor along with V2V communication provides a larger capacity increase than using sensors alone, which suggests the superiority of CACC system compared with the ACC system.

Analytical approaches are based on macroscopic traffic flow models and allow us to identify and explain the impact of a limited number of factors introduced by CACC vehicles. However, analytical approaches typically model the traffic flow in equilibrium states, and do not capture well the nonlinear phenomena in traffic flow such as flow instability and capacity drop. In this regard, the capacity estimated via analytical approaches is often higher than the maximum throughput in observation.

In order to assess the achievable roadway capacity with CACC vehicles, a number of studies evaluate the impacts through microscopic traffic simulations. How the car-following behaviour of CACC vehicles is modelled determines to a large extent the resulting capacity. There are three types of car-following models for CACC vehicles typically used in existing simulations. The first group of studies uses a car-following model for manually driven vehicles with different time gap settings for automated vehicles. The intelligent driver model (IDM) was chosen for simulating adaptive cruise control vehicles in Kesting et al. (2008) and connected vehicles in Guériau et al. (2016), and the optimal velocity model (OVM) was selected for connected cruise control vehicles in Ge and Orosz (2017). Although this method is easy to be implemented, the human driver models are not able to produce realistic behaviour of automated vehicles since they neglect the multiple sub-controllers and various driving modes in an automated control system and their resulting complicated vehicle behaviour. The second group of studies uses the desired accelerations of the CACC control algorithms, either the linear constant time gap control or more sophisticated nonlinear algorithms with safety constraints to avoid rear-end collisions (Wang et al., 2016b), as actual vehicle accelerations (Makridis et al., 2017; Schakel et al., 2010; Shladover et al., 2012; Talebpour & Mahmassani, 2016; Tientrakool et al., 2011; van Arem et al., 2006; VanderWerf et al., 2002; Zhao & Sun, 2013). However, the outputs of CACC controllers do not represent closed-loop CACC vehicle behaviour, since the mechanical driveline dynamics and rolling and aerodynamic resistance are not taken into account. The third group of studies uses an empirical CACC car-following model that is derived from field test experiments, relating the realized vehicle accelerations/speeds with relative speed and distance to predecessors. An empirical model was established in Milanés and Shladover (2014) and calibrated using vehicle trajectory from a field test of four CACC vehicles on public roads. This model is able to produce realistic CACC vehicle response within the high-speed range in which the field test data has been collected, but is not collision-free in a low-speed range. To apply it in a microscopic simulation, a previous study (Xiao et al., 2017) extended the empirical model into a full-speed-range CACC car-following model. It includes a speed-varying spacing margin for low-speed range and a driver-automation interaction module in which a driver can deactivate the CACC system and take over vehicle control. This model offers a realistic speed and acceleration profile for CACC vehicles in several typical scenarios with explicitly captured driver-automation interaction.

In addition to the car-following model, the network topology and CACC market penetration rate (MPR) are also critical factors for the capacity estimation in simulation-based studies. In the simulations of a single-lane highway with an on-ramp and off-ramp, the maximum lane throughput increases with a decrease of desired time gap (VanderWerf et al., 2001) and exhibits a quadratic increase with CACC MPR (VanderWerf et al., 2002). Based on a hypothetical single lane highway with an on-ramp, another study investigated the impacts of CACC vehicles on string stability and throughput and confirmed that CACC vehicles increase throughput (Talebpour & Mahmassani, 2016). However, the results of single-lane simulations cannot represent the capacity of multi-lane highways because the influences of lane changes are not taken into account. In this regard, other studies examined the CACC impacts in a simulated multi-lane highway. A lane drop scenario from a 4-lane section to a 3-lane section is simulated in van Arem et al. (2006). With the analysis of traffic performance with increasing CACC vehicles, this study showed that using CACC vehicles has potential positive impacts on the roadway capacity near a lane drop but a low CACC penetration below 40% does not show significant effects. Liu et al. (2018b) investigated the multi-lane throughput at various CACC MPRs in a simple merging segment. A quadratic relationship is found between the merging throughput and CACC MPR, suggesting that the traffic performance of an on-ramp merging area can also be improved by CACC vehicles. For a weaving segment, Tilg et al. (2018) evaluated the effects of the reduced reaction time by vehicle automation on flow operation via a hybrid multi-class model. The results show a non-linear increase of the capacity in the weaving segment with an increasing vehicle MPR. Hartmann et al. (2017) and Makridis et al. (2017) simulated CACC vehicles in German highway network and the ring road of Antwerp respectively for different market penetration rates. Both simulation results confirmed the potential of CACC vehicles to increase roadway capacity in a real traffic network. Additionaly, Makridis et al. (2017) pointed out that the capacity increase in a basic multi-lane segment and merging segment are only up to around 45% and 40% in the 100% CACC case. Zhao and Sun (2013) and Arnaout and Bowling (2011) investigated the impacts of CACC MPR on roadway capacity/throughput in a multi-lane highway, but they assumed no lane change is performed during the simulation. The pipeline capacity of a two-lane highway is around 3000 veh/h/lane with 100% CACC (Zhao & Sun, 2013), while the maximum throughput at an on-ramp merging section is proportional to the CACC MPR and vehicle arrival rate, at around 1952 veh/h/lane with an 8000 veh/h arriving rate in 100% CACC vehicles case (Arnaout & Bowling, 2011).

Apart from car-following models and simulation networks, roadway capacity is highly related to the assumptions made for vehicle time gaps in simulations. It is noticed that most abovementioned studies (Arnaout & Bowling, 2011; van Arem et al., 2006; VanderWerf et al., 2002; Zhao & Sun, 2013) use a 0.5 second time gap for CACC vehicles. It is a much smaller value compared to the time gap of manual driving, and therefore it contributes significantly to the roadway capacity increase. However, in real traffic, drivers choose different time gaps settings of automated vehicles, and most of them are larger than 0.5 second (Nowakowski et al., 2011). Using a realistic distribution of time gap setting from a field test, the lane capacity based on a single-lane simulation is reduced to 3970 veh/h/lane in 100% CACC case (Nowakowski et al., 2011), compared to 4550 veh/h/lane in the earlier studies (VanderWerf et al., 2002). This shows that CACC time gap setting plays a determinate role in the resulting capacity in simulations and a higher desired time gap leads to a lower attainable capacity increase. The CACC MPR straightforwardly determines the weight of CACC time gaps among the overall traffic and thus the capacity increase is highly sensitive to both CACC MPR and time gaps. A similar conclusion has been drawn by Kesting et al. (2010) in impact analysis of ACC vehicles.

In summary, the estimated roadway capacity with CACC vehicles varies largely in different simulation studies. Difference can be explained by the differences in the car-following and lane change models, desired time gap settings, simulation networks, and CACC MPRs. Among these studies, assumptions without empirical evidence were widely made, such as (1) using vehicle control algorithm as car-following response; (2) no authority transitions involved with CACC operation; (3) overestimated CACC performance in maintaining desired time gaps less than 0.5 s and (4) infinite CACC string length. To this end, the actual impacts of CACC vehicles on road flows remain uncertain. This study keeps the simulation realism as much as possible in order to provide a reliable evaluation of the CACC vehicle impacts on traffic flow characteristics. The simulation realism includes using an empirically underpinned car-following model, realistic time gap settings, plausible lane change behaviour induced by CACC authority transitions, and a practical constraint in CACC string length. Moreover, another contribution of this study is to show to what extent CACC vehicles can increase the roadway capacity at different MPRs, given the realistic behavioural model and time gaps. In particular, we focus on both the free-flow capacity and the queue discharge rate, which is paid less attention to by most of the existing CACC studies. Thus, the two-capacity phenomenon (Banks, 1991) and capacity drop can be discussed in this paper. The setting allows the discovery of both equilibrium and dynamical characteristics of congested flow in relation to different CACC MPRs.

This paper builds on the multi-regime car-following model for CACC systems proposed in our previous study (Xiao et al., 2017). The model extends the empirical model (Milanés & Shladover, 2014) to full speed range, generates constant time gap behaviour at equilibrium conditions, and captures two types of authority transitions (system-initiated and driver-initiated). In this study, we further improve this model into a multi-lane scenario by integrating the car-following model into a Lane Change Model with Relaxation and Synchronization (LMRS) (Schakel et al., 2012). The integrated simulation model is applied to a merging bottleneck where systematic simulation experiments are conducted. The experiment provides an evaluation of the CACC vehicle impacts on traffic flow characteristics, with a focus on flow-density relations, capacity and capacity drop. The evaluation is conducted for different levels of CACC market penetration rates, to show the changes by increased numbers of CACC vehicles in the near and long-term future.

In Section 2 we introduce the CACC behaviour model for multi-lane traffic, including the car-following model, lane change model, the driver-system interaction and string operation. Section 3 presents the experimental design for the impact analysis of CACC vehicle market penetration rates for a pipeline scenario and a merging bottleneck scenario. The simulation results are shown in Section 4, followed by a discussion in Section 5. Conclusions and future work are provided in Section 6.

3.2 CACC Behaviour model for multi-lane traffic

In this section, we first look into the car-following models of CACC vehicles and conventional vehicles respectively and then the lane change model for multi-lane traffic. After that, we present the assumptions of CACC system deactivation and reactivation, as well as the switching conditions for different vehicle modes and the vehicle behaviour in transitions. Next, we elaborate on CACC string operation including the string definition, properties and manoeuvres. Finally, we describe the model implementation in a microscopic simulation framework.

3.2.1 Car-following model

3.2.1.1 Control framework

A multi-regime car-following model of CACC vehicles has been previously elaborated in Xiao et al. (2017), where the longitudinal vehicle response is modelled with two parallel control loops. Both the human driver control loop and the (C)ACC control loop are based on a three-stage (perception - decision-making - actuation) control structure and it represents the sequential procedure for the underlying physics of vehicle longitudinal behaviour in discrete time steps (Milanés et al., 2014). Figure 3.1 illustrates the dual loop control, where v_i, x_i and a_i refer to the speed, position and realized acceleration of vehicle *i*. At each time step, the speed and position of preceding vehicle *i*-1 and subject vehicle *i* at a previous time step, as well as the desired time gap and the cruising speed, are used either by the CACC algorithm or by the human driver to determine the acceleration or speed command to the vehicle. The lower-level vehicle actuators will execute the acceleration/speed command and generate the (realized) acceleration/speed response. Note that the realized speed and acceleration may differ from the commanded values due to the driveline dynamics and resistance of rolling and aerodynamic drag mentioned in the Introduction section. Our car-following model captures the relation between the realized acceleration/speed and the vehicle position and speeds rather than detailing the ACC/CACC algorithms and lower-level vehicle dynamics.

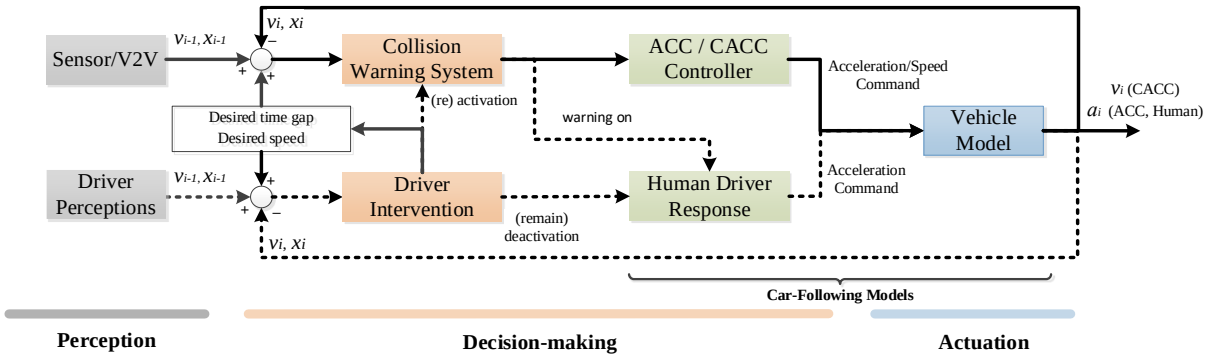

Figure 3.1 Conceptual longitudinal model for CACC vehicles in simulations.

3.2.1.2 Model specification

With the dual loop control, the CACC vehicles have three possible vehicle operating systems: manual driving, ACC operation and CACC operation. The ACC and CACC operation include sub-controllers for three different control objectives (Milanés & Shladover, 2015):

- a cruising controller to maintain a user-set desired speed if a preceding vehicle is absent;
- a gap-regulating controller to maintain a constant time gap with its predecessor in car-following situations;
- a gap-closing controller performing a transition from the cruising controller to the gap regulation controller when an ACC/CACC vehicle approaches its leader from long distance.

The vehicle state using a particular sub-controller is referred as the vehicle mode in our study. Each mode in these operations has its own car-following model, of which the mathematical specifications and the switching logics are described as following.

Cruising mode

The control objective of the cruising mode is to maintain the user-desired speed when the preceding vehicle is absent or far away and the vehicle acceleration is modelled as:

$$a_{i,k} = k_0 \cdot \left(v_{set} - v_{i,k-1} \right) \tag{3.1}$$

where the control gain k_0 is a parameter to determine the rate of speed error for acceleration and v_{set} is the driver's desired speed. The value of k_0 is assumed as 0.4 s^{-1} (Xiao et al., 2017).

Gap-regulating mode

In the gap-regulating mode, the car-following response of ACC vehicles is described by

$$a_{i,k} = k_1 \cdot e_{i,k} + k_2 \cdot (v_{i-1,k-1} - v_{i,k-1}) \tag{3.2}$$

where $e_{i,k}$ is the gap error of vehicle i at time step k. It shows that the vehicle acceleration depends on a gap error and a speed difference with the preceding vehicle, where their feedback gains k_1 and k_2 are 0.23 s^{-2} and 0.07 s^{-1} respectively (Milanés & Shladover, 2014).

For vehicles under CACC control, vehicle's speed is calculated by the speed in previous time step $v_{i,k-1}$, the gap error $e_{i,k-1}$ in the previous time step and its derivative, according to

$$v_{i,k} = v_{i,k-1} + k_p \cdot e_{i,k-1} + k_d \cdot \frac{\left(e_{i,k-1} - e_{i,k-2} \right)}{\Delta t} \tag{3.3}$$

where k_p and k_d are 0.45 s^{-1} (Milanés & Shladover, 2014) and 0.0125 (Liu et al., 2018a)

The gap error in equations (3.2) and (3.3) is determined by equation (3.4), where the inter-vehicle spacing ($x_{i-1,k-1} - x_{i,k-1}$), desired time gap t_{des}, subject vehicle speed $v_{i,k-1}$, vehicle length L and spacing margin d_0 are included.

$$e_{i,k} = x_{i-1,k-1} - x_{i,k-1} - L - t_{des} \cdot v_{i,k-1} - d_0 \tag{3.4}$$

ACC and CACC car-following models require a different spacing margin, since their collision risks at low speeds are different. Preliminary tests showed that the ACC model should have a 2-meter additional clearance at a speed under 10 m/s while the CACC model requires only 1 meter of spacing margin at speeds below 2 m/s. The dynamic spacing margins for ACC and CACC models are therefore formulated as a function of vehicle speed, as shown in equations (3.5) and (3.6) respectively.

$$d_0 = \begin{cases} 0 & v \geq 15 \text{ m/s} \\ \dfrac{75}{v} - 5 & 10.8 \leq v < 15 \text{ m/s} \\ 2 & v < 10.8 \text{ m/s} \end{cases} \tag{3.5}$$

$$d_0 = \begin{cases} 0 & v \geq 10 \text{ m/s} \\ -0.125v + 1.25 & v < 10 \text{ m/s} \end{cases} \tag{3.6}$$

Gap-closing mode

Reducing the speed difference and shortening the gap are the control objectives of the gap-closing controller. To achieve a safe approach, we increase the feedback gain on speed error and reduce the feedback gain on gap error. After tuning, k_1 and k_2 are 0.04 s^{-2} and 0.8 s^{-1} in equation (3.2), k_p and k_d are 0.005 s^{-1} and 0.05 in equation (3.3). These approaching models in combination with the driver intervention are able to guarantee collision-free driving when a CACC vehicle approaches a standstill vehicle, either under ACC control or CACC control (Xiao et al., 2017).

Three driving modes fulfil the different purposes of a vehicle moving and the switches among them are responses to the interaction between the subject vehicle and the environment. The cruising mode is operated when there is no leader in front and the vehicle maintains the desired speed. If a leader is found, depending on the distance with the leader, either the gap-regulating or gap-closing mode takes over. If the actual gap to the leader is larger than 1.5 times of the desired gap, the subject vehicle operates at the gap-closing mode, otherwise it operates at gap-regulating mode. The criterion of switching from gap-closing mode to gap-regulating mode is that the gap error is smaller than 0.05 m (Xiao et al., 2017).

Two assumptions are made for the accelerations determined in different driving modes. Firstly, to prevent CACC vehicles exceeding their desired speeds, the free-flow acceleration calculated by the cruising model is taken as the upper bound of the accelerations in gap-regulating and gap-closing models. If the gap-regulating model or gap-closing model generates higher accelerations than the free-flow acceleration, the latter will be used. Secondly, the accelerations from ACC/CACC models are limited to a range from -4 m/s^2 to 2 m/s^2. This assumption is made according to the internal acceleration limitations posed on production ACC vehicles (Milanés & Shladover, 2014).

Manual driving

The car-following model for human drivers is a modified version of the Intelligent Driver Model (Treiber et al., 2000), referred to as IDM+ (Schakel et al., 2010). The IDM+ provides the desired acceleration as the minimum of the acceleration of driving towards the desired speed and the acceleration towards the desired headway. Compare to the IDM, the IDM+ is able to achieve more reasonable values of capacity.

3.2.2 Lane change model

The lane change model we implemented for all vehicle types is based on the Lane Change Model with Relaxation and Synchronization (LMRS) in Schakel et al. (2012). In the LMRS, the lane change behaviour is predicted by a decision model that calculates the lane change desire first and determines whether a lane change is needed and which type of lane change should be executed. The lane change desire is the weighted summation of multiple lane change incentives for following the route, gaining speeds and respecting traffic rules such as keep-right directive. The route incentive is a mandatory incentive while the other two incentives are discretionary incentives. The weight for discretionary incentives becomes smaller when the route incentive appears (Schakel et al., 2012). The lane change desire is formulated as:

$$d^{ij} = d_r^{ij} + \theta^{ij} \cdot \left(d_s^{ij} + d_b^{ij}\right) \tag{3.7}$$

where d^{ij} is the overall lane change desire from lane i to lane j. d_r^{ij}, d_s^{ij} and d_b^{ij} represent the incentives for the route, speed and a directional bias respectively, and θ^{ij} is a weight factor reflecting the relative importance of discretionary incentives.

The magnitude of the lane change desire results in four different types of lane change behaviour, being No Lane Change (No LC), free lane changes (FLC), synchronized lane changes (SLC) and cooperative lane changes (CLC). Figure 3.2 shows the relationships between lane change desire and the resulting lane change behaviour, with behavioural changes in synchronization and gap-creation. The synchronization refers to the speed synchronization between the lane changer and its target leader, and the gap-creation refers to a courtesy provided by the potential follower in the target lane to facilitate the lane change. In SLC, the lane changer aligns its speed with that of the leader in the target lane, but the follower in the target lane does not actively create a gap for the lane changer. As the desire exceeds the CLC criteria, cooperative lane changes (CLC) are expected, in which the lane changing vehicle synchronizes its speed with the potential leader in the target lane and the potential follower in target lane actively creates a gap in front for the lane changer.

The interaction between the lateral and longitudinal vehicle behaviour is modelled by expressing the acceptable gap and acceleration level as functions of the lane change desire. Larger lane change desires lead to smaller acceptable headways and larger decelerations. When the lane change desire is larger than the synchronized lane change threshold, drivers apply the car following model to a leading vehicle in the adjacent lane, resulting in an acceleration for speed synchronization by the subject vehicle or gap creation by the potential follower in the target lane if the desire is even larger and above the cooperation threshold. This acceleration is constrained by a minimum value for comfort and safety. For detailed formulas and specifications of the lane change model and gap acceptance model, we refer to Schakel et al. (2012).

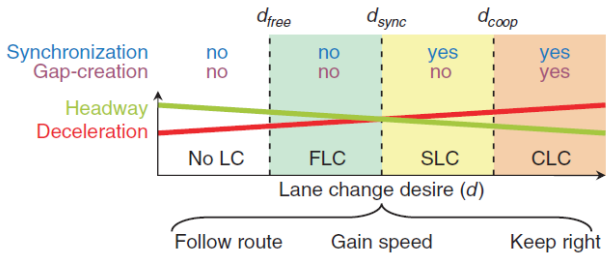

Figure 3.2 Four types of lane change behaviour corresponding to the level of lane change desire (Schakel et al., 2012).

The LMRS was extended and calibrated for situations with U.S. traffic, including the use of dedicated lanes in a previous study (Xiao et al., 2017). The resulting extended LMRS is capable of reproducing traffic flow characteristics in a complex network with interacting bottlenecks and HOV lanes, for a long simulation time period during which traffic demand varies considerably.

For CACC systems, it is the responsibility of drivers to make the lane change decisions and perform lane change control. Thus the same lane change model is used for CACC vehicles. When drivers need to change lane to follower route or perform synchronized and cooperative lane changes, drivers need to dynamically adjust the gap and speed to prepare for lane change. In these conditions, deactivating the CACC is needed to pass the vehicle control from the automated system to the human driver.

3.2.3 System deactivation and reactivation

Studies of automation-driver interaction suggest that authority transitions of automated vehicles have a large influence on traffic flow and they should be taken into account when the impacts of CACC vehicles are investigated (Klunder et al., 2009; Pauwelussen & Feenstra, 2010; Pauwelussen & Minderhoud, 2008; Varotto et al., 2015; Viti et al., 2008). The authority transition of CACC vehicles includes the deactivation and reactivation of the automation system. CACC might be deactivated for discretionary overruling, e.g. speed adaptation before a lane change or due to courtesy yielding behaviour, as well as for mandatory overruling such as reaching the system control boundaries or system failures (Klunder et al., 2009; Pauwelussen & Feenstra, 2010; Pauwelussen & Minderhoud, 2008; Varotto et al., 2015). Once CACC is deactivated, it can be reactivated after a certain time period (Viti et al., 2008). During the inactive period, the human drivers take over control and increase the CACC time gap to a manual driving gap, which has great implications for roadway capacity and flow heterogeneity.

3.2.3.1 Assumptions

The connection and interaction between the ACC/CACC car-following models and the human driver car-following model take place through the system activation/deactivation module. The system activation/deactivation module specifies the switching logic between these two parallel control loops and defines the vehicle behaviour during the transitional period.

One important assumption in this CACC simulation is that drivers intend to use the CACC system as much as possible. With an activated CACC system, three types of system deactivation could take place according to the drivers' intentions. Table 3.1 lists the deactivation types with detailed scenarios and the minimum time period of remaining deactivated to avoid frequent deactivation within a short time period. In addition, we assume that the CACC system cannot be (re)activated for vehicles braking over 2 m/s^2 or performing a lane-change. Drivers' continuous attention of surrounding environment is assumed for the activation and deactivation of CACC, which is plausible since drivers are kept in the control loop for Level 1 driving automation according to SAE.

Table 3.1 Clarification of CACC system deactivations

Deactivation Types	Scenario	Reactivation after
Type I Safety-related	Collision warning	5 s
	Critical approaching	10 s
Type II Lane-change-related	Synchronization for lane change	2 s
	Create a gap for cooperative lane changes	2 s
Type III Route-related	Taking exits, merging, lane drop	Arriving at the target lane

The first type of system deactivation is due to increased risk of rear-end collisions. It includes the system-initiated deactivation and the driver-initiated deactivation (see Figure 3.1). For system-initiated deactivation, a collision warning model is employed for identifying the safety-critical situations and if a warning is issued, the CACC system will be deactivated and the model switches to human driver mode. The collision warning is determined by an empirically underpinned indicator based on inverse time-to-collision (Kiefer et al., 2005). For driver-initiated deactivation, the driver actively resumes vehicle control in the high-relative-speed

approaching scenario, which implies a high risk of rear-end collisions for ACC/CACC vehicles due to the large deviation from equilibrium conditions that cannot be handled by the linear ACC/CACC controller. We assume that if the subject CACC vehicle is approaching the low-speed leader with a relative speed larger than 15 m/s and the gap is less than 150 m, the driver-initiated deactivation will take place.

The second type of system deactivation is related to lane changes, in particular in demanding lane change scenarios where drivers need to actively adjust the longitudinal speed to prepare a lane change or to yield a gap for another lane changer. The deactivation is considered as driver-initiated and the demanding scenarios are captured in the LMRS with high lane change desire. The lane-change-related deactivation appears in synchronized lane changes (SLC) and cooperative lane changes (CLC). When a CACC vehicle has to synchronize its speed with the target leader in the adjacent lane, the ACC/CACC will be first deactivated and then the vehicle switches to human-driven mode. When a CACC vehicle is involved in a cooperative lane change either as the lane changer who synchronizes its speed with the target leader or as the target follower who slows down to yield a gap for the potential lane changer in the adjacent lane, the human driver resumes vehicle control as well after the system deactivation. There is no difference in deactivation in terms of timing and conditions for ACC and CACC. The ACC/CACC system remains active for free lane change (FLC), during which a vehicle does not have to adjust its speed before or after the lane change.

The third type of system deactivation is related to mandatory lane changes, assuming that when vehicles have to make mandatory lane changes, drivers will resume control to avoid frequent switching between automation and human-driven modes. Mandatory lane change is captured by the route incentive in the LMRS model. Once the route incentive has appeared, as soon as the vehicles start to change lanes, the ACC/CACC system is switched off and it will remain inactive until no more lane changes for the route are required. After the route incentive vanishes, the ACC/CACC system can be re-activated if the activation conditions are met.

3.2.3.2 Switching and transitions

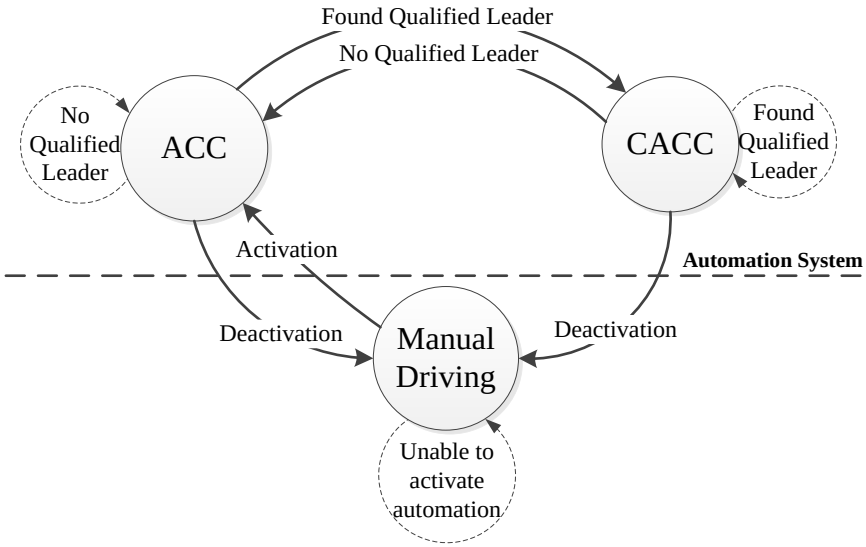

Figure 3.3 Switching paths between manual driving, ACC and CACC.

As Figure 3.3 illustrates, the switching path of system activation is different than the path of system deactivation. The CACC is considered as an advanced version of the ACC since it

additionally requires a DSRC-equipped leader for system activation. If the leader of a CACC vehicle is not equipped with DSRC, the system degrades to ACC operation. ACC operation is therefore chosen as the default control in the automation system and the activation of CACC operation is only possible via the ACC, instead of a direct activation from manual driving. This corresponds well to driver behaviour that drivers only choose to activate the automation system, rather than choose the ACC or CACC in particularly. For automation deactivation, both ACC and CACC operations can directly be switched to the manual driving, since human drivers should be able to resume controls from any automation status for any aforementioned reason at current SAE Level 1 automation that the driving automation system only executes parts of the lateral and longitudinal vehicle motion control.

The model assumes a gradual transition from automated control to manual driving, since vehicle motions are constrained by vehicle acceleration capability, safety and driving comfort. One notable difference in the behaviour of a CACC vehicle in different modes is the equilibrium time gap. Hence, switching between modes entails transition from one desired time gap to another. For CACC control, the desired time gaps range from 0.6 s to 1.1 s, which are smaller than the 1.4 s of manual driving. Switching the desired time gap from the CACC system to IDM+ instantaneously may cause large decelerations and disturbances to upstream flows, which is disfavoured by drivers and considered unrealistic. We model the transition by gradually changing the time gap of ACC/CACC to that of human drivers under a relaxation process, as suggested in Milanés and Shladover (2015) for a change in desired time in a cut-in scenario. This relaxation process during mode transition produces a smooth acceleration profile for the involved vehicles.

3.2.4 CACC string operation

A CACC vehicle string is defined as a cluster of CACC vehicles travelling in a lane with short following gaps using V2V communication. The vehicle in the first (front) position of a string is referred to as the string leader and the other vehicles in the string are called string followers. Each follower receives the kinematic information from the string leader and the directly preceding vehicle. This connectivity structure comes from the CACC vehicle string in the field test where the empirical models have been derived, and any non-CACC vehicle travelling between CACC vehicles causes a separation in connectivity. The destinations and desired time gaps of CACC vehicles in a string do not have to be identical (Rajamani et al., 2000).

A CACC vehicle is considered as a CACC string follower when all following three conditions are met: 1) the automation system is activated and the CACC vehicle is in CACC operation; 2) the vehicle is in gap-regulating mode; 3) the vehicle maintains the intra-string gap as the desired time gap instead of the inter-string gap. If one of the conditions is not met, a CACC vehicle is considered as a string leader.

The intra-string and inter-string gap is related to the implementation of string length control. Shladover et al. (2015) suggests that the CACC vehicle string length cannot go to infinity due to V2V communication range limitation, string instability and potential problems it brings at merging/weaving sections. In this regard, we implement a string length limit of 10 vehicles in the simulation to prevent overlong CACC vehicle strings, and a large inter-string gap is defined for the separation between strings. The length limit is assumed based on the maximum vehicle number travelling at highway speed within a V2V communication range of 300 meters. Such string operation has been considered in macroscopic modelling (Chen et al., 2017; Hall & Li, 1999; Michael et al., 1998), but is rarely taken into account in microscopic simulations for CACC impact evaluation. The length limit constrains the *string join manoeuvre* that a CACC

vehicle or a string of vehicles intend to join an existing string: only when the total string length after the join manoeuvre does not exceed the length limit will the join and intra-string gap be allowed. Otherwise, the leader of the upstream string operates at CACC mode with the inter-string gap to the tail vehicle of the downstream string.

We assume an ad-hoc clustering strategy for CACC strings in our simulation. The formation is conducted by a vehicle or a string joining an existing string. The *join manoeuvre* takes place at the string head or tail when a fast-speed follower/string catches up the leading vehicle/string under the string length limit, and also possible in the middle of a string that a CACC vehicle performs a lane change to the middle position of a string, but this could subject to CACC deactivations and a string separation. The *leave manoeuvre* can take place in any position of the string and consists of three steps. The driver of a leaving vehicle firstly deactivates the CACC operation, and then resumes vehicle control after the transition period in which the gap is gradually increased. When an acceptable gap is found in the target lane, the vehicle performs a lane change and the *leave manoeuvre* is completed. Based on these two manoeuvres, a dynamic CACC string operation can be implemented in the simulation.

3.2.5 Model implementation

The CACC simulation model was implemented in an open-source microscopic traffic simulation MOTUS for its explicit knowledge of simulated objects and a flexible framework that is easy to be extended for CACC algorithms (Schakel). Different simulation modules in MOTUS were extended or modified for new vehicle hardware and additional control functionalities. Most of the changes were made to the *Vehicle* module, especially on its secondary On-Board Units (OBU) module for ACC/CACC algorithms and the *Driver* module for new driver behaviour.

The *On-Board Unit* module enables modelling of vehicle connectivity and ACC/CACC electronic control units (ECU). The cyber-physical process of vehicle sensor and V2V communication is not modelled explicitly. Instead, the vehicle information provided by them is realized via accessible data within a certain range and the data is assumed accurate and reliable without any delay or loss. The ACC/CACC algorithm is written in ACC/CACC ECU that is designed depending on the architecture of the controllers in the CACC system. Both of them are substitute for human driver controls when the automation system is activated. Driver behaviour as well as their interaction with the automation systems are implemented in the *Driver* module.

3.3 Experiment design

To study the impacts of CACC on traffic flow characteristics, we simulate a merging bottleneck where jams often emerge on highways and the capacity drop exists. The simulated network consists of a four-lane highway segment with a single-lane on-ramp. As shown in Figure 3.4 , the network is 11 km in length and the on-ramp is located at 8 km downstream from the beginning, with an acceleration lane of 250 meters. In the first 3 km of the simulated network, the individually generated CACC vehicles will naturally form CACC strings via the *join manoeuvre*. Thus the first 3 km is used as a warm-up section in the simulation.

Three groups of detectors are placed at the locations illustrated as D1, D2, and D3 in Figure 3.4 at 8000 m, 8450 m and 10750 m respectively. D1 is placed at the beginning of the onramp section and aims to determine the traffic states of the merging section. D2 aims to collect the maximum throughput after the merge and therefore it is placed at 200 m downstream from

where the onramp section ends. D3 is placed at a further downstream section that is 2500 m away, aiming to collect the queue discharge rate in stable flow conditions according to Yuan et al. (2015). All detectors provide 5-min data for flow and speed.

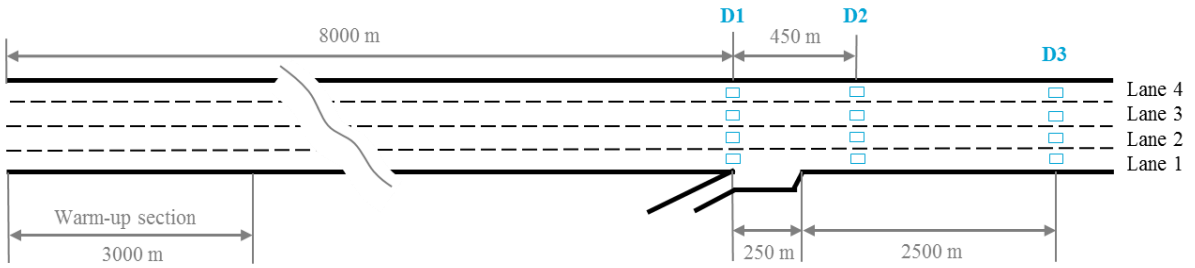

Figure 3.4 Road sketch of a simple merging network with detector locations.

To explore the traffic characteristics of mixed CACC vehicles at merging bottlenecks, the CACC MPR is the main control variable. In addition, the on-ramp demand is used as another control variable to simulate different merging disturbances. The CACC MPR increases from 0% to 100% with a 20% increment and applies to all traffic demands, including the mainline and merging traffic. The on-ramp demand is set to 400, 800, 1200 and 1600 veh/h, in order to evoke different levels of merging disturbances. In total, we simulated 24 scenarios, with 5 repetitions of each scenario with different random seeds. The random seed assigns the vehicle class, desired speed and the arriving interval between two vehicles at the simulation generators. The simulation lasts for one hour with a 0.1 second time step and the first 10 minutes is taken as a warm-up period. In addition, the mainline demand is set to 80% of the capacity of the corresponding CACC MPRs in a pipeline section, assuring that mainline flows are sensitive to the merging disturbances and they could experience the free flow, capacity flow and congested flow at each CACC MPR with the change to the on-ramp demands.

The parameters of the car-following model and simulation settings are listed in Table 3.2. We assume there is no difference in the vehicle size between the conventional vehicles and CACC vehicles and they both follow the same free-flow speed distribution. The manual driving time gap is assumed as 1.4 s from the calibration outputs of our previous study (Xiao et al., 2017), and the desired time gaps for CACC are selected from drivers' realistic choices in the field test (Shladover et al., 2012). When CACC vehicles are operated under ACC, the desired time gap is set to 1.1s.

We use the section-based harmonic speed as the traffic state indicator to distinguish the free flows and congested flows from merging bottlenecks. When the speed at D1 is above 80 km/h, traffic is considered to be in free flow and the flow count at D2 is recorded. When the speed is below 80km/h, traffic is considered congested and the flow count at D3 is stored. The merging capacity is the maximum recorded flow counts at D2, while the queue discharge rate is the averaged throughput stored at D3 for a stable value without influenced by a stop-and-go wave.

In order to estimate the pipeline capacity of mixed CACC vehicle traffic to set the demand inputs for mainline generators, we conducted simulations on an 11 km long section with four lanes, identical to the network in Figure 3.4 except the on-ramp. Similarly, the CACC MPR varies from 0% to 100% by a 20% interval. The capacity was estimated by slowly increasing the traffic demand until the generated vehicles are held at the beginning of the network. The demand was increased by 100 veh/h/lane. The throughput was collected by a group of detectors located at 10 km downstream. The 5-min flow data was aggregated into a 15-min data and the

average of the maximum 15-min throughput from five cases is denoted as the pipeline capacity (HCM, 2000).

Table 3.2 Typical values of parameters used in simulation

Parameters	Typical value
Conventional vehicles (IDM+)	
Maximum acceleration a	1.25 m/s^2
Maximum deceleration b	2.09 m/s^2
Stopping distance s0	3 m
Shared with conventional vehicles and CACC vehicles	
Desired time gap under manual driving	1.4 s
Vehicle length	4 m
Free-flow speeds	N (125, 8.75) km/h
Only for CACC vehicles	
V2V communication range	300 m
Sensor range	120 m
Desired time gap under ACC	1.1 s
Desired time gap under CACC	0.6 s (57%), 0.7 s (24%), 0.9 s (7%), 1.1 s (12%)
CACC inter-string gap	1.5 s
CACC string length limit	10 vehicles
ACC-CACC lower acceleration limit	-4 m/s^2
ACC-CACC upper acceleration limit	2 m/s^2

3.4 Results

In this section, the fundamental diagrams of mixed CACC vehicle traffic flow are firstly presented, giving a general overview of the changes in traffic characteristics e.g. capacity and data scattering. It is followed by a table of capacities including the theoretical capacity upper bound, pipeline capacity and merging capacity, analysed with the CACC MPR and CACC time usage. After that, we pay attention to the capacity drop and investigate the causes of the capacity drop in terms of CACC deactivation, and lastly we show the interaction between CACC deactivation and large following gaps by vehicle trajectory data.

3.4.1 Fundamental diagram

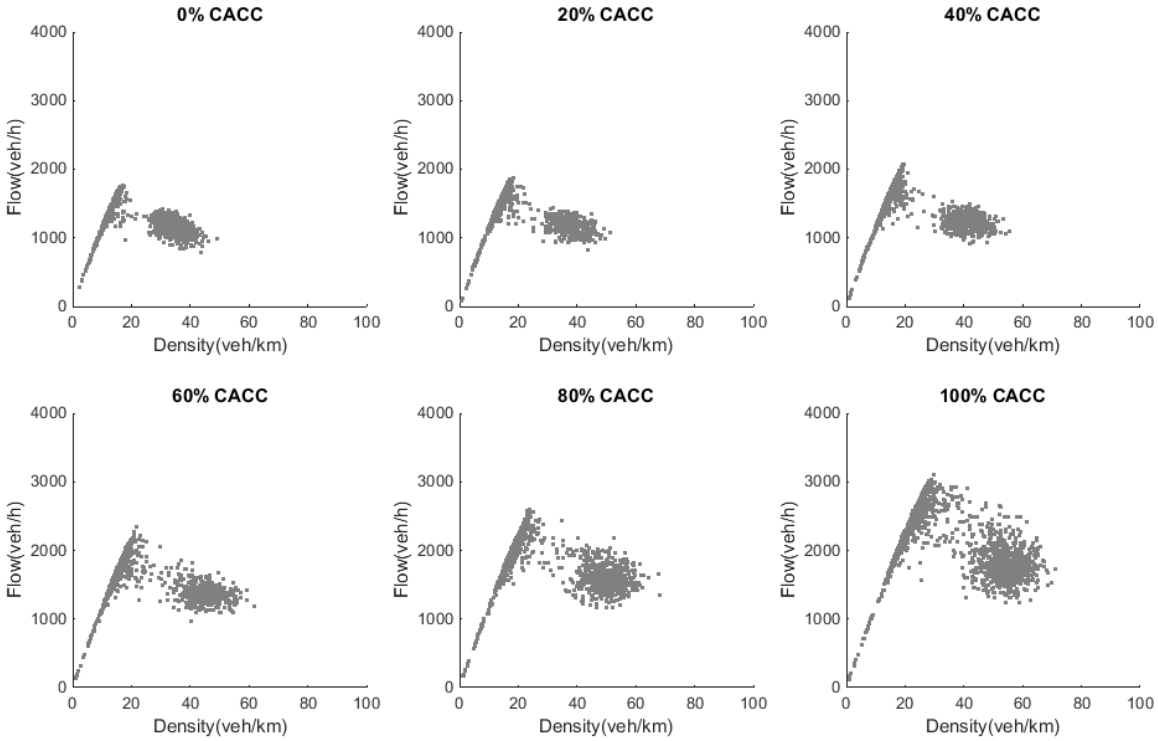

(a) Flow-Density plots with CACC MPRs

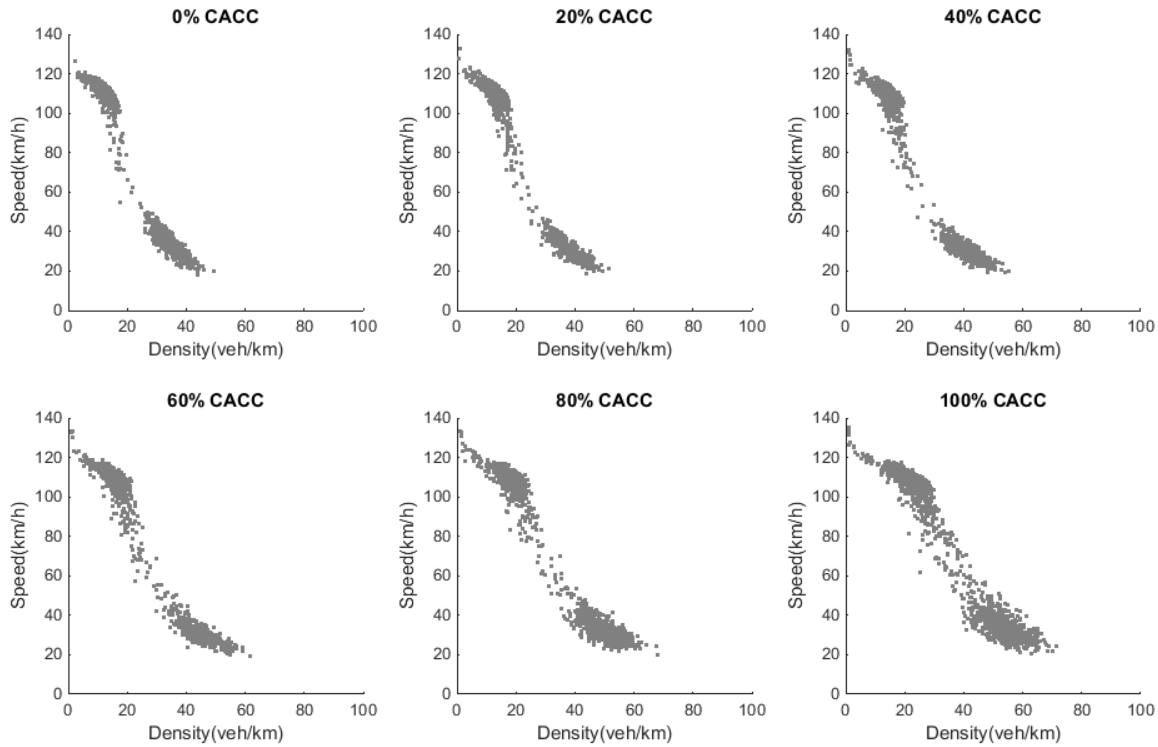

(b) Speed-Density plots with CACC MPRs

Figure 3.5 Fundamental diagrams at merging bottleneck (Detector D1) at different CACC market penetration rates.

Figure 3.5 shows the flow-density and speed-density relationship at the merging bottleneck with an increased CACC MPR, deriving from detectors at D1 using section-based flow and harmonic speed. As observed, the general shape of the fundamental diagram does not show clear changes with the appearance of CACC vehicles: the flow-density plots follow the reverse-λ curve described in Wu (2002) for manually-driven vehicle traffic, unlike the triangular fundamental diagram assumed in Bose and Ioannou (2003) and Levin and Boyles (2016) for automated vehicle traffic. A discontinuity between the free-flow regime and congested-flow regime, which is an implication of capacity drop, is the characteristic of a reverse-λ fundamental diagram as opposed to the triangular fundamental diagram. Therefore, the above flow-density plots suggest the existence of the capacity drop in mixed traffic with conventional vehicles and CACC vehicles (Treiber et al., 2006). Another characteristic that remains unchanged is the free-flow speed in the speed-density plot. The reason behind the unchanged free-flow speed is that the intended speeds of CACC vehicles follow the same distribution of intended speeds of conventional vehicles.

One noticeable change in the flow-density plots is that the data points are more scattered as usual in the congested-flow regime than the free-flow regime, and the scatter increases with CACC MPRs. The scatters can be largely attributed to different operational modes (cruising, gap-closing and gap-regulating) of ACC and CACC, as well as the vehicle controls switching among human driver, ACC and CACC system, which essentially increase the heterogeneity of road user behaviours. Moreover, the string instability of the ACC car-following model can be another explanation for the scattering. The amplified overshoot in the ACC following response has been shown in Milanés and Shladover (2014) in both field tests and simulations, and it may create shock waves that cause largely scattered data in congested flow. This finding is different from previous studies (Talebpour & Mahmassani, 2016) which suggested that the scatter in the fundamental diagram decreases as MPR of automated vehicles (using the CACC algorithm by van Arem et al. (2006)) increases from 50% to 100%. In Talebpour and Mahmassani (2016), a single-lane simulation was conducted with a mainline flow of 1800 veh/h and on-ramp demand set as 360 veh/h, which barely reaches the capacity at high MPRs of automated vehicles. The observed data located only in the free-flow regime and the scatter in the fundamental diagram naturally decreased, compared to the low MPRs case where data were also observed in the congested-flow regime. Apart from the different demand level, the different driving modes and authority transitions of CACC system were not modelled in Talebpour and Mahmassani (2016). That resulted in a more homogeneous and equilibrium flow state compared to our simulation.

3.4.2 Theoretical capacity upper bound, pipeline capacity and merging capacity

From the fundamental diagrams, the changes in throughput with the increase of CACC vehicles are clearly observed. Table 3.3 lists the theoretical upper bounds for the roadway capacity, and the simulated capacities at each CACC MPR for the pipeline network and merging bottleneck, with increases compared to the 0% CACC reference case. The theoretical capacity upper bound is calculated based on the probability of each vehicle class follow the other vehicle class and corresponding time gap settings, as well as the vehicle length and vehicle percentage, assuming the critical speed is 100 km/h (observed from the Figure 3.5b). The bounds give an indication of the maximum possible throughput when traffic is in the equilibrium state.

Table 3.3 Free-flow capacity and queue discharge rate with CACC market penetration rates, compared to theoretical upper bound and the pipeline capacity.

veh/h/lane	CACC Market Penetration Rates					
	0%	20%	40%	60%	80%	100%
Theoretical upper bound	2332	2452	2645	2945	3397	3877
Pipeline Capacity	2124	2222	2353	2620	3092	3824
Δ	-	4.6%	10.8%	23.3%	45.6%	80.1%
Merging Capacity	2031	2094	2197	2400	2708	3293
Δ	-	3.1%	8.2%	18.2%	33.3%	62.1%
Queue Discharge Flow	1684	1774	1837	1999	2268	2725
Δ	-	5.3%	9.1%	18.7%	43.3%	61.8%
Capacity Drop	347	320	360	401	440	568
%	17.1%	15.4%	16.4%	16.7%	16.0%	17.2%

The theoretical capacity upper bound, pipeline capacity and merging capacity exhibit a marginal increase at low CACC MPRs and a large increase at high CACC MPRs. The marginal increase at low CACC MPRs can be explained by the low time usage of the CACC system. The ad hoc clustering probability of two CACC vehicles is approximately the squared vehicle market penetration rates, which is very small at low MPRs. Since the CACC system is only activated when another CACC vehicle is found directly in front, most of CACC vehicles actually travel under ACC operation instead of CACC operation at low MPRs, with a time gap larger than CACC settings but smaller than that of a human driver. Similarly, the strong increase of capacity at high CACC MPRs is the result of increased CACC operation. As the CACC vehicle propotion increases, the clustering probability increases strongly and thus more vehicles operate in CACC system, so that the throughput is enhanced by small car-following time gaps.

Although the increasing trends are similar, discrepancies exist among the theoretical capacity, pipeline capacity and merging capacity. In 100% CACC vehicles scenario, the theoretical upper bound is around 3877 veh/h/lane, while the value decreases slightly to 3824 veh/h/lane for pipeline capacity and dramatically to 3293 veh/h/lane for merging capacity. First of all, the theoretical upper bound is the highest value at each CACC MPR as the equilibrium traffic flow was estimated. Regardless of the traffic dynamics and lane change behaviour, the theoretical capacity shows the greatest potential of CACC vehicles for throughput increase in an ideal situation. The merging capacity is lower than the pipeline capacity at all CACC MPRs as disturbances are introduced by the bottleneck. Due to many lane changes in the vicinity of the bottleneck, CACC systems degrade to ACC or human-driven modes with larger gaps, which result in a reduction in throughput. Because the pipeline capacity does not include disturbance at realistic traffic networks, it tends to overestimate the capacity of highways with CACC system. The merging capacity shows a more achievable and reliable potential of CACC vehicles in a realistic traffic network.

Since the increase of capacity is closely related to the operation of the CACC system, we investigate the relation between the merging capacity and the CACC operation ratio illustrated in Figure 3.6(a). The CACC operation ratio is given as the ratio of time that the system operates in CACC mode over the time of all vehicles, analysed from the vehicle trajectories at the merging bottleneck (7950 - 8050 m). The merging capacity is found as a quadratic function of

the CACC operation ratio and in fact the actual CACC operation ratios are far below the corresponding CACC MPRs. In Figure 3.6(b), a bar plot of vehicle percentage in time under CACC, ACC and human driver control (deactivated) is provided to explain the operation states of CACC vehicles with the vehicle percentage of conventional vehicles. The results show that in mixed CACC vehicle flow, a considerable percentage of CACC vehicles are operated under ACC, while a certain percentage of CACC is deactivated and under manual driving at the merging bottleneck. For instance, at the 20% CACC MPR, only 3.5% of vehicles are operated by CACC, while 14.3% of vehicles are operated under ACC and a 2.2% of vehicles are operated in the manually driven mode. As the CACC MPR increases, the percentage of CACC operation increases and that of ACC operation decreases, contributing to a much higher usage of CACC at high MPRs.

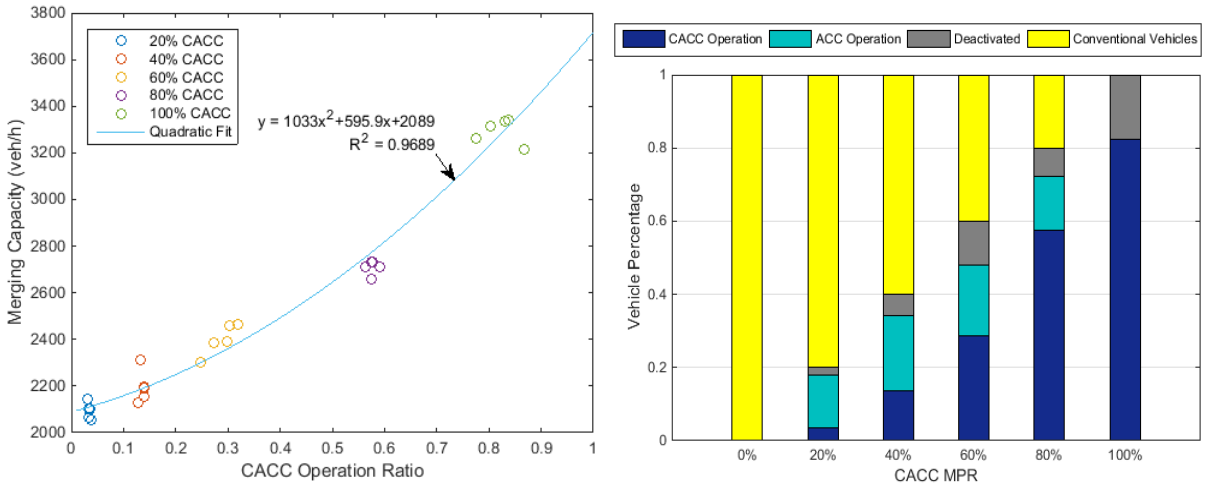

(a) (b)

Figure 3.6 (a) A relation between merging capacity and CACC operation ratio (b) vehicle percentage in CACC operation with CACC MPRs, based on trajectory data collected from the 7950 – 8050 m section.

The percentage of deactivated CACC systems generally increases with CACC MPRs, from 2.2% at 20% CACC MPR to 17.5% in the 100% CACC case. The deactivated CACC operation, which is mainly due to the lane-change-related deactivation at the merge, leaves a gap between the ideal CACC usage and the actual CACC usage at the bottleneck. Thus, it is an important explanation for the discrepancies between pipeline capacity and merging capacity in Table 3.3. As it increases with CACC MPRs, the discrepancy increases because there are more CACC deactivations due to lane changes. This further hinders the potential of CACC systems in increasing capacity of a merging bottleneck.

3.4.3 Capacity drop and CACC deactivation

Table 3.3 lists the queue discharge flow at each CACC MPR from the scenario that the averaged throughput in congestion is the highest at different on-ramp demands. The queue discharge flow shows a similar increasing trend with the merging capacity that there is a small increase at low CACC MPRs and a fast increase at high CACC MPRs.

The difference between the merging capacity and queue discharge rate is referred as a capacity drop (Yuan et al., 2017). In Table 3.3, it ranges from 320 to 586 veh/h/lane and generally

increases with CACC MPRs. The capacity drop for conventional vehicle traffic is 17.1%, and it varies between 15.4%-17.2% for traffic with CACC vehicles. The results suggest that the capacity drop in CACC traffic exists and its extent is comparable to that in conventional vehicular traffic.

According to the relation between the capacity/throughput and CACC usage, it is reasonable to investigate the capacity drop in terms of CACC deactivation. InTable 3.4, we retrieve the time ratios of different operation modes from vehicle trajectories at the merging bottlenck (7950 - 8050 m) when the merging capacity and queue discharge rates are measured. The comparison of operation ratios in such two cases shows decreases in the CACC and ACC operation time, but an increase time ratio of deactivation at all CACC MPRs. It suggests that more CACC are deactivated, either from ACC or CACC operation, at the merging bottleneck after traffic breakdown. In fact, at CACC MPRs below 40%, the increased ratio of deactivated CACC come from more ACC than CACC operation, while at high MPRs above 60%, more CACC operation than ACC operation is deactivated. Since the time gap of CACC is much smaller than that of the ACC, the change of car-following time gap from CACC operation is larger than that from ACC operation. For this reason, a higher CACC MPR leads to a larger throughput in the capacity drop, explaining the similar deactivated CACC ratio in 80% and 100% but with a different capacity drop in vehicle number.

Table 3.4 Operation ratios of CACC, ACC and manual driving (deactivated) in the free-flow capacity case and queue discharge rate case at the merging bottleneck.

Operation	CACC MPR				
	20%	40%	60%	80%	100%
CACC	3.5% / 2.8%	13.6% / 9.9%	28.8% / 22.4%	57.6% / 39.5%	82.3% / 57.8%
ACC	14.3% / 10.8%	20.7% / 14.6%	19.3% / 14.3%	14.6% / 9.0%	0.2% / 0.1%
Deactivated	2.2% / 6.4%	5.7% / 15.5%	11.9% / 23.4%	7.8% / 31.5%	17.5% / 42.2%

Note: CACC operation ratios in free-flow capacity case / CACC operation ratios in quque discharge rate case.

At the macroscopic level, a relation in space and time exists between the congestion pattern and the number of deactivations. The number of deactivations refers to the instance that the CACC system switches to the manual driving within a 5-min time interval in a 1-km section, and it includes the multiple deactivations of a CACC vehicle. One simulation run of 60% CACC with 1200 veh/h on-ramp demand is shown as an example in Figure 3.7. At the merging section (8-9 km) and its upstream section, the increase of the number of deactivations shows a consistent time-space pattern with the traffic congestion shown as speed and flow reduction in Figure 3.7(a) and Figure 3.7(c). The speed reduction at the merging bottleneck appears at 28 min and the number of deactivation starts to dramatically increase at the same time and location. When the congestion propagates to upstream sections, the number of deactivations in the upstream section also increases, showing a strong interaction between the traffic congestion and number of deactivations. In addition, the capacity drop before and after traffic breakdown is clearly observed in Figure 3.7(c).

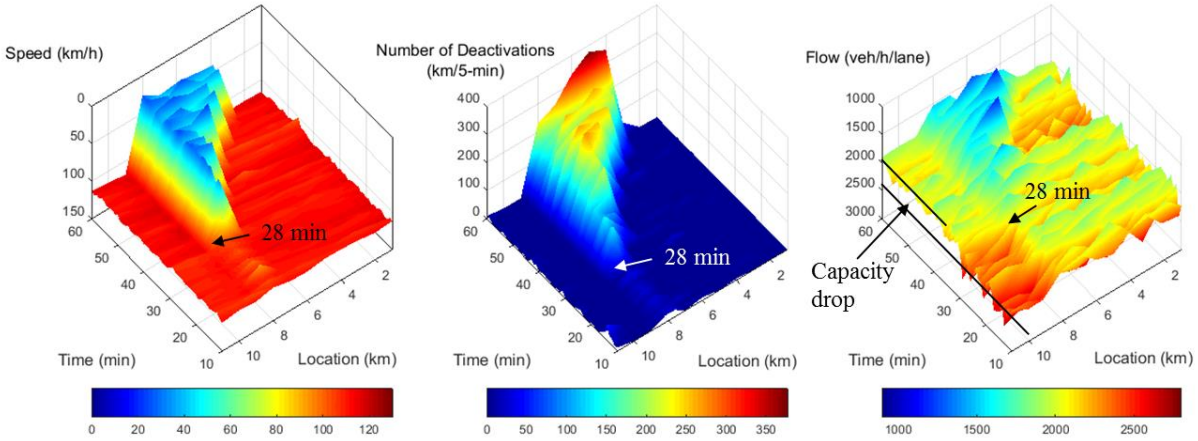

(a) (b) (c)

Figure 3.7 The relations among congestion pattern and number of deactivations. An example in the 60% CACC scenario with a 1200 veh/h on-ramp demand.

Figure 3.8 shows the relationship between the traffic flow speed and number of deactivations per km·5-min. As it is clearly observed, the number of deactivations is below 50 at high speeds above 80 km/h and it dramatically increases to a large number between 100 and 200 at speeds around 30 km/h. The deactivations at high speeds are found related to the lane changes for merging traffic and the deactivations at low speeds are the results of collision warning during the shock waves in congestion propagation. In this regard, this figure implies a mutual interaction between the traffic congestion, capacity drop and CACC deactivation.

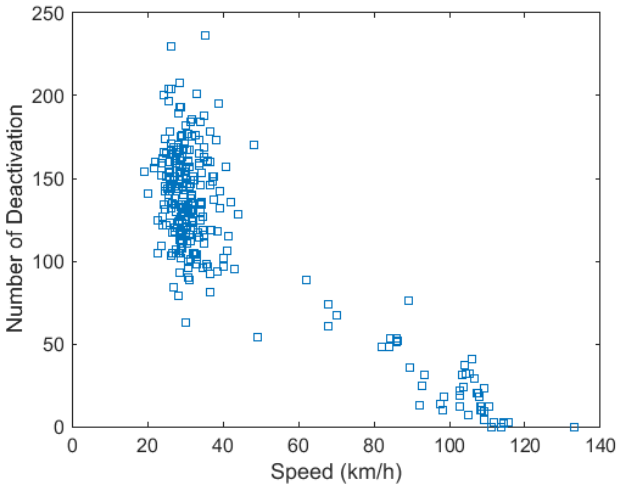

Figure 3.8 Plot of speed reduction and numbers of deactivation within 8-9 km. Data from simulation runs of the 60% CACC scenario with a 1200 veh/h on-ramp demand.

In addition to CACC deactivation, the asymmetric CACC acceleration upper and lower limits could result in capacity drop. As shown in Table 3.2, the upper acceleration limit of ACC/CACC controller is assumed 2 m/s^2 and the lower acceleration limit is -4 m/s^2. Although the full-speed range CACC could has symmetric response in deceleration and acceleration under the gap-regulating mode, the different acceleration limits result in asymmetric realized accelerations that causing capacity reduction at the downstream section of congestions.

Meanwhile, the time gap relaxation after lane changes, assumed in the manual lane change model LMRS, is another reason for the capacity drops. At the merging section, a lane changing vehicle accepts small following time gap to a leader in the target lane when the lane change desire is large. After a lane change is completed, the desired time gap will be relaxed back to the value for stable vehicle following. Such relaxation of desired time gap leads to lower traffic flow density after merging than that at merging section. The asymmetric deceleration/acceleration behaviour and time gap relaxation after lane change are also the mechanism of capacity drop in the conventional traffic.

3.4.4 Verification by vehicle trajectory

CACC system deactivation results in switches among control systems and operational modes that lead to larger vehicle gaps. Under CACC mode, CACC vehicles maintain a gap no larger than 1.1 s, but the desired gap of human-driven vehicles is 1.4 s. System deactivation inevitably causes an increase of time gap, which corresponds to a lower flow. Figure 3.9(a) presents the equilibrium gap-speed relationship under different operating modes, from the rightmost lane of a simulation run with 60% CACC and 1200 veh/h on-ramp demand. The vehicle trajectories were collected within 7-9 km for the whole simulation period, and the equilibrium state refers to the condition that a CACC vehicle is operated in the gap-regulating mode. Firstly, it is evident that the CACC has a shorter following gap than ACC in equilibrium state and also than manual driving. Secondly, vehicles under CACC perform more stable following behaviour than vehicles under ACC and manual driving, shown as the less scattered gap-speed observations in each desired time gap setting under CACC mode than the observations under the other modes. This pattern will prevail with different CACC MPRs since the equilibrium states under ACC and CACC are only related to their car-following models and time gap settings.

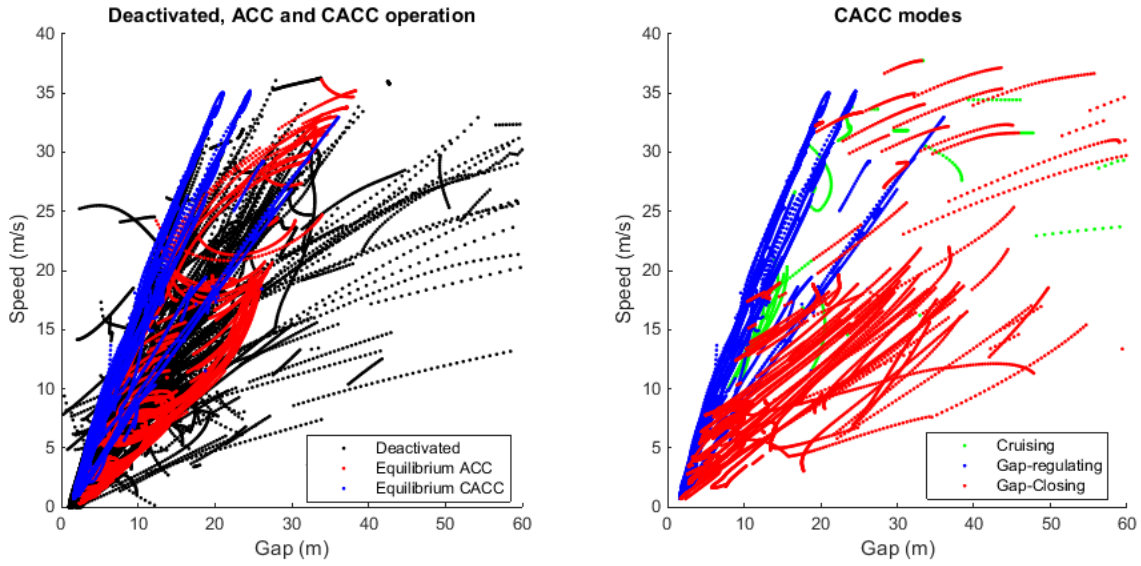

(a) (b)

Figure 3.9 (a) The Speed-Gap plot for manual driving, equilibrium ACC and equilibrium CACC operation; (b) the Speed-Gap plot for Cruising, Gap-regulating and Gap-closing mode under CACC operation.

A secondary consequence of CACC deactivation appears after the CACC system is reactivated. Immediately after the re-activation, most CACC vehicles are operated in gap-closing mode, since the gap is too large to implement the gap-regulating mode. The gap-closing mode

gradually reduces the time gap until the switching threshold of gap-regulation mode is met. As can be seen from the speed-gap plot in Figure 3.9(b), the gaps under gap-closing mode are larger than the gap-regulating mode, coresponding to a low throughput after the reactivation. Figure 3.9 establishes a connection between the microscopic vehicle behaviour and macroscopic traffic flow, points out the changes in flow state after CACC deactivation and gives an insight into the impacts of the switches among control systems and driving modes.

In addition to the speed-gap plot, vehicle trajectories provide evidence of increased following gaps due to the deactivation of CACC. In Figure 3.10, the trajectories near the merging point of two CACC vehicles, from the rightmost lane of a simulation run with 60% CACC and 1200 veh/h on-ramp demand, are highlighted and marked as 1 and 2. For each of them, a virtual trajectory is plotted (marked as 1' and 2') as a dashed line using the speed of the leader at each time step and by calculating the position of the virtual CACC follower assuming the CACC vehicle were not deactivated. These two pairs of vehicle trajectories present the deactivation of CACC string followers during a shock wave caused by a merging vehicle (marked as a cross). Before the deactivation, they are all in CACC gap-regulating mode and they enter the gap-closing mode after the CACC resumes control, which results in a larger gap than the gap-regulating mode as shown by the virtual trajectories. In combination with the speed-gap plots, we present evidence of increased time gaps after CACC deactivations caused not only by the different desired time gap settings between ACC, CACC and manual driving, but also by the changes in driving mode in CACC systems.

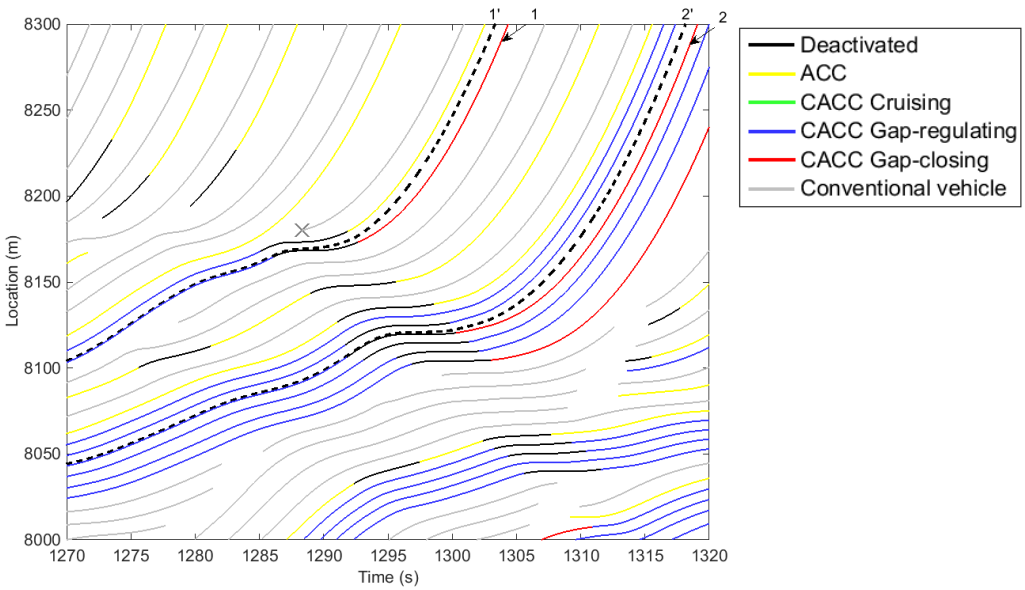

Figure 3.10 Virtual CACC vehicle trajectories showing the increased large following gaps by CACC deactivation.

3.5 Discussion

Our study shows several new insights into the traffic flow characteristics with CACC vehicles. One interesting finding is that introducing CACC vehicles into manually driven vehicle traffic does not change the inverse-λ shape of fundamental diagram. The free-flow regime and congested-flow regime are clearly observed, and they retain their characteristics with a discontinuity between two regimes. The results imply the existence of a two-capacity

phenomenon in mixed CACC vehicle flow, which has been widely observed in conventional vehicle traffic but has not previously been discussed in CACC studies.

Another important finding is that CACC vehicles increase the roadway capacity both at road segments and merging bottlenecks, with a trend of a small increase at low CACC MPRs (20 – 40%) and a strong increase at high CACC MPRs (60 – 100%). These results are in line with those of previous studies (Shladover et al., 2012; Tientrakool et al., 2011; van Arem et al., 2006; VanderWerf et al., 2002). Moreover, we found that the increase in throughput is not only related to the CACC MPRs, but also to the probability of two CACC vehicles being clustered and the system deactivations due to lane changes. For a more direct and accurate description, the capacity is closely related to the time usage of activated CACC operation, a consequence of realized ACC/CACC time gaps determined by CACC MRPs.

In addition, the deactivation of CACC is found as an important factor in reducing the capacity at the merging bottleneck compared to the pipeline capacity. It also contributes to the capacity drop. As CACC MPR increases, the influence of a bottleneck with network heterogeneity becomes stronger because of a higher percentage of CACC deactivation caused by (mandatory) lane changes. The capacity drop in vehicle per hour increases with CACC MPRs but it does not strongly vary by percentage in throughput. The number of CACC deactivations is found to be consistent with the congestion pattern in time and location, and is related to the speed of traffic flow. The capacity drop in mixed CACC vehicle traffic has not been investigated previously and our study provides new insights into the relation between the capacity drop and CACC deactivations.

These findings may help vehicle manufacturers to refine or even redesign their systems to improve traffic flow performance. Vehicle manufacturers should work on extending the operational design domain of ACC/CACC systems such that they can handle more traffic situations such as safety-critical situations and low speed operations, to reduce the number of system deactivation. In addition, with the use of V2V connectivity, the merging vehicles and vehicles in the mainline could work in a more coordinated way, which could potentially increase the capacity at a merging bottleneck (Milanés & Shladover, 2015; Wang et al., 2015). The enhanced system functionalities can improve the resilience of traffic flow and further increase the merging capacity.

The insights into traffic flow characteristics from our simulations also have implications for highway traffic management. It is noteworthy for road operators that the capacity benefit of CACC systems should be evaluated at highway bottlenecks and at low MPRs the potential of CACC systems is marginal due to the low probability of CACC vehicles following each other. Increasing the activated CACC operation ratio is more effective than increasing the CACC vehicle MPR in terms of improving the traffic flow operation. Especially at the early stage of implementing CACC, road operators may explore strategies in either increasing the clustering probability of CACC vehicles, such as a dedicated lane operation and active platooning strategy, or increasing the number of vehicles equipped with V2V communication. Another paradigm of highway management strategy involves the use of Infrastructure-to-Vehicle (I2V) communications connecting traffic control with vehicle control systems to harmonize traffic flow or resolve stop-and-go traffic, which will potentially reduce the system deactivations. This has shown to be effective in simulations (Baskar et al., 2012; Roncoli et al., 2016; Wang et al., 2016a).

Our study focuses on the merging bottleneck but the findings also bear significance for other bottlenecks such as weaving section and lane drops. In a weaving section, there is additional exiting traffic that interacts with the mainline and merging traffic within a short section, which often leads to a larger speed reduction than a merging bottleneck. For CACC vehicles taking

exits, more deactivations are anticipated due to the lane change requests for following routes, and the influence of system deactivation is therefore expected to be stronger compared to a merging bottleneck. This expectation is consistent with Hartmann et al. (2017), concluding that the capacity of mixed CACC traffic at weaving sections is lower than the merging bottleneck. In a lane drop scenario, vehicles have to change lane to follow the route similar to the merging bottleneck scenario, but the lane changes could be performed at upstream sections in advance whenever the gap is available and thus less deactivations of CACC happen in the mainline for cooperative lane changes. In this way, the negative impacts of a lane drop bottleneck will be less than that of the merging bottleneck.

It should be noted that our assumptions on CACC activation and deactivation might not be complete. For example, our model does not include the deactivation for courtesy lane changes, during which the courtesy provider might actively deactivate the system to yield gap for the lane changer. On the other hand, drivers with activated CACC might be less inclined to provide cooperation or courtesy, resulting in fewer CACC deactivations.

3.6 Conclusions and outlook

In this paper, we formulated the extension of a realistic CACC behaviour model with system deactivation/reactivation and a string length constraint, which are essential determinants of roadway capacity. The CACC model was implemented in the simulation model MOTUS, with which we conducted simulations to investigate impacts of CACC vehicles on traffic flow characteristics at a merging bottleneck, particularly on the fundamental diagram and roadway capacity.

Our work reveals that there are some noticeable changes in the fundamental diagram, especially, a wider spread of traffic states in the congested branch of the fundamental diagram with the increase of CACC MPRs. This is explained by the multi-regime nature of the full-speed-range CACC controllers and the degradation of CACC to ACC and human-driven modes.

The simulation results show that roadway capacity increases with CACC MPRs both on homogeneous highway sections and merging bottlenecks, up to 3824 veh/h/lane and 3293 veh/h/lane respectively for a four-lane highway with 100% CACC vehicles. The pipeline capacity and merging capacity both exhibit a slow increase at CACC MPRs below 40% and a rapid increase at CACC MPRs above 60%. The merging capacity is 6% -14% lower than the pipeline capacity at the same CACC MPR since the merging disturbances greatly limit the flow increase by the increased CACC MPRs. Drivers have to take over vehicle control to enable cooperative lane changes, and that significantly compromises the capacity benefits of CACC systems.

The capacity drop at merging bottleneck is explained by the CACC deactivation, which increases the time gap between CACC vehicles and their predecessors consequently. After traffic congestion appears, the number of deactivations increases substantially due to safety concerns and lane change requests, which leads to a larger number of vehicle control switches from CACC to manual driving and from gap-regulating mode to gap-closing mode after CACC reactivation. The changes among multiple vehicle operations and modes result in large time gaps and thus lead to a capacity drop.

The capacity drop can be further investigated by CACC deactivation types. Future research can focus on segregating the effect of each deactivation type on reducing throughput at different traffic bottlenecks, i.e. merging, splitting, weaving and lane drop. Other than roadway capacity, special attention can be paid to string stability of the proposed CACC car-following model. The discrete-time property, multi-regime state and the inclusion of historical vehicle state pose

challenges to the string stability analysis. Deactivation in approaching scenarios can potentially be reduced by including a quadratic term of relative speed in the approaching model, which makes the model nonlinear. Moreover, future study points to the extension of CACC simulations of highway corridors with multiple interacting bottlenecks to see the impacts of CACC vehicles in mitigating congestion. In addition, the considerable capacity drop due to CACC deactivation suggests a need for developing a better strategy for CACC vehicle cooperation or coordination at merging sections. Future study will pay attention to the cooperative merging control to further boost the roadway capacity by CACC vehicles. Besides, lane management strategies such as a CACC vehicle dedicated lane can be used to maximize the positive effects of CACC vehicles in low MPRs and it remains as an interesting topic to be studied. Learning-based car-following models that capture more historical information and provide higher prediction capability (Wang et al., 2018; Zhou et al., 2017) could be applied to model future CACC vehicles, and impact assessment of such systems on traffic flow is also a nice topic to be explored.

4 An enhanced lane change model for a continuous-access dedicated lane

The evaluation of traffic performance at merging bottlenecks in Chapter 3 implies that the benefits of CACCs are greatly limited by the interacting traffic. In this regard, creating a dedicated lane for CACC vehicles is considered as a promising lane management strategy to reduce such interactions, which could improve traffic flow operations. In order to construct a dedicated lane scenario, it is important to simulate the relevant lane change behaviour. This chapter therefore extends the Lane change Model with Relaxation and Synchronization (LMRS) for a continuous-access dedicated-lane scenario. The lane change behaviours of eligible and ineligible vehicles are modelled separately, and the model is calibrated using traffic data from SR-99 in California, where a High Occupancy Vehicle (HOV) lane is operational.

Section 4.1 reviews lane change models for simulating dedicated lane operations and selects the LMRS to be further extended. Section 4.2 describes the additional lane change incentives for dedicated lanes and integrates them into the default framework of the LMRS. In Section 4.3, the traffic operation of the SR-99 corridor is presented, and the methodology of model calibration is introduced. The simulation results focusing on congestion pattern, fundamental diagram and friction effects are delivered in Section 4.4, followed by conclusions in Section 4.5.

This chapter is an edited version of the following paper:

Xiao, L., M. Wang, W. J. Schakel, S. E. Shladover and B. van Arem. (2016). *Modeling Lane Change Behavior on A Highway with A High Occupancy Vehicle Lane with Continuous Access and Egress*. Paper presented at the Transportation Research Board, Washington, D.C

Abstract—A realistic lane change model plays an essential role to reproduce traffic characteristics and ensures the validity of traffic simulation results. In the presence of a High Occupancy Vehicle (HOV), lane alternatives change for eligible and ineligible vehicles and thus the lane change behaviour changes. If the lane change model is not adjusted properly to that new behaviour, the simulation may not provide reliable results. This paper puts forward a model for the lane change behaviour on highways with continuous access HOV lanes for both eligible and ineligible vehicles. The model formulates lane change desire based on lane change incentives, representing both mandatory and discretionary lane changes in relation to HOV lanes. Speed gain and drivers' preference on HOV lanes are assumed as incentives for using HOV lanes. The speed gain incentive is modelled using the speed difference between the current lane and adjacent lanes while the drivers' preference is modelled as a directional bias toward the HOV lane. We apply the model to the SR99 corridor in California with one HOV lane, and calibrate the model against loop detector data. The results show that the proposed model reproduces lane change behaviour during the transition between deactivation and activation of the HOV lane, as well as section-specific fundamental diagrams and congestion pattern at the network level. In addition, we offer an explicit representation of lane change behaviour that leads to the friction effect of HOV lanes.

4.1 Introduction

A High Occupancy Vehicle (HOV) lane is a lane reserved for access only by vehicles with one or more passengers in addition to the driver. HOV lanes are expected to encourage car-pooling and consequently reduce the person-based delay during traffic congestion (Giuliano et al., 1990). In the USA, more than 130 HOV freeway facilities and over 1000 miles HOV lanes have been put into practices. Limited-access HOV lanes use physical barriers or solid double white line between HOV lanes and General Purpose (GP) lanes. HOVs enter and exit the HOV lanes at restricted road sections which can easily become road bottlenecks (Cassidy et al., 2015a). On the other hand, continuous-access HOV lanes use dashed white lane markers, allowing HOVs to access and egress the HOV lanes continuously at any point. In this case, lane change manoeuvres are found more spread along the highways (Qi et al., 2016), which cause complex interactions between HOV lanes and GP lanes. Our study focuses on HOV lanes with continuous access and egress, since they avoid additional bottlenecks and can be converted to GP lanes during off-peak hours (Choudhury, 2005), both of which ensure a better use of the non-separated HOV lanes compared to their separated counterpart.

HOV lanes with continuous access and egress have been found to have particular impacts on traffic flow characteristics. A friction effect of HOV lanes has been observed from the empirical data, characterized as a speed reduction on the HOV lane when the adjacent GP lane is congested. This phenomenon can be explained because HOV drivers in the HOV lane may reduce speeds when passing low-speed vehicles in the adjacent GP lane, associated with the disturbances caused by possible lane changes between GP lanes and HOV lanes (Chen et al., 2005; Guin et al., 2008; Jang et al., 2012; Menendez, 2006).

Existing studies focusing on the impact assessment of HOV lanes are usually based on microscopic traffic simulations in order to elaborately represent vehicle behaviour in car following and lane change situations. To reproduce realistic traffic characteristics, modelling the difference between HOVs and Single-Occupant Vehicles (SOVs) in the lane change behaviour is essential. The lane change behaviour of SOVs is often modelled by limiting the accessibility of SOVs to the HOV lane, while that of HOVs is modelled by several approaches as follows.

Lane changes of HOVs can be modelled through the process of traffic assignment, defining HOV lanes as independent routes for HOV drivers (Gomes et al., 2004; Zhang et al., 2009). Consequently, HOVs use HOV lanes as soon as they enter the highway regardless of traffic flow conditions on HOV and GP lanes. This results in mandatory lane changes at fixed locations of HOV lanes, which is, in fact, a separated-HOV-lane model. Even for barrier-separated HOV lanes, lane change decisions without considering traffic conditions are unrealistic.

The lane change behaviour can also be considered as a consequence of lane choice models and gap acceptance models. Lane selections specifically taking HOV lanes into consideration is a distinct characteristic of HOV drivers, compared to lane selections of SOV drivers. Choudhury (2006) modelled the lane choice of HOVs based on the utility theory. A target lane model was proposed by using an extra dummy variable in the utility function for eligible users of HOV lanes. This model assumes that HOV lanes can offer a benefit for HOV drivers and this benefit is invariant with traffic conditions. Disadvantages of this model include the non-physical interpretation of the dummy parameter and the difficulties in the parameter calibration. Besides, Chow et al. (2010) introduced prospect theory in the lane choice for HOV lanes and proposed a cumulative-prospect-theory-based logit model for two-lane highways. This model is able to capture the heterogeneity of weights across drivers on the speed gain from HOV lanes, but the model has limited applicability since two-lane highways with one HOV lane rarely exist.

In addition to utility-based models, also rule-based models are considered as another category of lane choice models (Rahman et al., 2013). Menendez (2006) modelled the lane change decisions based on lane change probabilities, in which the speed gains between the current lane and HOV lanes were taken as the only influential factor. Later research developed and calibrated this model to simulate the lane change behaviour in separated and non-separated HOV lanes (Cassidy et al., 2015a, 2015b). However, this model neglects possible speed reductions from neighbouring lane, which is likely to produce lane changes even when the intermediate lanes are heavily congested. Moreover, Hao et al. (2017) introduced two lane change rules toward HOV lanes: eligible vehicles seeking short-term speed gain or anticipated long-term speed benefit on HOV lanes. This model is integrated into a cell transmission model where successive multi-lanes lane changes cannot be explicitly modelled and lane change locations are highly dependent on the node numbers in the network. Furthermore, factors related to driver characteristics, e.g. HOV drivers' preferences for HOV lanes, were not captured in these two models.

In this paper, we propose a new and intuitive lane change model, which is capable of reflecting drivers' lane change decisions in the presence of HOV lanes. Lane change decisions are based on a lane change desire accumulated by multiple lane change incentives. The incentives for HOV lanes are modelled as a speed incentive and a lane preference bias, while the incentive of SOVs leave HOV lanes is modelled by a strong bias toward GP lanes. The model is calibrated against empirical data and is verified by section-specific fundamental diagrams and congestion pattern at the network level. This study makes contributions to offer an understanding of adaptive driving behaviour and provides a new insight into the interaction between HOV lanes and GP lanes.

The remaining paper is structured as follows. In Section II, we discuss possible incentives for HOV drivers to use HOV lanes and review the recently developed Lane Change model with Relaxation and Synchronization (LMRS), which will be extended to an application in the presence of HOV lanes. Section III describes the calibration framework and results of the model when it is applied to a real network with interacting bottlenecks, followed by an observation and an analysis of the friction effect in the simulation as well as the face validity of the simulated vehicle behaviour. Conclusion and further work are discussed in Section IV.

4.2 Incentive-based lane change model

In this section, spontaneous desires and underlying incentives for the use of HOV lanes are discussed firstly. Based on that, an incentive-based lane change model is described, followed by the extensions made for modelling HOV traffic and adaptions made for U.S. traffic features.

4.2.1 Incentives toward HOV lanes

Many factors substantially contribute to the attractiveness of HOV lanes, e.g. level of traffic congestion, eligibility requirements and infrastructure design (Turnbull et al., 2016). Among them, travel time saving is acknowledged as the most important element that attracts HOV drivers to move from GP lanes to HOV lanes. Time saving depends on many features including the flow on HOV lanes, congestion levels on GP lanes, the length of the facility and access configuration. The saving of travel time can be considered equivalent to speed gain from GP lanes to HOV lanes. The higher the speed gain is, the stronger the desire toward HOV lanes can be.

Literature also suggests other incentives to use HOV lanes. Some SOV drivers were found to pay for the usage of High Occupancy Toll (HOT) lane (an exclusive lane which SOVs can enter by payment) even when the speed difference between the HOT lane and GP lanes is insignificant (Burris et al., 2012). This implies that there may be other incentives for selecting an exclusive lane than just for travel time saving. These incentives may be related to psychological attributes of drivers, e.g. the feelings of jumping a queue on GP lanes and getting a premium service by HOV lanes, or the positive experiences on travelling in HOV lanes with more reliable travel time. Following a parsimonious modelling principle, we assume these incentives are captured by an overall HOV lane preference by HOV drivers, which is independent of traffic conditions. The same assumption has been made in the studies of Gomes et al. (2004) and Choudhury (2006).

In summary, the speed incentive and the lane preference are two essential factors in the HOV lane change model. They reflect the motivations to change lane toward HOV lanes from the perception aspect (situation-based principles) and the experience aspect (personal-related features) respectively in the decision-making process.

4.2.2 Basic LMRS model

Based on the aforementioned lane change incentives, the Lane Change Model with Relaxation and Synchronization (LMRS) is selected as the seminal model (Schakel et al., 2012). This model was developed for asymmetrical traffic (with keep-right rules) and has been calibrated using traffic data of the Dutch A20 freeway. The LMRS is based on an intuitive and straightforward concept for lane change desire and provides a flexible structure to easily integrate additional incentives. The lane change behaviour is predicted by a transparent decision model using driver-dependent desires and condition-dependent acceptable gap relaxation. It has been implemented in an open source traffic simulator, in which all the model implementations can be fully accessed and modified.

The LMRS model describes the lane change decision by a combination of multiple incentives. In the original model, a lane change desire is calculated by three incentives of following the route, gaining speeds and keeping right:

$$d^{ij} = d^{ij}_{route} + \theta^{ij}_{voluntary} \cdot \left(d^{ij}_{speed} + d^{ij}_{b} \right) \tag{4.1}$$

where d^{ij} is the overall lane change desire from lane i to lane j. d^{ij}_{routes}, d^{ij}_{speed} and d^{ij}_{b} represent the incentives for the route, speed and a bias to the right lane respectively, and $\theta^{ij}_{voluntary}$ is a weight factor reflecting the relative importance of discretionary incentives.

Lane change incentives are categorized as mandatory and voluntary incentives, related to mandatory and discretionary lane change behaviours respectively. Following the route is considered as a mandatory incentive and it plays an important role when vehicles are in preparation for entering/exiting the main freeway. The route incentive is based on a parameter t_0 indicating for how long in advance per lane that vehicles start to consider lane changes for following routes. The other two incentives are considered as voluntary incentives, which are partially included by a weight factor $\theta^{ij}_{voluntary}$ which is larger as d^{ij}_{routes} is closer to zero. It can be interpreted as that the driver is caring less about the speed gain and keep-right regulation in adjacent lanes when the vehicle is approaching its destination. $\theta^{ij}_{voluntary}$ is formulated as equation (4.2).

$$\theta^{ij}_{voluntary} = \begin{cases} 0 & d^{ij}_{route} \cdot (d^{ij}_{speed} + d^{ij}_{b}) < 0 \text{ and } \left|d^{ij}_{route}\right| \geq d_{coop} \\ \dfrac{d_{coop} - \left|d^{ij}_{route}\right|}{d_{coop} - d_{sync}} & d^{ij}_{route} \cdot (d^{ij}_{speed} + d^{ij}_{b}) < 0 \text{ and } d_{sync} \leq \left|d^{ij}_{route}\right| \leq d_{coop} \\ 1 & d^{ij}_{route} \cdot (d^{ij}_{speed} + d^{ij}_{b}) \geq 0 \text{ and } \left|d^{ij}_{route}\right| \leq d_{sync} \end{cases} \tag{4.2}$$

Meaningful desires range from -1 to 1, where negative values suggest that a lane change is not desired. Based on the total lane change desire, different types of lane change behaviour can be distinguished by three thresholds: d_{free}, d_{sync} and d_{coop}, with $0 < d_{free} < d_{sync} < d_{coop} < 1$. As shown in Figure 4.1, a lane change desire d smaller than d_{free} means that no lane change (No LC) is performed. When d is between d_{free} *and* d_{sync}, vehicles execute free lane changes (FLC). When d is within the range of $[d_{sync}\ d_{coop}]$, the lane changing vehicle performs synchronized lane changes (SLC) where it aligns speed with that of the leader in the target lane, but the follower in the target lane does not actively create a gap for the lane changer. As the desire d exceeds d_{coop}, cooperative lane changes (CLC) are expected, in which the lane changing vehicle synchronizes its speed with the potential leader in the target lane and the potential follower in target lane actively creates a gap in front to facilitate the lane change.

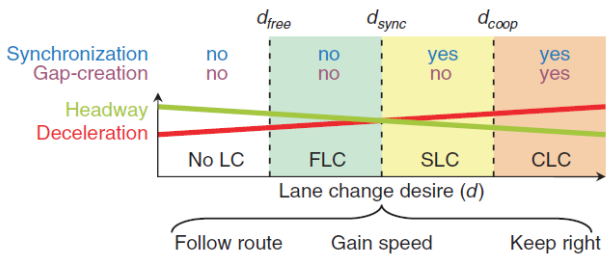

Figure 4.1 Four types of lane change behaviour corresponding to the level of lane change desire (Schakel et al., 2012).

This incentive-based lane change model is integrated with a modified version of Intelligent Driver Model by Treiber et al. (2000), hereinafter referred as IDM+ (Schakel et al., 2010). The

IDM+ provides the desired acceleration as the minimum of the acceleration of driving towards the desired speed and the acceleration towards the desired headway. This model has been proved to be capable of producing crucial traffic phenomena such as capacity drop (Kesting et al., 2010). The interaction between the lateral and longitudinal vehicle behaviour is modelled by expressing the acceptable gap and acceleration level as functions of the lane change desire. As shown in Figure 4.1, larger lane change desires lead to smaller acceptable headways and larger decelerations. When the lane change desire is above d_{sync} or d_{coop}, drivers apply the car following model on a leading vehicle in an adjacent lane resulting in an acceleration for speed synchronization by the lane changer or gap creation by the potential follower in the target lane. This acceleration is constrained by a minimum value for comfort and safety.

4.2.3 Extended LMRS for HOVs

The model extension focuses on modelling two lane change incentives of HOVs, being speed incentive and lane preference. The incentive for gaining speed on an adjacent HOV lane is captured by the original LMRS. For HOVs travelling on GP lanes that are further away from the HOV lanes, speed incentives are indirectly captured by accumulated adjacent speed gain in each lane change process. In this way, the lane speeds during intermediate lane change process in multiple highways can be taken into consideration. Drivers' preferences on HOV lane are formulated as a particular direction bias of lane changes, i.e. to-left or to-right. Since in LMRS vehicles only consider the lane change desire to directly adjacent lanes, a specific preference for HOV lanes could result in a desire to change multiple lanes until HOVs have arrived at the HOV lanes.

Based on the aforementioned discussions, a direction bias toward HOV lane (denoted as d^{ij}_{HOV}) is proposed in the LMRS framework. Similar to the keep-right bias in the default model, this direction bias is modelled as a discretionary incentive, weighted by a factor $\theta^{ij}_{voluntary}$ relative to the route incentive in equation (4.2). Since here we particularly aim to model the HOV lanes implemented in the USA where keep-right do not apply, the bias for keeping right is thus removed. The extended LMRS model for HOVs is formulated as equation (4.3).

$$d^{ij} = \begin{cases} d^{ij}_{route} + \theta^{ij}_{voluntary} \cdot d^{ij}_{speed} & \text{no HOV lanes in the direction of lane } j \\ d^{ij}_{route} + \theta^{ij}_{voluntary} \cdot \left(d^{ij}_{speed} + d^{ij}_{HOV} \right) & \text{HOV lanes exist in the direction of lane } j \end{cases} \tag{4.3}$$

The value of HOV bias determines the strength of lane preferences, leading to diverse demanding lane change desires within different lane change categories. Table 4.1 lists the range of the HOV bias with corresponding lane change behaviour.

Table 4.1 HOV bias ranges with corresponding lane change behaviour

HOV bias Range	HOV lane change behaviour
0 - d_{free}	A lane change towards HOV lanes when the current lane is congested and speed incentive is sufficiently high.
d_{free} - d_{sync}	A lane change toward HOV lanes when the gaps are available.
d_{sync} - d_{coop}	HOVs actively synchronize their speeds in order to change lane to the side of HOV lanes.
d_{coop} - 1	HOVs do cooperative lane changes toward the side of HOV lanes.

The discretionary lane change desire of HOVs is calculated by both speed incentive and HOV bias. HOV bias is positive, i.e. HOVs drivers always have a preference for HOV lanes, while the calculated speed incentive can be negative. Therefore, the preference towards HOV lanes can be compensated by a negative speed incentive. This is plausible as the HOV drivers are less likely to use HOV lanes if the HOV lane speed is lower than that on their current lane. If a severe speed reduction is encountered on HOV lanes, the HOV drivers aware of the performances of adjacent GP lanes are expected to change to the GP lanes. To this end, we suggest that the HOV bias should not exceed the threshold d_{sync} to generate a reasonable level of lane change desires toward HOV lanes and a responsive behaviour to the speed gain in adjacent GP lanes. Importantly, this vehicle behaviour is essential to model the lane changes in HOV lanes with continuous access and egress and reproduce the friction effect of HOV lanes. Overall, by adding a simple direction bias, the incentives for HOV lanes can be simulated and modelled, avoiding complex computation and calibration of utility functions in discrete choice models.

4.2.4 Extended LMRS for SOVs

The presence and operation of HOV lanes may influence the behaviour of single-occupant vehicle (SOV) drivers as well. Dynamic operation of HOV lanes may lead to a transition phase in which some SOVs are still in HOV lanes after the HOV lanes have just been activated. Those SOV drivers are obliged to leave the HOV lanes but they may not find sufficient gaps in the adjacent GP lanes at the beginning and thus may gradually leave the HOV lanes when acceptable gaps are found. The behaviour of egressing the HOV lanes is similar to the other lane change behaviour, but may exhibit more aggressiveness due to the high lane change desire. These actions correspond to the synchronized and cooperative lane change behaviours and they can be modelled by adding a direction bias d^{ij}_b toward GP lanes. Once the SOVs have left the HOV lanes, the desire toward HOV lanes is infinitely negative, indicating that they will not change back to HOV lanes. Equation (4.4) gives the formula of lane change desire for SOVs. Unlike other simulation models which instantly set the HOV lanes inaccessible for SOVs and result in mandatory lane changes, our model produces sequential lane changes over the transition period that are closer to the reality.

$$d^{ij} = \begin{cases} d^{ij}_{route} + \theta^{ij}_{voluntary} \cdot \left(d^{ij}_{speed} + d^{ij}_{b} \right) & \text{lane } i \text{ is an activated HOV lane, lane } j \text{ is a GP lane} \\ \text{-}Inf & \text{lane } j \text{ is a activated HOV lane} \\ d^{ij}_{route} + \theta^{ij}_{voluntary} \cdot d^{ij}_{speed} & \text{others} \end{cases} \quad (4.4)$$

4.2.5 Model adaptions for traffic in the U.S.

The traffic in the U.S. is different from EU continental (in particular Dutch) traffic, in the aspects of traffic regulations, driving behaviour and traffic flow characteristics. To better mimic the vehicle behaviours in the U.S. where the majority of HOV lanes were implemented, additional improvements on lane change model for trucks and SOVs have been done.

The keep right bias in the default LMRS model is removed since it is not regulated in the U.S. traffic. As a result, vehicles will not intend to change to the right as much as possible and vehicles are more evenly distributed over the lanes. Besides, trucks mostly travel on the two lanes from the right-side. Thus a lane bias available for trucks is used in the simulation, keeping trucks within those two lanes. It is denoted as d_{truck} and specified in equation (4.5) when two

conditions are met: the current lane is not the rightmost two lanes and a to-right lane change desire is calculated.

$$d^{ij} = d^{ij}_{route} + \theta^{ij}_{voluntary} \cdot \left(d^{ij}_{speed} + d_{truck} \right) \tag{4.5}$$

We suggest a value equals to d_{free} to the truck bias in order to encourage a free-flow lane change behaviour.

Moreover, two more advanced direction biases are applied for SOVs in order to replicate the specific lane flow distribution on the studied corridor. Comparison of simulation with detector data showed too low flows and speeds on the second lane from the left and those discrepancies become larger at merging sections. The first bias encourages low desire-speed vehicles to leave the second lane heading to the right-side and the second bias encourages high desire-speed vehicles to move to the second lane only at the upstream of merge sections. They are performed in equation (4.1) as $d^{ij}{}_b$ when their conditions are satisfied. The first bias is applied to a to-right lane change desire when the vehicle is in the second lane. The second bias works on a to-left lane change desire when the vehicle is travelling in the right-side of the second lane, when a downstream merge section is within 800 meters. These two biases were calibrated by a set of SR99 traffic data without HOV lane operations and a value of 0.25 is recommended for both of them. After calibration, low desired-speed vehicles are determined if a ratio– vehicle desired speed over speed limit – is lower than 0.79, while the ratio for high desired-speed vehicles should be over 0.91.

4.3 Performance and calibration

In order to calibrate and validate the developed model, a simulation study on a network including HOV lanes is conducted. The network configuration, source data and general traffic performances are introduced firstly, followed by the methodologies used in calibration and the calibration results. After that, the friction effect of HOV lanes is examined in the simulation and the face validity of simulated vehicle behaviour is inspected.

4.3.1 Case study network

The SR99 corridor to the south of Sacramento, California, is selected as the studied network. The network starts from the on-ramp of Elk Grove to the off-ramp toward SR50, with 20 km in length, 16 on-ramps and 12 off-ramps. The considered time period is from 4:00 AM to 12:00 PM. Loop detector data in this corridor were obtained from the Caltrans Performance Measurement System (PeMS), which provides 5-mins flow and speed data for each lane on the mainline of the corridor. We chose the data of October 6, 2015 - a typical weekday without incident reports during the selected time period. Unreliable data violating the principle of vehicle conservation were removed, resulting in 16 reliable groups of mainline detectors for demand imputation and calibration.

The SR99 Corridor has a median exclusive HOV lane with continuous access and egress operating only from 6:00 AM to10:00 AM. Data from both free-flow and congested-flow can be obtained due to recurrent congestion, providing sufficient data for model calibration. The empirical data reveal a complex congestion pattern with interacting bottlenecks in the morning peak. Propagation and recovery of the congestion can also be recognized.

4.3.2 Calibration approach

The aim of our calibration is to achieve a simulated congestion pattern which represents the key characteristics of the congestion from empirical data, while lane-level errors of flows and speeds are within an acceptable range. We consider three key features of a congestion pattern: (I) the time and location of the start of each congestion, (II) the time and section where the congestion propagates to, and (III) the time when the traffic recovers from congestion. To quantify the performance of the proposed model, the Mean-Absolute-Percentage-Errors (MAPEs) of flow and speed are selected as measures. MAPE is formulated as equation (4.6).

$$MAPE = \frac{1}{N \cdot T} \sum_{n=1}^{N} \sum_{t=1}^{T} \frac{M_{n,t}^{real} - M_{n,t}^{sim}}{M_{n,t}^{real}} \tag{4.6}$$

where N is the detector number and T is the number of data time interval. $M_{n,t}^{real}$ and $M_{n,t}^{sim}$ are the data of detector n at time t from ground-truth data and simulation data respectively.

Before the model calibration, we first estimated the OD matrix based on the traffic counts at the network boundaries. For computation efficiency, the routes were estimated for every 30 mins – a time interval allowing a stable traffic status whilst avoiding large fluctuating traffic counts caused by congestions. Within each 30 mins, each generated vehicle was assigned to a downstream destination by a probability. The probability of reaching a certain destination is calculated as the split ratio at each off-ramp which is the off-ramp flow over upstream mainline flow. This method provides flow consistency at network destinations. In the next step, the traffic composition is estimated. There are three types of vehicles in simulation: HOVs, SOVs and trucks. The percentage of trucks in total traffic is assumed to be 3.82%, an average of detected truck flow over total mainline flow by Caltrans Performance Measurement System. On the most upstream mainline section, the HOV lane generator only produces HOVs when HOV lanes are activated, while 10% of the traffic from vehicle generators on GP lanes are assumed to be HOVs and the rest are SOVs and trucks. This assumption is based on a largely increased HOV lane flow and slightly reduced GP lane flow at nearby downstream detectors. For on-ramps with an HOV bypass lane, the percentage of HOVs is assumed to be 10 % higher than the detected value during the uncongested period under the assumption that a number of HOVs do not use the HOV bypass lanes at the on-ramp when there is no congestion. For on-ramps without HOV bypass lanes, we assume that 19% of the traffic is HOVs based on the average ratio of HOV flows on the main freeway.

Model calibration is an optimization process for a minimal difference between simulated and observed data, by tuning the parameters of the LMRS and IDM+ model. The objective function used for searching the optimized parameter set is formulated by Schakel et al. (2012). It combines the Root-Mean-Square-Error (RMSE) of flow and speed together with different weights and the formula is shown in equation (4.7). RMSE is chosen as the indicator for optimization for its large deviation range of value and it is more sensitive to the measure variations.

$$\varepsilon = \sqrt{\frac{\sum_{n=1}^{N} \sum_{t=1}^{T} (12 \cdot (q_{n,t}^{real} - q_{n,t}^{sim}))^2}{N \cdot H}} + 25 \cdot \sqrt{\frac{\sum_{n=1}^{N} \sum_{t=1}^{T} (v_{n,t}^{real} - v_{n,t}^{sim})^2}{N \cdot H}} + m \tag{4.7}$$

where m is the number of deleted vehicles in the simulation. The coefficient of squared flow error is 12 and it is different from the value in Schakel et al (2012), due to a different time interval of source data.

The parameter optimization started from the free-flow scenario where parameters corresponding to free driving behaviour are determined, see Schakel et al (2012) for the list of calibrated parameters. For each parameter set, we ran the simulation five times with different random seeds. The set of parameters with the minimum values of the objective function was selected as the calibrated parameters for free flow conditions. Next, the parameters were calibrated in a scenario with congested conditions. Following the procedures in the previous stage, a sensitivity analysis of the results with varying parameters helped us to narrow down the range of each parameter. Then we checked the congestion pattern before the quantitative analysis of errors and searched the parameter values by congestion pattern with acceptable errors. A repetition of simulation runs with five different random seeds is also used in this scenario.

4.3.3 Calibration results

The calibration resulted in a representative congestion pattern, with MAPE of section-based flow and speed reaching 7.93% and 19.21% respectively, which were considered as reasonable results for calibration. The calibrated parameters are shown in Table 4.2.

Table 4.2 Calibrated parameters of the SR99 corridor.

Parameter/Symbol	Original values	Calibrated values
Sensitivity to speed gain / v_{gain}	69.6 km/h	54 km/h
Free lane change criteria/ d_{free}	0.365	0.25
Synchronized lane change criteria/ d_{sync}	0.577	0.5
Cooperative lane change criteria/ d_{coop}	0.788	0.75
Average minimum headway/T_{min}	0.56 s	0.52 s
Average maximum headway/T_{max}	1.2 s	1.4 s
Lane change desire per lane/ t_0	43 s	52 s
Averaged free-flow speed/ $V_{des,car}$	123.7 km/h	125 km/h
σ_{car}	12 km/h	8.75 km/h
HOV bias/ d_{HOV}	-	0.45
SOV bias/ d_b	-	0.5
Low desire-speed bias	-	0.25
Local high desire-speed bias	-	0.25

As we can see from Table 4.2, differences can be found in parameter values between the calibrated results and default values. A smaller speed gain in our results implies that simulated U.S. vehicle drivers are more sensitive to the speed change from target lane and a low value of d_{free} suggests that drivers are more likely to change lanes compared to the Dutch traffic. Changes of T_{min} and T_{max} indicates a less centralized distribution of vehicle headway in the simulated corridor and an increased *t0* means that vehicle drivers start the exiting preparations at an early time when they are heading to the off-ramps. A larger value of d_{HOV} than d_{free} implies that HOVs intentionally change lanes in the direction of HOV lanes when there is a gap available. The difference between d_{HOV} and d_{sync} is 0.05, suggesting that a speed gain of 2.7 m/s (calculated by v_{gain}) in the adjacent lane can stimulate a more aggressive synchronized lane change.

The calibrated model represents several key features of the observed traffic flow phenomena of the corridor. Firstly, congestion patterns (via the speed contour in spatio-temporal dimension) from simulation and field data are compared for the general traffic performance at the corridor level. For a detailed and complete congestion pattern, eight more mainline detector groups are included for their reliable speed data. As it is illustrated in Figure 4.2, the simulated congestion appears at around 6:30 AM at two bottlenecks: Florin Road Ramps and Shelden Road Ramps, in line with the observations from field data. Congestion at both bottlenecks spilled back to upstream sections and they last for a period until the traffic demand started to decrease after 8:50 AM. The speed reductions at each bottleneck have been effectively reproduced and the spatio-temporal congestion dynamics have been qualitatively reproduced, proving the model validity at the network level.

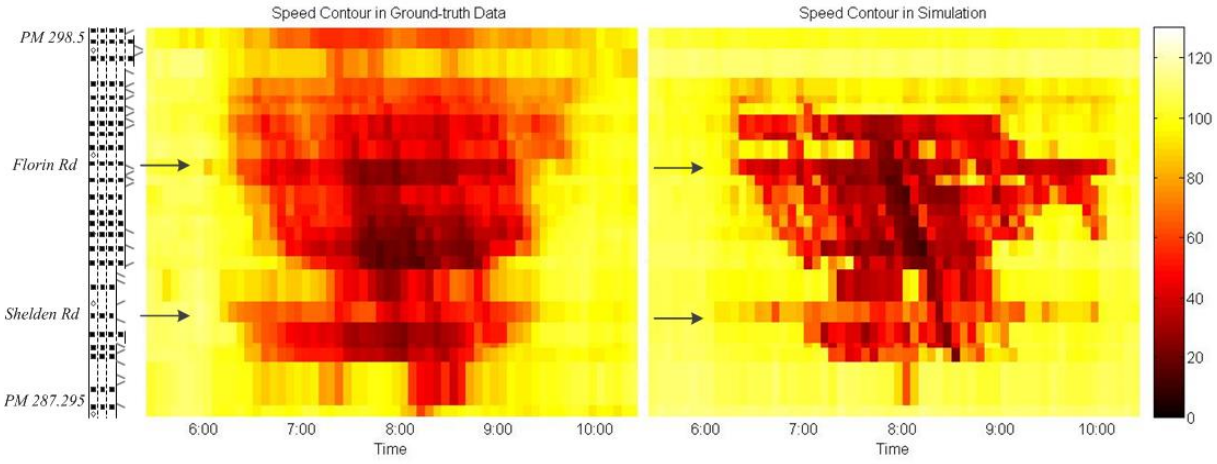

(*a*) (*b*)

Figure 4.2 (*a*) Detected congestion pattern and (b) simulated congestion pattern.

Fundamental diagrams and lane flow distributions of a road bottleneck and homogeneous highway section are plotted to gain insights into the performance of the model at the section level. The detectors located at a weaving section near Florin Road Ramps (the primary bottleneck in this corridor), and their adjacent upstream detectors are analysed and presented in Figure 4.3. From the fundamental diagrams, the simulation data are consistently in line with ground-truth data in the free flow branch. In the congested branch, the range of scattered data is also coincident with field data. This shows the general flow-speed relations are in accordance with the empirics at both bottlenecks and sections.

Plots of lane flow distribution show the flow relocation within lanes with the change of section density. Especially before the critical density, lane flow distribution is an important indicator suggesting the drivers' lane preferences. From the distributions of the bottleneck and section in Figure 4.3, it is found that the proposed lane preference biases (both bias for HOVs and SOVs) can reproduce the similar trends of each lane flow share. Particularly the flow share of the HOV lane increases significantly from free flow density to congested density range. The goodness of fit between simulated data and real data suggests that our simulation is capable of modelling the traffic with HOV lanes at the section and lane levels.

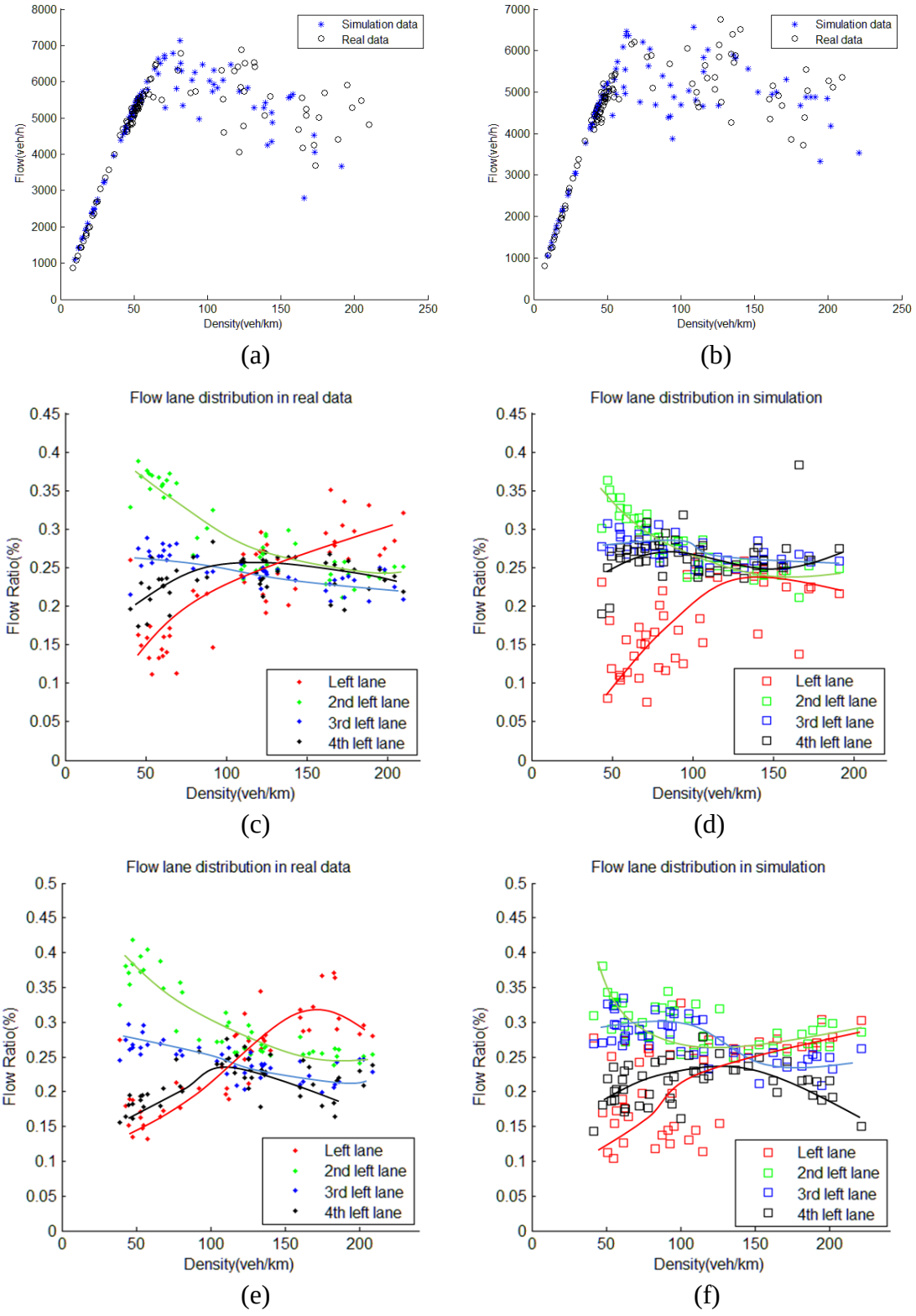

Figure 4.3 Fundamental diagrams of (a) a road section and (b) a bottleneck; lane flow distributions at road section from (c) real data and (d) simulation, and lane flow distributions at road bottleneck from (e) real data and (f) simulation.

4.3.3.1 Friction effects

To verify that our model can reproduce the "friction effect" of HOV lanes, we compare lane-specific speed between the HOV lane and the adjacent GP lane. Figure 4.4 shows the speed contour plots of the two lanes separately. The speed reductions on HOV lanes can be easily found corresponding to the congestion appeared in the adjacent GP lane, especially at the bottleneck of Florin Road. The friction effects at bottleneck Shelden Road are not apparent due to the insufficient HOV demand.

Three hypothetical causes for the friction effect can be explained as (a) intrinsically slow HOVs block the lane, (b) lane changing manoeuvers between HOV and GP lanes disrupt the flow on the HOV lane, and (c) HOVs slow down because of the perceived risk from the high speed difference between the HOV and GP lanes (Chen et al., 2005; Guin et al., 2008; Jang et al., 2012; Menendez, 2006). In our simulation, we observe a speed reduction on HOV lanes caused by the second hypothesis. When the GP lanes are congested and the HOV lane is in free flow, HOVs on the GP lanes have high desires to move to the HOV lane in a cooperative way. This increases the lane changes as well as the disturbance to the HOV lane and leads to inevitable speed reductions. At the same time, due to the negative speed incentive on the adjacent GP lane, HOVs on the dedicated lane are reluctant to leave the HOV lane until the distances to their exits are too short and the mandatory lane change incentive is large enough to outperform the discretionary incentives. This results in a strong lane change desire for HOVs corresponding to synchronized and cooperative lane changes where HOVs slow down to synchronize the low speed of GP lanes. For a single HOV lane, this contributes to the speed reduction substantially.

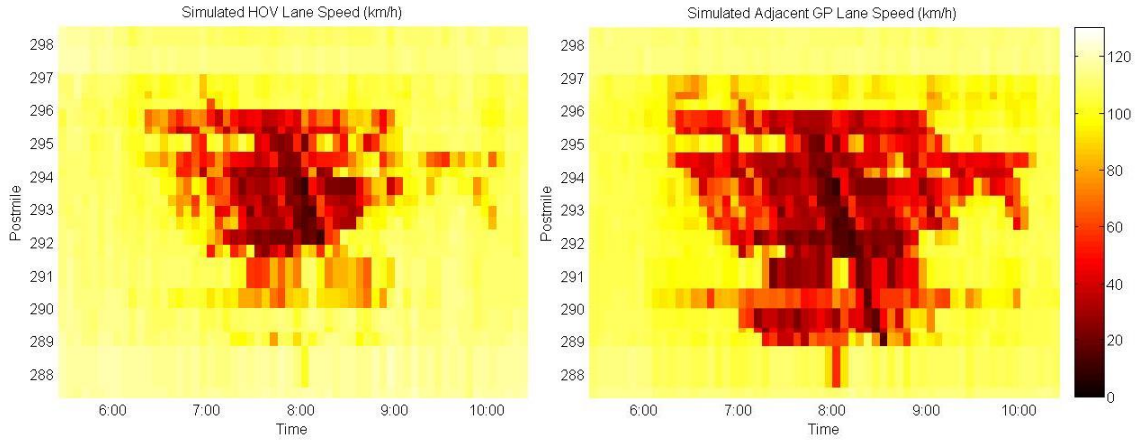

(a) (b)

Figure 4.4 Friction effects of HOV lane in simulation: (a) speed contour of HOV lane and (b) adjacent GP lane.

4.3.3.2 Face validity of lane change behaviour

We verify the extended LMRS model by observing the vehicle behaviour during the simulation. With the proposed simulation model, a number of reasonable and realistic vehicle behaviours are identified.

- SOVs travelling in the HOV lane gradually leave the HOV lane within five minutes after the HOV lanes are activated at 6:00 AM.
- In free flow conditions where the speed incentives are not substantial, the lane change behaviour of HOVs is dominated by HOV bias. The bias is below d_{free} which leads to low possibilities of lane changes and HOVs remain in their current (GP) lanes without heading directly to HOV lanes.

- When a speed reduction of the current GP lane is observed, free lane changes and synchronized lane changes are triggered. HOVs start to change lane to HOV lanes.
- When HOVs approach a bottleneck where GP lanes are congested and the HOV lane is uncongested, the speed incentive to left increase across lanes from right to left. HOVs gradually change to HOV lane due to the co-existence of speed incentive and HOV bias. The higher the speed difference is, the more cooperative and aggressive the lane changes are.
- For the conditions that HOVs face congestion in all lanes of a downstream section, HOVs in the GP lanes do not change lane frequently because of the ineffective speed incentives.

Based on the face validation, the model is considered capable of representing the driving behaviours on the freeway with HOV lanes.

4.4 Conclusions and future work

In this paper, we have proposed a new model to represent freeway traffic with continuously accessible HOV lanes. In the presence of HOV lanes, drivers of both HOVs and SOVs may adapt their behaviours according to their own benefits. Speed incentives and lane preference are found as two main attributes attracting HOV drivers to use HOV lanes. To take both of them into account, the proposed model, developed from an incentive-based LMRS model, models the speed incentives by default and replaces the lane preference by an invariant direction bias as discretionary desires. By applying a similar direction bias, the model is also proven to be capable of simulating mandatory lane changes of SOVs when they leave activated HOV lanes.

The proposed model shows validity in reproducing traffic flow characteristics in a complex network with HOV lanes and interacting bottlenecks. The model was verified by face-validation on vehicle behaviours and calibrated by loop detector data from the SR99 corridor in California. The reproduced congestion pattern at the corridor level, fundamental diagrams at the section level and lane flow distributions are in accordance with empirics. Furthermore, our model reproduces the friction effects and provides new insights into this phenomenon. Our model supports the hypothesis that the lane changes between HOV and GP lanes lead to a significant speed reduction of HOV lanes. The proposed model can be used by highway agencies as a tool to assess different HOV lane designs and operation strategies.

In future work, we plan to compare our simulation results with the HOV lane modelling study of Lu et al. (2017), in order to provide a comparable model performance. Verification of the lane change model by vehicle trajectory data and model extensions to capture the lane restriction violations and the conversion of HOV lanes to HOT lanes are also interesting topics. Meanwhile, the model provides the possibility for further extension of dedicated lane operation for certain vehicle types, such as Cooperative Adaptive Cruise Control (CACC) vehicle strings. Therefore, the integrated design of CACC string strategies and dedicated lane operations can also be a future research topic.

5 Traffic flow impacts of converting an HOV lane into a dedicated CACC lane

Based on the car-following model proposed in chapter 2 and the lane change model developed in Chapter 4, we conduct simulations to investigate the traffic flow impacts of mixed CACC traffic using dedicated lane strategies. This chapter focuses on the changes in traffic congestion that stem from increasing CACC vehicle market penetration rates (MPRs), revealing the combined influence of CACC MPRs and a CACC lane on traffic flows. Via comparison with the California reference case, this simulation reveals the conditions in which to convert an HOV lane to a CACC lane, as a reaction to increasing CACC vehicles in mixed traffic. Section 5.1 reviews the impact analysis of a CACC-dedicated lane on traffic flow operations. Section 5.2 briefly presents the car-following model and lane change model for CACC vehicles, as well as the extended driver-system authority transitions and the assumptions for CACC string operation. In section 5.3, an experiment for CACC impact assessment in the SR-99 corridor in California is designed and set up. After that, the simulation results are shown in section 5.4, highlighting congestion patterns, along with the flow operation, travel time reliability and clustering effects of CACC lanes. Section 5.5 draws the conclusions and suggests directions for future work.

This chapter is an edited version of the following paper:

Xiao, L., M. Wang and B. Van Arem. (2020). Traffic flow impacts of converting an HOV lane into a dedicated CACC lane on a freeway corridor. *IEEE Intelligent Transportation Systems Magazine, vol 12(1), pp. 60 -73*.

Abstract—Cooperative Adaptive Cruise Control (CACC) systems can increase roadway capacity, but the benefits are marginal at low market penetration rates (MPRs). Thus, a CACC dedicated lane is considered to group CACC vehicles for efficient traffic stream. Concepts of converting existing High Occupancy Vehicle (HOV) lanes into CACC lanes emerge, which leverages the infrastructural facilities and experience with HOV lanes. However, it is unclear to which extent changing HOV lanes to CACC lanes can influence freeway operations. This study examines the traffic flow impacts of converting HOV lanes into CACC lanes regarding CACC MPRs on a complex freeway corridor with multiple interacting bottlenecks in California. A simulation model capable of reproducing flow characteristics with HOV lane and CACC systems is employed for the assessment. Special attention is paid to macroscopic congestion patterns, CACC lane utilization, travel time reliability and CACC operation characteristics. The results show that converting to CACC lanes at low MPRs (<30%) can exacerbate congestion in general purpose lanes, whereas at intermediate CACC MPRs (40%–50%) the congestion is drastically alleviated due to a large share of traffic carried by CACC lanes.

5.1 Introduction

Automated vehicles (AV) may bring fundamental changes to the traffic flow characteristics and congestion problems we are facing today (Hoogendoorn et al., 2014). In recent years, Cooperative Adaptive Cruise Control (CACC) systems that enable an equipped vehicle to maintain a small time gap to its predecessor automatically with Vehicle-Vehicle (V2V) communication, develop in a fast way that it have attracted considerable attention (Shladover et al., 2015).

In the presence of CACC vehicles, traffic flow features will change since the vehicle behaviour under CACC is different from that under human driver control. The impact of CACC vehicles needs to be carefully investigated before they are deployed widely in real traffic. There has been a variety of studies taking efforts to investigate the impacts of CACC vehicles on roadway capacity. Several studies (Hall & Li, 1999; Kanaris et al., 1997; Michael et al., 1998; Swaroop et al., 1994) used analytical approaches to conclude that the capacity increase can be considerable by the reduced time gaps between two vehicles. A group of studies based on macroscopic simulations, where the traffic dynamics are taken into account, show that CACC vehicles not only increase the dynamic equilibrium capacity but also the flow stability (Delis et al., 2016; Ngoduy, 2013). Another group of studies assess the impacts of CACC vehicles via microscopic traffic simulations, in which the individual dynamic behaviour of CACC vehicles can be explicitly modelled. The effects in increasing capacity/throughput of CACC vehicles were confirmed (Arnaout & Arnaout, 2014; Hartmann et al., 2017; Makridis et al., 2017; Shladover et al., 2012; Talebpour & Mahmassani, 2016; van Arem et al., 2006; VanderWerf et al., 2002; Zhao & Sun, 2013) and a quadratic relationship is found between roadway capacity and CACC market penetration rates (MPRs) (Shladover et al., 2012; VanderWerf et al., 2002). The capacity increase at high CACC MPRs is significant; however, the increase in capacity at low CACC MPRs is marginal (Arnaout & Arnaout, 2014; van Arem et al., 2006) due to the low probability of forming CACC strings in an ad-hoc way (Xiao et al., 2018) or even negative if a conservative time gap is in use (Hartmann et al., 2017). In this regard, a dedicated lane for CACC vehicles has been proposed as one of the solutions to facilitate the clustering of CACC vehicles and enhance the CACC string operation.

Existing studies regarding a special lane for CACC vehicles can be categorized into two groups. The studies in the first group assume an exclusive CACC lane allowing only CACC vehicles to travel in that lane. The simulation study of (van Arem et al., 2006) showed that a CACC lane

contributes to higher throughput and speed at a lane-drop bottleneck when the MPR of CACC vehicles is more than 40%. Focusing on a merging bottleneck, the simulation in Talebpour et al. (2017) showed that a dedicated lane for autonomous vehicles (using CACC algorithms) mitigated congestion and reduced scatters in the fundamental diagram when MPR is above 30%. Another recent simulation study (Liu et al., 2018b) demonstrated that both the pipeline capacity and merging capacity increase by deploying a CACC lane at 40% and 60% CACC MPRs. These three studies pointed out that the effectiveness of CACC lanes is highly related to the CACC market penetration rate, being consistent with the findings of an analytical study regarding the deployment of an AV lane (Chen et al., 2016). However, van Arem et al. (2006) focused on a single lane-drop bottleneck without on/off ramps, where the impacts of CACC vehicles' lane changes in preparation for entering CACC lanes and exiting highway are neglected; and the simulations of the hypothetical merging segments and the real multi-ramp network in Talebpour et al. (2017) and Liu et al. (2018b) do not provide a realistic and reliable estimation of CACC vehicle impacts in a traffic corridor level. The simulated real network in Talebpour et al. (2017) is too short (less than 6 km) to fairly show the CACC benefits for a multi-ramp corridor because the actual travelling distance by CACC in dedicated lanes might not be sufficient to reveal substantial benefits. The simulation of the SR99 corridor in Liu et al. (2018b) only investigated the impacts of CACC vehicles with a combined strategy of a CACC lane and connected vehicles at the 20% CACC level. The impacts of only deploying CACC lanes at other CACC MPRs are not specified.

Instead of assuming exclusive CACC lanes, the second group of studies assume CACC vehicles can access existing dedicated lanes, e.g. high occupancy vehicle (HOV) lanes. In Arnaout and Bowling (2015), 20% of overall traffic with CACC vehicles were assigned in the HOV lane in addition to 10% of overall traffic with HOVs. This results in a higher throughput but a lower average speed at high traffic demands, compared to the cases of 0% CACC and 20% CACC vehicles travelling across all the lanes without a dedicated lane. In Qom et al. (2016) a tolling discount for CACC vehicles travelling in a tolling HOV lane is assumed in the lane choice model during dynamic traffic assignment. It is concluded that opening the HOV lane for CACC vehicles is not beneficial for increasing the use of HOV lanes and bottleneck speeds at 20% CACC MPRs, but it is beneficial at 60%-100% CACC MPRs. In both studies, no lane change activity was taken into account for CACC vehicles so the concluded impacts are more related to the steady state operations of barrier-separated HOV lanes.

Beyond the categorization, a study (Chen et al., 2017) discussed the optimal lane deployments in terms of roadway capacity in equilibrium states, from the aspects of mixed-use or separated-use lanes for regular vehicles and AVs. At low MPRs, the optimum capacity is achieved when all lanes are mixed-used lanes and all AVs are allocated only in one of them; at high MPRs, the optimum lane deployment will be a combination of a separated-used lane for AVs and mixed-used lanes for regular vehicles. However, from the aspect of CACC vehicle strings operation, the presence of regular vehicles can easily cause string separations and CACC degradations to ACC. Thus a mixed-used lane is not ideal to cluster CACC vehicles for string operation. In this study, we focus on the exclusive lane for CACC vehicles, termed CACC lanes.

Overall, the literature pointed out that the traffic impacts of a CACC lane are complex, and correlate with traffic demand and CACC MPRs. Although the literature has shown that a CACC lane can increase throughput/capacity and alleviate congestion at either a lane-drop or a merging bottleneck, those benefits are generally overestimated when it is discussed at a realistic corridor due to the negative influence by the additional lane changes of CACC vehicles from on/off ramps. The combined effects of a CACC lane and CACC MPRs at a corridor with multiple interacting bottlenecks have not been addressed, and the question of how to deploy CACC dedicated lanes is still challenging to road operators, especially whether it is beneficial

to leverage existing HOV lanes to encourage early deployment of CACC. In this regard, this research investigates the traffic impacts of converting an HOV lane into a CACC lane and reveals the effects of a CACC lane at different CACC MPRs on congestion pattern, travel time reliability and CACC system operation at a highway corridor. We select a realistic traffic corridor with an HOV lane as the reference case and identify at which CACC MPRs it is beneficial to convert an HOV lane to a CACC lane. The main contribution of this study is to offer new insights into the impacts of a CACC lane at various CACC MPRs at a corridor level with interacting bottlenecks as distinguished from a single bottleneck (Liu et al., 2018b; Talebpour et al., 2017; van Arem et al., 2006; Xiao et al., 2018). The simulated network is sufficient in length to show the benefits of CACC operation in long-distance trips and the network complexity of various merging, diverging, and weaving sections is able to generate realistic traffic disturbances and the nonlinear traffic flow phenomena. In addition, the simulation model captures the CACC operational characteristics and driver-automation interaction. Thus, the trade-off between the positive effect of the CACC lane in clustering CACC vehicles and the negative effect of inducing more lane changes and more CACC deactivations can be evaluated.

The paper is structured as follows. Section 2 introduces the car-following model for CACC vehicles and conventional vehicles in our simulation and the lane change model particularly applied to the continuous-access dedicated lane scenario. Section 3 elaborates the simulation experiment design and set-up to explore the impacts of CACC MPRs in a scenario with a CACC dedicated lane. After that, simulation results are presented and discussed in the fourth section, followed by the conclusion and future work in Section 5.

5.2 Car-following and lane change models for microscopic simulations

This section summarizes the vehicle behavioural models proposed in our previous studies (Xiao et al., 2016; Xiao et al., 2017) for CACC vehicles and manually driven vehicles in microscopic simulations. A framework for integrated lane change and car-following model is presented, followed by brief descriptions of CACC and manually driving car-following model, as well as the lane change model for dedicated lane scenarios.

5.2.1 Framework for integrated lane change and car-following model

Figure 5.1 shows the framework of how the lane change model and car-following model are integrated with the hierarchical structure of driving tasks. The lane change model is placed at the tactical level, where drivers make the decisions for lane change and gap acceptance; the car-following model is located at the operational level, where acceleration models are executed. The outputs of the lane change model are used as the inputs of car-following models.

The possible outputs from the lane change model are three lane change intentions: stay in the lane, lane change preparation and change lane to left or right. The stay in the lane is the result of either no lane change desire shows up or the gap for a free lane change is rejected. The decision of change lane to left or right is made when lane change desire is larger than a minimum value and the gap is acceptable. The lane change preparation occurs only when a lane change decision has been made with large desires but the current gap is unacceptable. The vehicle has to adjust its car-following behaviour or request cooperation from other vehicles to conduct the lane change.

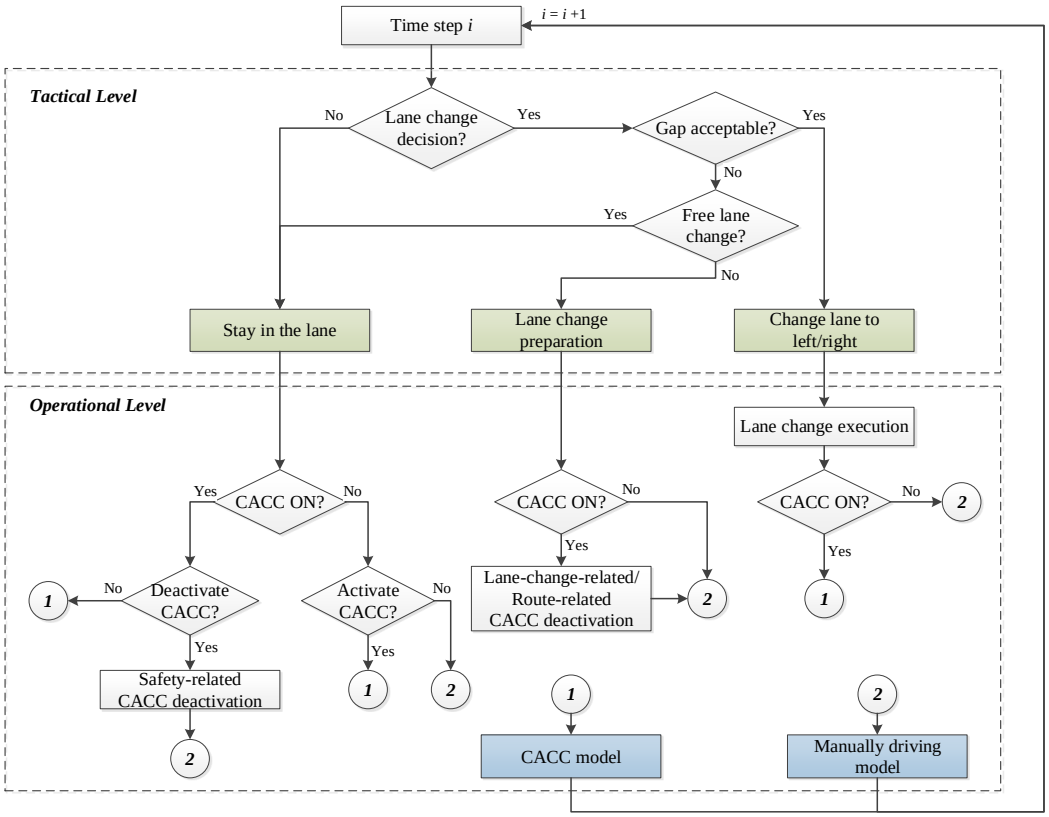

Figure 5.1 Framework for the integrated lane change and car-following model.

The three different lane change intentions determine different paths to choose between the CACC and the manually driving car-following models at the operational level. Following the intention of stay in the lane, CACC vehicles can be activated or deactivated by the driver. In the lane change preparation, CACC will be deactivated and the manually driving model will be the only option because the preparation behaviour is only assumed to be conducted by human drivers. During the lane change execution, no switch between CACC and manual driving is allowed. Therefore, the dominating car-following model remains as it is. After the execution of car-following models, the time moves to the next time step. This set of the hierarchically integrated lane change and car-following models represent the driving behaviour of a CACC vehicle in both lateral and longitudinal response.

5.2.2 Car-following models under CACC

5.2.2.1 Car-following models in three operation modes

The ACC and CACC controllers consist of three modes for three different control objectives (Milanés & Shladover, 2014; Milanés & Shladover, 2015; Milanés et al., 2014). The cruising mode is designed to maintain a user-set desired speed if a preceding vehicle is out of detection range or faster than the subject vehicle's desired speed; the gap-regulating mode works for the car-following situation and aims to maintain a constant time gap with its predecessor. The gap-closing mode performs a transition from the cruising controller to the gap-regulating controller when an ACC/CACC approaches its leader from a long range.

Each mode has its own car-following model as formulated in Table 5.1. The ACC and CACC systems share the same model for the cruising mode since the V2V communication does not

play a role when the vehicle is only targeting the desired speed. The gap-regulating mode and gap-closing mode also have the same model structure, whereas the control gains in different modes vary. For a detailed specification of the models, we refer to (Xiao et al., 2017).

The desired speed and desired following time gap are the model inputs. We assume the same desired speed under ACC/CACC as it is under the manually driving, and the desired time gap follows a realistic distribution of time gap setting collected from a field test (Nowakowski et al., 2011). The maximum CACC string length is 10 vehicles and the minimum desired time gap between two strings (inter-string gap) is assumed to be 1.5 seconds (Liu et al., 2018a).

Table 5.1 Model specifications for three operation modes under ACC and CACC

Driving modes	Model specifications
ACC Cruising	$a_{i,k} = 0.4 \cdot (v_{des} - v_{i,k-1})$
ACC Gap-regulating	$a_{i,k} = 0.23 \cdot e_{i,k} + 0.07 \cdot (v_{i-1,k-1} - v_{i,k-1})$
ACC Gap-closing	$a_{i,k} = 0.04 \cdot e_{i,k} + 0.8 \cdot (v_{i-1,k-1} - v_{i,k-1})$
CACC Cruising	$a_{i,k} = 0.4 \cdot (v_{des} - v_{i,k-1})$
CACC Gap-regulating	$v_{i,k} = v_{i,k-1} + 0.45 \cdot e_{i,k-1} + 0.0125 \cdot \frac{d(e_{i,k-1})}{dk}$
CACC Gap-closing	$v_{i,k} = v_{i,k-1} + 0.005 \cdot e_{i,k-1} + 0.05 \cdot \frac{d(e_{i,k-1})}{dk}$
	$e_{i,k} = x_{i-1,k-1} - x_{i,k-1} - t_{des} \cdot v_{i,k-1} - d_0$

Note: i is the vehicle sequence; *k* is the simulation time step; *a*, *v and e* are the vehicle acceleration (m/s^2), speed (m/s) and gap error (m); v_{des} is the desired speed (m/s); t_{des} is the desired time gap (s) and d_0 is a dynamic spacing margin (m) proposed in (Xiao et al., 2017).

5.2.2.2 Automation system activation and deactivation

System activation and deactivation, as driver's interaction with the automation system, specify the switching logic between the CACC and manually driving car-following models. In this study, system activation is based on the assumption that drivers intend to use the ACC/CACC system as much as possible. Thus, the ACC/CACC will be switched on as long as the operational design domain allows. In two situations the ACC/CACC system will not be activated: the vehicle is braking over 2 m/s^2 and the vehicle is performing a lane change.

There are three types of system deactivation and there is a minimum time period of remaining deactivated to avoid frequent deactivation within a short time period. The first type of system deactivation is safety-related, including the system-initiated deactivation and the driver-initiated deactivation for avoiding rear-end collisions. From the system-initiated aspect, a collision warning based on inverse time-to-collision (Kiefer et al., 2005) is employed to identify safety-critical situations and inform the driver to take over vehicle control. The ACC/CACC system is allowed to be re-activated 5 seconds after the collision warning has terminated. In addition, drivers are also assumed to actively resume vehicle control in a high-relative-speed approach scenario, and re-activation is possible 10 seconds after the deactivation criterion is not satisfied. The second type of system deactivation is related to lane change behaviour, in particular when drivers need to synchronize their speeds for a lane change or create a gap in front to facilitate a vehicle to merge. Drivers override systems to conduct such lane change preparations and once the lane change is completed, CACC is reactivated in 2 seconds. This type of deactivation highly depends on the lane change desire, which will be explicitly explained in the following lane change model section. The last type of deactivation is related to

the route. It is assumed that when vehicles have to make mandatory lane changes to follow a particular route, drivers will resume control until the vehicle arrives the target lane to avoid the frequent switch between automation and human-driven system.

5.2.3 Car-following model under manual driving

The car-following model for human drivers is a modified version of the Intelligent Driver Model (Treiber et al., 2000), referred as IDM+ (Schakel et al., 2010). The IDM+ outputs the vehicle acceleration as the minimum of the acceleration of driving towards the desired speed and the acceleration towards the desired headway. It is formulated as

$$\dot{v} = a \cdot min(1 - (v/v_{des})^4, 1 - (s^*/s)^2) \tag{5.1}$$

and

$$s^* = s_0 + v \cdot T + v \cdot \Delta v/2\sqrt{a \cdot b} \tag{5.2}$$

where a, b are the maximum acceleration and comfortable deceleration in m/s^2, v_{des} is vehicle's desired speed in m/s, and s^* is the dynamic desired distance headway in the meter. T and s are the time gap in second and distance gap in meter, whereas the s_0 is the stopping distance and Δv is the approaching rate to a leader in m/s. The IDM+ is able to generate more reasonable capacity values compared to the IDM.

The time gap is relaxed between a minimum time gap T_{min} at a maximum lane change desire and an equilibrium following time gap T_{max} which is defined as a constant value during the entire simulation period. However, to simulate a long road network which has complex road configurations such as varying lane numbers and multiple types of bottlenecks, a constant T_{max} is not adequate to depict the characteristics of driving behaviour adapted to different road configurations. Thus, we introduce a location-based fraction of T_{max} for better reproduction of traffic flows, e.g. roadway capacity, and the fractions are to be calibrated in each case study.

5.2.4 Lane change model for dedicated lane operation

The lane change model, for both CACC and manually driven vehicles, is based on the Lane Change Model with Relaxation and Synchronization (LMRS) in (Schakel et al., 2012). In order to model the adapted vehicle behaviour with the presence of dedicated lanes, we extended this model for eligible users and ineligible users in terms of the accessibility to dedicated lanes.

5.2.4.1 Basic LMRS

In the LMRS, the lane change behaviour is predicted by a decision model that calculates the lane change desire to decide whether to change lane and what type of lane change is needed. This is followed by a gap acceptance model to determine if the available gap is acceptable at the current desire level. The lane change desire consists of multiple lane change incentives for following the routes, gaining speeds and directional bias representing traffic rules. The route incentive is a mandatory lane change incentive, which arises if the current lane will not allow a vehicle to follow its route. It is determined either by the remaining distance or by the remaining anticipated travel time to the target lane that can continue to follow the route. A driver's desire to change lane for higher anticipated speed is defined as the speed incentive. It is expressed as a function of the anticipated speed gain from the target lane. The directional bias is applied in accordance with the keep-right traffic rule, which is implemented as a constant bias to the right lane. The speed incentive and directional bias are discretionary lane change incentives, which

are only partially included when the route incentive appears. The model is generally formulated as

$$d^{ij} = d_r^{ij} + \theta^{ij} \cdot \left(d_s^{ij} + d_b^{ij}\right) \tag{5.3}$$

where d^{ij} is the overall lane change desire from lane i to lane j. d_r^{ij}, d_s^{ij} and d_b^{ij} represent the incentives for the route, speed and a directional bias respectively, and θ^{ij} is a weight factor reflecting the relative importance of discretionary incentives.

Four types of lane change behaviour are specified according to the overall lane change desire, being No Lane Change (No LC), free lane changes (FLC), synchronized lane changes (SLC) and cooperative lane changes (CLC). The relationships between lane change desire and resulting lane change behaviour are shown in Figure 5.2 with behavioural changes in synchronization and gap-creation. The synchronization refers to the speed synchronization of the lane changer to its target leader, and the gap-creation refers to the courtesy behaviour of the potential follower in the target lane to facilitate the lane change. As lane change desire increases, lane changing vehicles first intend to perform the FLC without additional strategies. As lane change desire falls into the SLC range, a lane changing vehicle aligns its speed with that of the leader in the target lane, but the follower in the target lane does not actively create a gap for the lane changer. When the desire exceeds the CLC criteria, cooperative lane changes (CLC) are expected, in which the lane changing vehicle synchronizes its speed with the potential leader in the target lane and the potential follower in target lane also actively creates a gap in front for the lane changer.

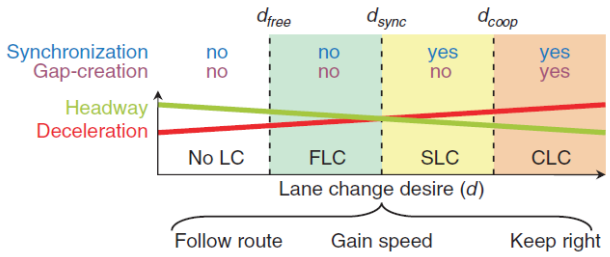

Figure 5.2 Four types of lane change behaviour corresponding to the level of lane change desire (Schakel et al., 2012).

In addition, the interaction between the lateral and longitudinal vehicle behaviour is modelled by expressing the acceptable gap and acceleration level as linear functions of the lane change desire. As lane change desire increases, the acceptable headway decreases and the acceptable deceleration increases, both of which increase the likelihood of successful lane changes. The mathematical formulation of the interaction can be found in reference (Schakel et al., 2012).

5.2.4.2 Eligible users to a dedicated lane

Speed incentive and lane preference are two lane change incentives toward dedicated lanes taken into account by eligible users. The speed incentive for gaining speed on an adjacent dedicated lane has been captured by the original LMRS, whereas for users travelling on general purpose (GP) lanes that are further away from the dedicated lanes, the speed incentives are indirectly captured by an accumulated adjacent speed gain in each lane change process. The lane preference on the dedicated lane by eligible users is considered as a particular direction bias of lane changes, i.e. to-left or to-right. This direction bias will increase the lane change desire toward dedicated lanes and it works during multiple lanes changes until a vehicle has arrived at the dedicated lanes.

A direction bias toward a dedicated lane (DL), denoted as d_{DL}^{ij}, is proposed in the LMRS framework as a discretionary incentive. The lane change desire of eligible users is thus formulated as equation (5.4), where the keep-right bias in the original model is removed because the keep-right rule does not apply in the simulated U.S. traffic.

$$d^{ij} = \begin{cases} d_r^{ij} + \theta^{ij}\left(d_s^{ij} + d_{DL}^{ij}\right) & head\ for\ DL; \\ d_r^{ij} + \theta^{ij} \cdot d_s^{ij} & otherwise. \end{cases} \tag{5.4}$$

5.2.4.3 Ineligible users to a dedicated lane

Ineligible users are obliged to leave the dedicated lanes when the dedicated lane is activated. They may leave the dedicated lane immediately or gradually if sufficient gaps in the adjacent GP lanes are not found. Such egressing behaviour can be modelled by a directional bias d_{leave}^{ij} to the direction of the adjacent GP lane. This bias increases the lane change desire of going to the adjacent GP lane and generally leads to a relatively active lane change behaviour, e.g. the SLC and CLC. Once the ineligible users have left the dedicated lanes, their desire toward dedicated lanes becomes infinitely negative, indicating that they will not change back to dedicated lanes. The lane change desire of ineligible users to dedicated lane is expressed in equation (5.5).

$$d^{ij} = \begin{cases} d_r^{ij} + \theta^{ij}\left(d_s^{ij} + d_{leave}^{ij}\right) & leaving\ DL; \\ -Inf & j\ is\ a\ DL; \\ d_r^{ij} + \theta^{ij} \cdot d_s^{ij} & otherwise. \end{cases} \tag{5.5}$$

This completes the description of the car-following model and lane change model for simulated CACC vehicles and manually driven vehicles in our study. This integrated model outperforms the other CACC simulation models for its capability in reproducing realistic CACC vehicle behaviour in simulations. It models the multi-mode operation of the CACC system and the interaction between the driver and the system, describing extensively the CACC vehicle states on road. The manually driving behaviour including the lane change behaviour adapted to dedicated lanes is explicitly modelled and properly calibrated. In the following section, the experiment and simulation set-up for determining the traffic impacts of a CACC lane will be provided.

5.3 Experimental setup

To investigate the impacts of CACC vehicles on traffic flow with a dedicated CACC lane and explore the interaction between CACC MPRs and a dedicated lane deployment, we conduct simulation experiments by introducing CACC vehicles and a left-most CACC lane in a realistic network with interacting bottlenecks.

The SR-99 corridor to the south of Sacramento in California is chosen as the simulation network. The corridor is 20-km long with 16 on-ramps, 12 off-ramps and 1 High Occupancy Vehicle (HOV) lane, heading from the Elk Grove Blvd to the interchange for SR-50. The number of lanes increases from three lanes to four lanes at the merge of Calvine Rd and further increase to five lanes after the interchange with Fruitridge Rd. The leftmost lane is a continuous-access HOV lane, where eligible vehicles are free to enter and exit at any location. In the morning, it is only activated during 6:00 – 10:00 AM. Figure 5.3 presents the lane configuration with lane-based loop detectors. In total, there are 16 reliable groups of detectors illustrated as rectangles with their post miles. The 5-min flow and speed provided by these detectors exhibit the traffic flow performance in this corridor, in which there is recurrent congestion in the morning peak contributed by three interacting bottlenecks: the merging section at Sheldon Rd.,

the weaving section at Florin Rd. and 47th Ave. Our simulation starts from 4:00 AM to 12:00 AM, covering the operations of free flows, traffic breakdown and congestion recovery, as well as the inactive and active periods of the HOV lanes.

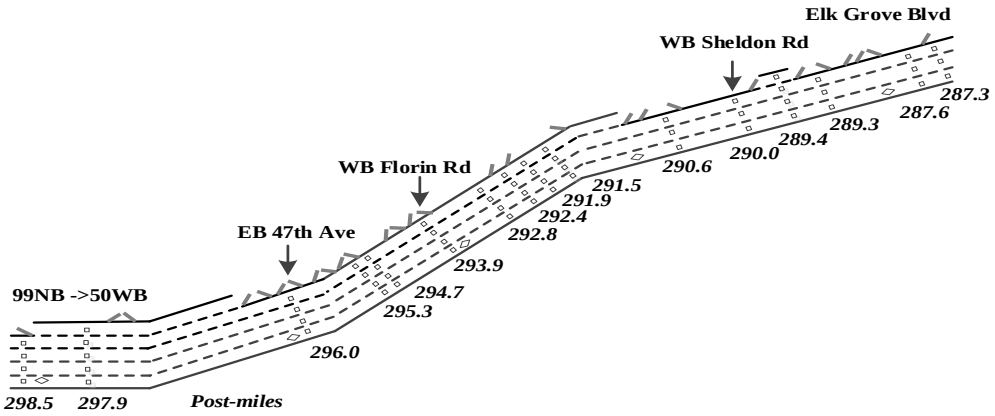

Figure 5.3 Lane configuration and road geometry of the SR-99 corridor.

The selected network and scenario were established in an open-source microscopic traffic simulator, MOTUS, where the basic LMRS and IDM+ are adopted and integrated. The lane change model has been extended in our previous work (Xiao et al., 2016) to model dedicated lane operations and the car-following and lane change models for CACC vehicles have been implemented in the simulator (Xiao et al., 2018). In the previous study (Xiao et al., 2016), we have calibrated the manually driving car-following model and lane change model using the loop detector data of October 6, 2015 from the Caltrans Performance Measurement System (PeMS), which is chosen for a typical weekday without incident reports during the simulated time period. Four parameters in the IDM+ and nine parameters in the extended LMRS were calibrated and the models are able to reproduce plausible vehicle behaviour and replicate a consistent congestion pattern, fundamental diagrams and lane flow distribution at network, section and lane level respectively with the PeMS data. The calibrated simulation is taken as the reference case for comparison with simulations of CACC vehicles in a CACC dedicated lane scenario.

In this experiment, we replace the HOV lane by a CACC lane. Similar to the HOV lanes, the CACC lane is only accessible to CACC vehicles once activated, but CACC vehicles can travel in all lanes. All the other simulation settings and parameters (see Table 5.2) remain unchanged except for a percentage of passenger cars changing into CACC vehicles. The truck percentage remains at 3.8% of all traffic, an average of truck flow over the mainline flow in this corridor. We use the largely time-variant demand pattern from the reference case and assume an invariant generated CACC percentage during the simulation period.

When a CACC dedicated lane is activated, the vehicles generated at that lane should only be CACC vehicles, instead of mixed vehicle types to avoid mandatory lane changes at the network beginning due to lane accessibility. In order to meet this requirement while ensuring CACC market penetration rate is respected as the simulation input, we distribute the mainline demand to the three mainline generators so that when the dedicated CACC lane is activated, only CACC vehicles are generated in this lane.

Table 5.2 Employed parameters in simulation

Parameters	Typical value
Car-following model	
Conventional vehicles	
Maximum acceleration	1.25 m/s^2
Comfortable deceleration	2.09 m/s^2
Stopping distance	3 m
Shared with conventional vehicles and CACC vehicles	
Desired time gap under manual driving	1.4 s
Vehicle length	4 m
Free-flow speeds	N(125, 8.75) km/h
CACC vehicles	
V2V communication range	300 m
Sensor range	120 m
Desired time gap under ACC	1.1 s
Desired time gap under CACC	0.6 s (57%), 0.7 s (24%) 0.9 s (7%), 1.1 s (12%)
CACC inter-string gap	1.5 s
CACC string length limit	10 vehicles
ACC-CACC lower acceleration limit	-4 m/s^2
ACC-CACC upper acceleration limit	2 m/s^2
Lane change model	
Free lane change criteria	0.25
Synchronized lane change criteria	0.5
Cooperative lane change criteria	0.75
Bias to head toward dedicated lanes	0.45
Bias to leave the dedicated lane	0.5

The simulated CACC vehicle percentages increase from 10% to 50% by an increment of 10%, and each CACC MPR is run five times with different random seeds. Impact analysis uses the simulated loop detector data on a 5-min interval and vehicle trajectory data on a 0.2-second interval. For the impacts of CACC vehicles on traffic congestion, the spatiotemporal speed contour of the corridor is plotted for the identification of the changes in congestion pattern. The congestion pattern is further explored with CACC lane operation and friction effects, which can be analysed via CACC lane throughput and speed. In addition, changes in travel time reliability in each CACC MPR scenario are investigated and statistics on CACC time usage and number of deactivations are provided to show the operation of CACC strings.

5.4 Simulation results

This section presents the simulation results with increasing CACC vehicle MPRs in terms of the macroscopic congestion pattern, the utilization of CACC dedicated lane, travel time reliability and CACC system operations. The analysis of congestion pattern and CACC lane utilization are carried out from the traffic flow perspective, whereas the discussions on travel time reliability and CACC operations are mainly at the platoon and vehicle/driver levels.

5.4.1 Traffic congestion pattern

Figure 5.4 shows the macroscopic flow operations with CACC MPRs via the speed plot in the time-space diagram. From 10% to 50% MPRs, the congested area at 10%-20% CACC MPRs is considerably large, then becomes small at 30% and further substantially reduces to a small area after 40% CACC MPRs. It depicts a general trend of alleviated congestion with increasing CACC MPR in the network. Compared to the reference case, a low CACC MPR with a CACC lane does not show positive impacts in reducing congestion. The congestion area at 10% and 20% CACC percentage is much larger than the reference case and at 30% MPRs the congestion area is just comparable to the reference case. The HOV ratio in the reference case is time-variant and the averaged HOV ratio is around 29% during 6:00 – 8:00 AM when the traffic congestion emerged and propagated in the network. The comparable vehicle percentages eligible for the dedicated lane in reference case and 30% CACC case can explain the similar congestion pattern in both cases and it suggests that the formation of congestions at 10%-30% CACC MPRs is mainly caused by closing one lane for manually driven vehicles whereas there is insufficient flow on the CACC lane. These results imply that the potential improvements by CACC vehicles are offset by the underutilization of a CACC lane at low MPRs.

Looking into the characteristics of traffic congestion, increasing the CACC MPR does not change the location of a bottleneck in the network. In Figure 5.4, it is clear to observe the activated bottlenecks at Sheldon Rd. (PM 290.0), Florin Rd. (PM 293.9) and 47th Ave (PM 296.0) at 10-30% CACC MPRs, which also are the bottlenecks identified in the reference case. However, increasing CACC MPRs delays the onset of congestion, especially for the Shelden bottleneck. The congestion starts at 6:40 AM in the reference case and at 6:20, 6:45 and 7:05 AM at 10%, 20% and 30 % MPRs respectively. Above 40% MPRs, the congestion at this bottleneck is entirely prevented, given the same demand as the reference case.

With the same demand setting for each scenario, the delayed timings for the onset of congestion suggest the potential of CACC vehicles, in combination with a CACC lane, in postponing or preventing traffic congestion. A CACC lane provides high vehicle throughput. When there is sufficient CACC demand, a considerable amount of traffic can be shared by CACC lanes, leading to less demand in GP lanes and therefore the congestion is less likely to appear. In addition, the CACC vehicles travelling in GP lanes are able to increase the throughput of GP lanes, which also prevents or postpones traffic breakdowns.

The changes in congestion pattern also reveal that the effectiveness of converting an HOV lane to a CACC lane is highly related to the percentage of CACC vehicles in traffic. At low MPRs, the CACC lanes may not be able to share sufficient traffic and the CACC vehicles remaining in GP lanes are also not effective to alleviate the congestion.

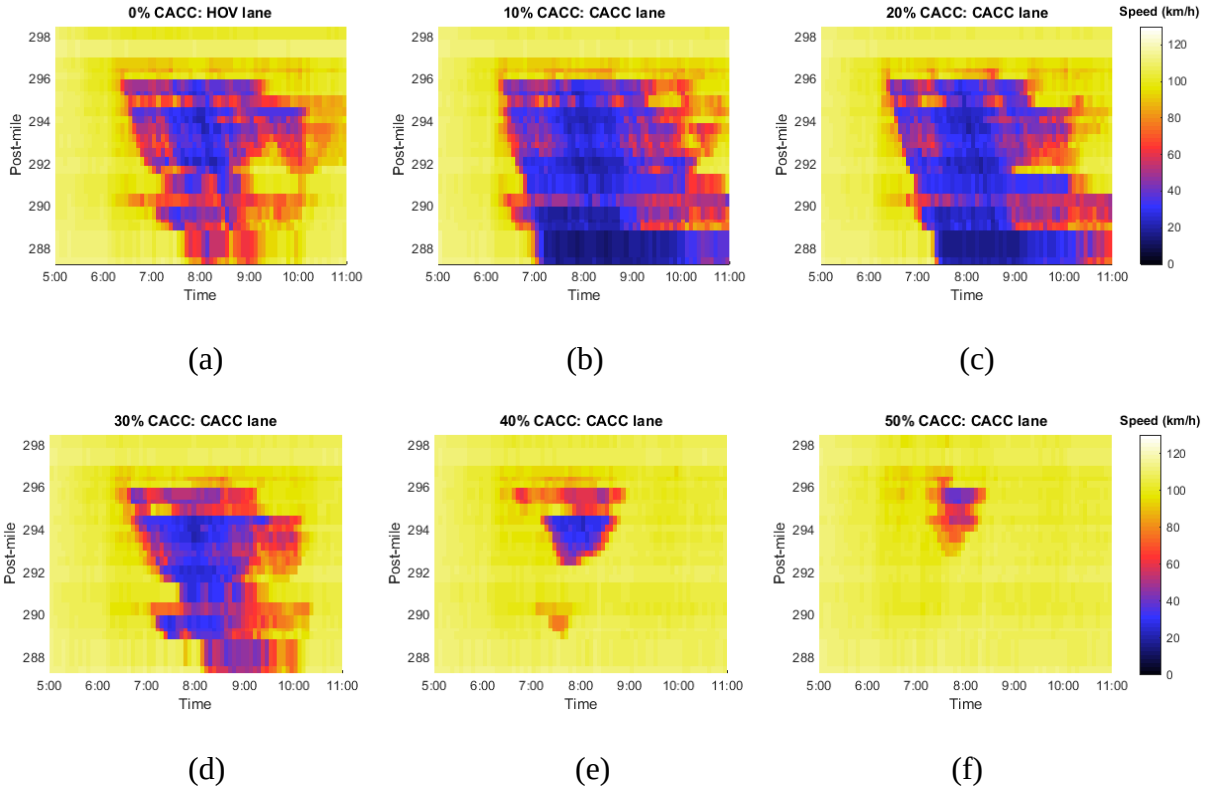

Figure 5.4 Traffic congestion pattern with increasing CACC MPRs in a CACC dedicated lane scenario.

5.4.2 CACC lane operation and friction effects

Figure 5.5 provides speed-flow plots at each bottleneck with different CACC MPRs during 6:00 – 7:30 AM that the congestion was formed. Firstly, the results show that the traffic volume/flow of CACC lanes increases with the CACC MPRs at each bottleneck and they are all below the lane capacity of 100% CACC vehicles which is around 3300 veh/h/lane at a merging bottleneck (Xiao et al., 2018). It implies that the traffic flow on CACC lanes is not oversaturated and CACC lanes can still carry more traffic when the overall CACC MPR is below 50%. Secondly, it is noted that sometimes the speed reduces substantially even though the flow remains at a low level. This suggests that the congestion in CACC lanes is not caused by high traffic demands but by lane changes of CACC vehicles between CACC lanes and GP lanes.

The speed reduction of dedicated lanes as a result of interacting traffic between dedicated lanes and adjacent GP lanes is described as the friction effect, and it is a general phenomenon for traffic flow with a continuous-access dedicated lane (Guin et al., 2008). A friction effect appears before dedicated lanes reaching the capacity and corresponds to the traffic congestion in adjacent GP lanes. To understand the interaction between the CACC lanes and GP lanes, the speed reductions in both lanes are investigated.

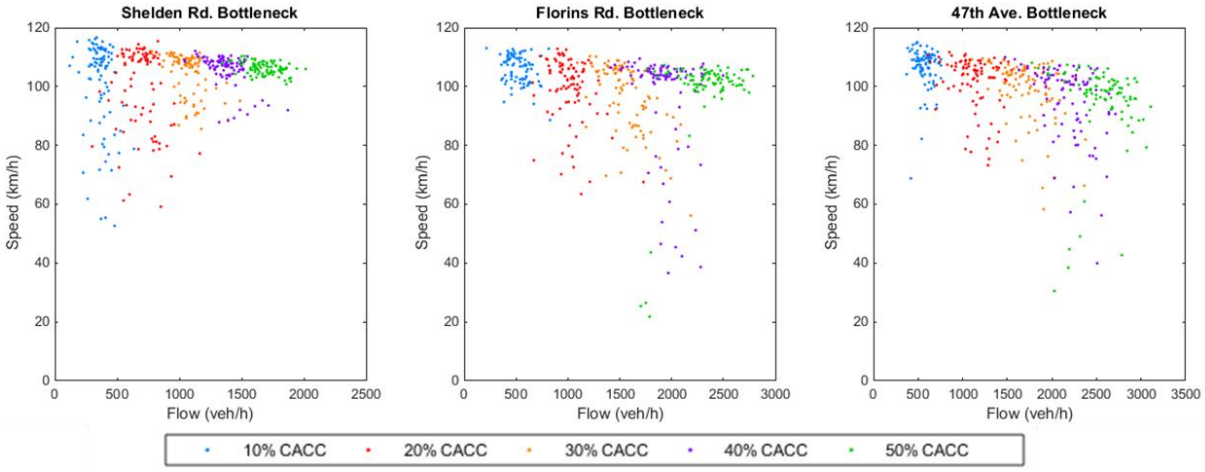

(a) (b) (c)

Figure 5.5 The speed-flow plots of the CACC lane during 6:00-7:30 AM at different CACC MPRs at three bottlenecks.

The speed contour plots of the CACC lanes and adjacent GP lanes, as well as the plots of their speed differences are presented in Figure 5.6. With a CACC dedicated lane, the friction effect remains observable at all tested CACC MPRs. At low CACC MPRs 10 – 30%, speed reductions in the CACC lanes are observed only at several particular sections. The speed differences between CACC lane and the adjacent GP lane are considerable, reaching up to 100 km/h at some locations that can lead to adverse consequences on safety. At high CACC MPRs, the time-space area of speed reductions in the dedicated lane is more comparable to the congestion in the adjacent GP lanes and the speed difference of the congested area is relatively small. Hence, the friction effect is more significant. This is consistent with the observation in (Xiao et al., 2016) that the friction effect does not occur when the demand in dedicated lanes is low.

In our model, the friction effect is mainly due to the lane change manoeuvres for entering and exiting the dedicated lane which disrupts the flow on the dedicated lane (Xiao et al., 2016). With a CACC string operation in the dedicated lanes, the following gaps between two vehicles are generally smaller than that between manually driven vehicles, which makes it difficult for a CACC vehicle to merge into the CACC lane. In this case, a cooperative lane change initiated by a CACC vehicle from the adjacent GP lane, requiring the potential follower in the CACC lane to intentionally create a sufficient gap, causes severe disruption in the CACC lane. In addition, the speed reduction in the CACC lane is also caused by CACC drivers slow down to search an acceptable gap for performing a lane change toward highway exits.

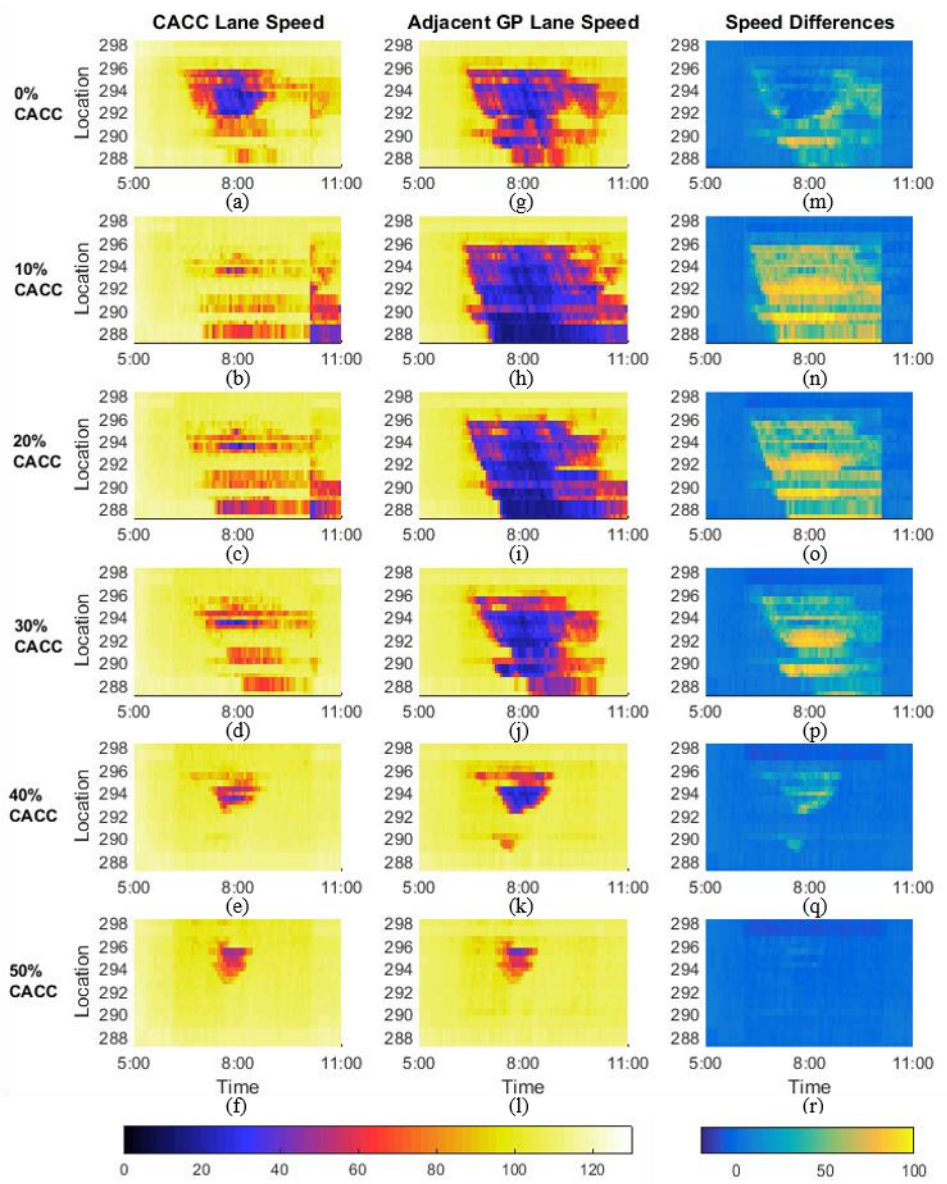

Figure 5.6 Speed differences of dedicated lanes and the adjacent general-purpose lanes at different CACC MPRs.

5.4.3 Travel time reliability

The speed difference between CACC lane and GP lanes implies unequal travel time for vehicles travelling in those lanes. Table 5.3 provides the statistical analysis of total travel time of all vehicles and average travel time delay per vehicle regardless of vehicle classes, by which the effects of CACC lanes at each CACC MPRs are quantified. The total travel time and averaged travel time delay firstly increase from 0% to 10% CACC MPRs and later decrease with CACC MPRs, which is consistent with the traffic congestion pattern in Figure 5.4. At the 10% and 20% MPRs which the CACC lanes worsen the traffic performance, the increases in travel time are as high as 42% and 31%, whereas the increases in travel time delay reach 110% and 75%. At 40% and 50% MPRs where less congestion is observed, the reductions in travel time are 31% and 36% and in travel time delay are 71% and 77%, a considerably large save.

The standard deviation of averaged travel time delay shows the impact of congestion on travel time reliability. As the results presented, more severe congestion is, less reliable the travel time is. Although at 30% CACC MPRs, it seems that the congestion pattern and travel time are comparable to the reference case, the results show a larger delay and standard deviation, implying reduced travel time reliability at this MPR due to a mixture of CACC and conventional vehicles.

Table 5.3 Travel time and delay analysis of all traffic in each CACC MPR

	CACC MPR					
	0%	10%	20%	30%	40%	50%
Total TT (h)	10961	15546	14337	10997	7586	7065
mean TTD (s/veh)	255	536	446	324	86	79
std TTD (s/veh)	381	861	723	555	110	89

Note: TT is travel time; TTD is travel time delay and std is the standard deviation.

To distinguish the travel time reliability of CACC and conventional vehicles, Figure 5.7 shows their averaged travel time delay and its deviation at each MPR separately. During the 10-30% CACC MPRs, the differences are substantial, suggesting that CACC dedicated lane does lead to less travel time delay and provide more reliable travel time to CACC vehicles. At 40% CACC MPRs, although the difference in delay is insignificant, the discrepancy in variation prevails. It is explained by the light traffic jam in this scenario that the travel time will not differ much between the CACC lanes and GP lanes. However, at 50% CACC MPRs, the variation of CACC vehicles in delay is slightly higher than conventional vehicles, which might be the consequences of additional lane changes heading toward and egressing the dedicated lanes. These results point out the effectiveness of CACC lanes in providing shorter travel time and higher travel time reliability to CACC vehicles in saturated traffic.

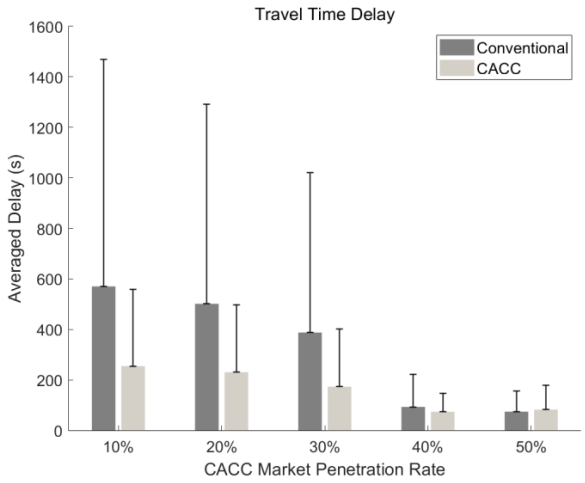

Figure 5.7 Mean and standard deviation of the travel time delay of conventional and CACC vehicles at each CACC MPRs.

5.4.4 CACC system operations

The operational characteristics of the CACC system reveal to what extent the CACC system is effectively and sufficiently used in mixed traffic. In this section, the CACC usage in each MPR scenarios is examined, illustrating the impacts of increasing MRPs on CACC operations with a presence of CACC lane.

CACC time usage is an important indicator of the operation of CACC systems. It is calculated for each CACC vehicle, based on vehicle trajectories, as the ratio of the accumulated time duration under CACC operation over the entire travel time. In Table 5.4, the CACC time usage increases as the percentage of CACC vehicles increases, which rise from 23.94% to 48.45%. It is explained by the increase in the probability of CACC vehicles following another CACC vehicle. Higher MPR leads to a higher probability and thus the CACC time usage increases.

Regarding string operation, the time usage under the CACC gap-regulating mode is investigated. For comparable results among different scenarios, it is calculated as the ratio of the accumulative time duration under gap-regulating mode over the time duration of CACC for each vehicle. Table 5.4 lists the average value of five simulation runs at each CACC MPR. The lower the CACC MPR is, the higher the ratio is. This trend is explained by the existence of a CACC dedicated lane. Since more severe congestions happen at low CACC MPRs, CACC vehicles on GP lanes have larger desires to change to the dedicated lane to gain speeds. CACC vehicles travelling in the dedicated lane experience less interference from merging and exiting traffic than that in GP lanes, therefore CACC vehicles are more likely to be operated in the CACC gap-regulating mode.

Table 5.4 CACC operational characteristics

	CACC MPRs				
	10%	20%	30%	40%	50%
Time Usage per CACC vehicle					
CACC System	23.94%	31.12%	38.1%	43.83%	48.45%
Gap-regulating Mode Ratio	57.39%	56.39%	52.47%	48.03%	45.55%
Number of Deactivations per CACC vehicle					
Total	5.86	6.06	4.66	3.32	3.43
Lane-change related	2.25	2.35	2.05	1.65	1.71
Safety-related	2.97	3.05	1.93	1.01	1.06
Route-related	0.64	0.66	0.68	0.67	0.66

The number of CACC deactivations reflects to what extent CACC operation is interrupted and it is highly related to throughput reduction in mixed traffic flows (Xiao et al., 2018). Table 5.4 provides the average number of CACC deactivations per CACC vehicle and also the number in each deactivation category. In general, the number of safety-related deactivation changes significantly with the MPRs, whereas the other two categories of deactivation vary insubstantially. The safety-related deactivation decreases from around 3 per vehicle at 10 – 20% CACC MPRs to 1 per vehicle at 50% MPRs as the CACC MPR increases, mainly because traffic congestion was mitigated with increasing CACC vehicles and less collision warning is issued thereof. The lane-change-related deactivation decreases at 40% and 50% CACC MPRs

as well. This can be explained by the fact that the traffic performance in CACC lane is not significantly better than the GP lanes and fewer lane changes are made by CACC vehicles toward the CACC lanes and fewer cooperative manoeuvres are needed.

5.5 Conclusions and future work

This study was designed to investigate the quantitative impacts of converting an HOV lane to a CACC dedicated lane on traffic flow, travel time and CACC string operation at low and medium CACC MPRs. Based on an enhanced car-following model for CACC vehicles and an extended lane change model for a dedicated lane scenario, we conducted microscopic simulations to reproduce the traffic flows with mixed CACC vehicles and manually driven vehicles with a leftmost CACC dedicated lane on a freeway corridor in California. The simulation results were compared to a reference case with an HOV lane and the comparison revealed the positive and negative impacts of CACC lanes in terms of traffic flow performance.

This study showed that converting an HOV lane to a CACC dedicated lane has different impacts depending on the market penetration rate of CACC vehicles. The results of 30% CACC MPR with a CACC lane is comparable to the reference case of an HOV lane which has around 29% HOVs during the congestion formation. At CACC MPRs below 30%, the CACC lane carries insufficient traffic and the GP lanes bear a higher demand than the reference case, which causes severe and long-lasting traffic congestion. The total travel time substantially increases and the travel time reliability decreases. However, at CACC MPRs ranging from 30% – 50%, the traffic congestion are considerably alleviated by a high lane flow share of the CACC lane and the CACC operation in GP lanes. In these cases, the travel time and delay dramatically decrease and the travel time reliability increases. At low CACC MPRs where congestions happen, this study also found that a CACC lane can provide smaller travel time delay and higher travel time reliability to CACC vehicles than that of the manually driven vehicles in GP lanes. In terms of CACC operations in a CACC lane scenario, the CACC time usage is found to be increasing with the CACC MPR, but the time ratio of CACC operations under gap-regulating mode is found to be decreasing as the CACC MPR increases.

The findings of this research provide new insights into the effects and operation of a CACC dedicated lane. An important implication to road operator is that the conversion from an existing HOV lane to a CACC lane should wait until the CACC MPR has risen to a certain level. Otherwise, the overall traffic can deteriorate due to a closed lane for manually driven vehicles. Mixed use of dedicated lane at low CACC MPRs is likely to be a transitional strategy before reaching sufficient CACC demand, which is in accordance with the literature.

The results of the friction effect between CACC lanes and GP lanes also raise a safety concern: at low CACC MPRs, the large speed difference between two lanes can result in high collision risk when a lane change is performed. Especially when CACC systems are activated, drivers pay less attention to surrounding vehicles, and they may not respond in time to resume vehicle controls and avoid collisions. To reduce the collision risks, communication and coordination between lane changing vehicles and vehicles in CACC lanes are essential. A future study will focus on strategies to increase the flow of CACC lanes as the CACC MRP is low, for instance, by allowing connected (conventional) vehicles to act as string leader and use CACC dedicated lanes. In addition, future research may pay attention to the save in travel time by CACC vehicles with different travel distance. It may provide a detailed quantitative analysis of CACC system usage for different CACC users. Moreover, future work may investigate the scenario of increasing CACC vehicles in a highway with an activated HOV lane, as the intermediate phase of converting an HOV lane to a CACC lane.

6 Conclusions and future work

This thesis addresses the challenges of modelling cooperative adaptive cruise control vehicles and provides systematic evaluations of their impacts on traffic flow performance. Chapter 1 outlined the research framework and formulated the scientific research questions, which were answered throughout Chapters 2-5.

This chapter summarizes the main findings, discusses the scientific and practical implications and gives recommendations for future work. Section 6.1 reviews the research findings in terms of the multi-regime CACC car-following model, capacity characteristics of mixed traffic flow, the enhanced lane change model for the dedicated lane scenario and the traffic flow impacts of deploying a CACC lane. Section 6.2 describes the relevance of research findings to practice and points out the possible future actions for each stakeholder. Section 6.3 discusses the research limitations in modelling and experiment design and illustrates the directions for future studies.

6.1 Scientific findings and conclusions

The objective of this thesis is to gain insights into the traffic flow characteristics of mixed traffic with CACC vehicles and conventional vehicles and reveal the impacts of CACC vehicles from the traffic efficiency point of view. To this end, car-following and lane change models representing the CACC vehicle behaviour were developed and impact analysis at different CACC MPRs was conducted. This section summarizes the main research findings and conclusions, answering the research questions in Chapter 1.

6.1.1 A multi-regime car-following model for CACC vehicles' longitudinal response

A multi-regime conceptual model for the CACC vehicle longitudinal response was proposed to answer the research question "*how to reproduce realistic behaviour of CACC vehicles in a microscopic simulation*". We examined the operational speed range limits of using an empirical CACC model in simulation and introduced the human driver takeover in the vehicle longitudinal control framework. The model framework we proposed pertains to a multi-regime model in which cruising, gap-regulating and gap-closing modes are distinguished. The distinction is necessary and in accordance with the multiple sub-controllers of CACC for different control objectives. A gap-closing mode is specifically designed to ensure the safety in vehicle approaching and it is activated when the CACC vehicle is closing a large gap with a higher speed than its predecessor. The multi-regime model incorporates both system-initiated and driver-initiated control authority transitions and this renders the CACC model applicable in full speed range conditions with a low number of vehicle collisions. The alternative manual driving is designed as a control loop parallel to the CACC loop and the interaction between two control loops is realized by assumptions about CACC activation and deactivation. In safety-critical situations, drivers overrule the system control and apply a deceleration larger than the braking capability of CACC, substantially reducing the collision risk. Therefore, the empirical CACC car-following model integrating driver takeover can be used for more traffic scenarios without rear-end collisions. In addition to that, a dynamic spacing margin is introduced at speeds below 10 m/s in order to offer additional safety margin at low-speed CACC operation.

Systematic simulation experiments were conducted to investigate the car-following performance and collision-free property of the proposed multi-regime model. Three typical simulation scenarios i.e. stop-and-go, cut-out and approaching scenarios, and two safety-critical scenarios, being hard braking and cut-in scenarios are included. It is shown that no collision takes place in the typical scenarios but high collision risk remains in the low-speed-range operation and the approaching scenarios. Driver-initiated and system-initiated takeovers effectively avoid collisions. In the cut-in scenario, a vehicle cutting-in with a speed difference below 6 m/s does not result in collisions. In the hard braking scenario, collision does not occur when a leader decelerates either less than 4 seconds at 2 m/s^2 or 1.5 seconds at 4 m/s^2. It is concluded that the proposed multi-regime car-following model, combining a realistic CACC system with driver intervention, can produce plausible following behaviour and it is collision free under typical traffic situations and most safety-critical situations.

6.1.2 Traffic flow characteristic of the mixed traffic with CACC vehicles

A systematic simulation experiment was conducted to investigate the fundamental diagram, capacity and capacity drop of the mixed traffic flow, answering to the research question "*what are the capacity characteristics of traffic flows with different CACC vehicle market penetration*

rates". The CACC MPR and on-ramp demand are two control variables to simulate the different levels of mixed traffic and merging disturbances. The CACC MPR increases from 0% to 100% with a 20% increment and the on-ramp demand increases from 400 to 1600 veh/h by every 400 veh/h. For each simulation setup, five repetitions with different random seeds for assigning vehicle class, desired speed and vehicle arriving interval are conducted and each simulation test lasts for one hour. Driver's choices in CACC desired time gaps from field tests were used to reproduce the realistic distribution of CACC time gaps.

The results firstly show that the general shape of the fundamental diagram does not alter substantially after introducing CACC vehicles into traffic. The reverse-λ shape in the flow-density plot remains unchanged at all levels of CACC market penetrate rate, implying the existence of the free-flow capacity, queue discharge flow and capacity drop in the mixed traffic. In the fundamental diagram, more scatters in the congested-flow regime are observed with the increased CACC MPRs. The scatters can be attributed to the increased flow heterogeneity due to the multiple ACC and CACC operation modes, control authority transition and the string instability of the ACC car-following model.

Secondly, the theoretical capacity upper bound, pipeline capacity and merging capacity (free-flow capacity) were examined with the varied CACC MPRs. They all exhibit an increasing trend with the increased CACC MPRs which suggests that CACC vehicles increase the roadway capacity at both road segments and merging bottlenecks. The increase in throughput is found to be closely related to the effective use of CACC, which is a consequence of CACC MPR, the probability of two CACC vehicles being clustered, and the percentage of system deactivation. At low CACC MPRs (20-40%), the CACC usage is relatively low since a large number of CACC vehicles cannot find a qualified CACC leader and therefore are operating in the ACC mode. At high CACC MPRs (60-100%), a higher percentage of CACC vehicles are operating in the CACC mode, thus a large capacity increase is observed. This finding is in accordance with the previous studies (Chen et al., 2017; Shladover et al., 2012; van Arem et al., 2006; VanderWerf et al., 2002) regarding the effects of CACC on roadway capacity.

The queue discharge flow at the merging bottleneck is found to increase with CACC MPRs as well, a similar trend with the merging capacity. The difference between the merging capacity and queue discharge flow, being the capacity drop, exists at all CACC MPRs and its extent is comparable to that in conventional vehicular traffic in the order of 15%-20%. Given that a strong correlation in space and time between traffic congestion and the number of CACC systems deactivations is found, the capacity drop at merging bottleneck can be explained by the CACC deactivation that increases the time gap between CACC vehicles and their predecessors consequently. After traffic congestion appears, the number of deactivations increases substantially due to safety concerns and lane change requests. This leads to a larger number of transitions from CACC to manual driving and from gap-regulating mode to gap-closing mode after CACC reactivation. The changes among these multiple vehicle operations and modes result in large time gaps and thus lead to the capacity drop.

6.1.3 An extended LMRS for the lane change behaviour regarding a dedicated lane

An extension of the lane change model with relaxation and synchronization (LMRS) is proposed to answer the research question "*how to model the lane change behaviour with the presence of a dedicated lane*". According to the different lane change purposes in relation to the dedicated lanes, this extended model is specified for eligible and ineligible users of the dedicated lane respectively once it is activated. For eligible users, two lane change incentives

are taken into consideration during the process of lane change decision-making. One incentive is the speed gain of travelling in the dedicated lane. It is modelled as the speed incentive based on the speed differences between the current lane and dedicated lanes. The other incentive is the driver's preference for the dedicated lane. The preference is modelled as directional bias heading toward the dedicated lane. Both the speed incentive and directional bias are discretionary incentives, which are discounted when the route incentive related to mandatory lane change appears. For ineligible users, the intention of leaving an activated dedicated lane is modelled by a directional bias heading toward the general purpose lanes.

A systematic calibration of the extended model was conducted with aggregate traffic flow measurements. The simulation was calibrated on SR99 corridor in California as the simulated network since a continuous access High Occupancy Vehicle (HOV) lane is currently operating in this corridor. The car-following and lane change parameters of the extended model are adjusted and tuned to achieve the minimum root-mean-square error of both flows and speeds from the loop detectors. It is shown that the extended model is capable of reproducing traffic flow characteristics in a complex network with HOV lanes and interacting bottlenecks. Key characteristics such as the congestion formation and propagation pattern at the corridor level and the lane flow distribution and fundamental diagram at the section level were explicitly replicated in the simulation. It strongly supports the capability of the extended model to model the lane change behaviour of eligible and ineligible users with the presence of a dedicated lane. Moreover, this model is cross-calibrated via a comparison with another model using the same data for calibration. The consistency between two calibration results shows the validity of both driving models and gives more confidence to users about the simulation results (Kan et al., 2019).

6.1.4 Traffic flow impacts of converting an HOV lane into a CACC lane

A simulation-based impact analysis of a CACC lane at various CACC MPRs was carried out and the traffic performance was compared to a reference case of an HOV lane, providing an answer to the research question "w*hat is the consequence of converting an HOV lane to a CACC lane in a realistic highway corridor".* The CACC car-following model proposed in Chapter 2 and the lane change model particularly developed for a dedicated lane scenario in Chapter 4 are integrated and applied to simulate an existing freeway corridor in California, where an HOV lane is replaced with a dedicated CACC lane at different MPRs. A simulation experiment is conducted with a CACC lane at CACC MPRs ranging from 10% to 50% and with the calibrated SR99 corridor as the reference case. The comparison of each CACC lane case with the HOV lane case reveals the impact of converting an HOV lane into a CACC lane at a certain CACC MPR.

From the traffic flow perspective, it is found that the effects of converting an HOV lane into a CACC lane are highly related to the CACC MPRs. At CACC MPRs below 30%, a CACC lane generally deteriorates the congestion in the general purpose (GP) lanes in the studied corridor because the CACC lane carries insufficient demand; however, at CACC MPRs ranging from 30% to 50%, the congestion is considerably alleviated due to both a high lane flow share of the CACC lane and the increased throughput by CACC operation in GP lanes. At all tested CACC MPRs, the traffic flow on CACC lanes is found below the lane capacity of 100% CACC vehicles, implying that the CACC lanes are not oversaturated. On the basis of that, the speed reduction on the CACC lane, referred to as the friction effect, is largely contributed by the lane changes between the dedicated lane and the adjacent GP lane.

From vehicle/driver perspective, it is found that the CACC vehicles experience less travel time delay and more reliable travel time than the conventional vehicles with the CACC lane. Especially when traffic congestion is severe at 10-30% CACC MPRs, the difference in travel time delay and travel time reliability between the CACC vehicles and conventional vehicles is substantial. It implies that a CACC lane can provide shorter travel time and higher travel time reliability to CACC vehicles when congestion occurs in general purpose lanes, contributing by the exclusive lane use with a relatively high travel speed. In addition, the CACC operational characteristics reveal to what extent the CACC system is effectively used in mixed traffic. The CACC time usage increases with the increasing CACC MPRs, due to a larger probability of a CACC vehicle following another CACC vehicle. It is also found that the average number of CACC system deactivation decreases as the congestion is alleviated. The safety-related deactivation contributes the most in the heavily congested traffic and the lane-change related deactivation plays the dominant role in the moderate congestion conditions.

6.2 Implications for practice

The methodology and analysis in this thesis are useful for the traffic flow impact assessment of emerging vehicle technologies in the development of vehicle automation. This is relevant to the researcher, policymaker, road operator, traffic engineer and car manufacturers. The findings and conclusions provide several practical implications for these stakeholders.

The integrated CACC car-following model and the extended lane change model for a dedicated lane scenario provide a useful toolbox to researchers, industries and policymakers to evaluate CACC vehicles in various scenarios in terms of traffic flow impacts. The use of an empirical model and the assumptions of human intervention enhance the model validity and ensure the collision-free property in a wide range of scenarios, leading to a successful traffic simulation with feasible computation time. With the calibrated lane change model and car-following model for manual driving, the integrated models can be applied to the simulation of various freeway network stretches with mixed traffic of CACC vehicles and conventional vehicles. Policymakers and road operators are advised to conduct the impact assessment before promoting CACC vehicles into the market since our study show unsubstantial improvement in road capacity at low CACC MPRs and even deteriorated general flow performance with a CACC dedicated lane at low MPRs.

Modelling the limitations of vehicle automation, being the operational design domain of CACC in this thesis, is important for the traffic impact assessment of automated vehicles. The CACC degrades to ACC when a qualified leader is not found and the CACC has to switch to the manual driving when the traffic condition is out of the operational design domain. These modelled vehicle control transitions not only explicitly depict the operational limitations of CACC, but also result in realistic flow characteristics of mixed traffic. It is found that the roadway capacity improvement by CACC at merging bottlenecks is substantially smaller than the theoretical estimation and that on homogeneous sections. Capacity drop pertains at all CACC MPRs and the flow heterogeneity increases with CACC MPR, all of which are due to the multi-regime car-following response as a result of limited CACC operational design domain. Thanks to these modelled CACC limitations, the investigated CACC traffic impacts are valid and reliable and the CACC benefit is not overestimated.

The insights into the capacity characteristics at various CACC MPRs offer important implications to road operators regarding the traffic management of the mixed traffic flow. Firstly, road operators can understand the nonlinear increase of road capacity with CACC MPRs and be aware of the small road capacity increase at the early stage of CACC deployment. Proactive strategies could be considered to adapt to the different features of the mixed flow.

Secondly, additional traffic management measures are needed for low CACC MPRs to maximized CACC benefits. Instead of increasing the CACC MPRs, road operator may pay attention to the strategies of increasing the activated CACC operation ratio, by increasing the number of human-driven vehicles equipped with V2V communication capability and implementing active platooning strategies at freeway network bottlenecks. Meanwhile, it is noted that a large number of CACC vehicles are operating under ACC at low vehicle market penetration rates. Road operator may have to develop control measures to deal with the flow instability resulting from the ACC operation. Last but not least, this thesis implies that deploying a CACC dedicated lane is not an effective strategy in improving overall traffic performance at low CACC MPRs scenarios although it increases the activated CACC operation ratio. The CACC benefit is compensated by the deteriorated congestion on the general purpose lanes and the average travel time for all vehicles become larger when a CACC lane is deployed at low MPRs. Road operators thus should only consider a dedicated CACC lane when the CACC vehicle demand is sufficient.

Unravelling the relations between CACC system deactivation and the capacity reduction at a merging bottleneck and the significant capacity drop after congestion shed lights on future directions in enhancing the benefits of CACC on traffic flow. Road operators can take specific ITS measures to enhance vehicle coordination and cooperation; policymakers can formulate policies to increase vehicle connectivity; and car manufacturers can refine or even redesign their CACC systems to handle more challenging traffic situations at freeway bottlenecks without driver takeover.

6.3 Recommendations for future work

The generalizability of the findings and conclusions is subject to the assumptions made in vehicle behavioural models and the simulation setup in experiments. Future research can challenge the model assumptions and address the shortcomings of experiment designs, as well as focus on new traffic management measures and vehicle control algorithms to deal with the CACC system degradation and deactivation found in this thesis.

This thesis proposes a multi-regime car-following model for CACC vehicles, which is based on an empirical model that is valid at speeds within 25.5m/s to 29.5 m/s. By integrating the driver takeover and manual driving control, the empirical model is extended for a full-speed-range operation, assuming that the vehicles under CACC behave the same way at the other speed ranges as in the high speed range. Our proposed model could be improved by validating this assumption through a field test that investigates the CACC car-following response at full speed ranges.

Several assumptions about the CACC system activation and deactivation have been made to operationalize the interaction between the CACC and manual driving control. It is assumed that CACC is activated as much as possible and it is deactivated under the safety-critical, mandatory and cooperative lane changing conditions. These assumptions might not be complete when taking human factors into account. Future research may integrate sophisticated human decision models to determine the situations of system activation and deactivation and the vehicle behaviour during the transitional period, e.g. regulating target speed (Varotto et al., 2018).

The lane change model of manually driving vehicles is currently used for CACC vehicles based on the assumptions that the lane change decision and manoeuvres of CACC vehicles are made and conducted only by human drivers. However, it is possible that drivers behave differently when they drive CACC vehicles. For example, drivers may prefer to stay in a CACC string and consequently they are reluctant to change lanes. Drivers may actively change lane to follow

another CACC vehicle or join a CACC string. A lane change model considering such lane change incentives could be an interesting topic for follow-up research.

The impacts of CACC vehicles on traffic flow performance are subject to the proposed simulation framework adopting specific ACC and CACC algorithms. Different control algorithms (i.e. non-linear ACC/CACC) and control gains could result in different vehicle behaviour, and the difference in behaviours among cars from different car manufactures could be substantial. Such heterogeneity in vehicle behaviour could be taken into account in future CACC impact research.

This thesis provides insights into the characteristics of mixed traffic flow mostly from the perspective of new CACC vehicle behaviour. Another perspective to look into the mixed traffic flow characteristics may be the behavioural adaptation of driving in conventional vehicles in the surrounding of CACC platoons. How does the conventional vehicle behave in mixed traffic could also place significant effects on flow efficiency and it has rarely been explored in existing studies.

In addition to the CACC dedicated lane strategy, allowing CACC vehicles to use an existing dedicated lane (e.g. HOV lane) and increasing the number of vehicles equipped with V2V communication are frequently discussed as alternative strategies for the low CACC MPR scenario. It would be an interesting topic to evaluate these two strategies as comparisons to the CACC lane strategy and determine the optimal intermediate strategy for maximum CACC benefit in simulation.

Since low clustering probability is the main reason for an unsubstantial capacity increase at low CACC MPRs, more attention can be paid to investigate the active platooning control that enables CACC vehicles to find a qualified leader and actively form a CACC string. The mixed traffic operation could largely benefit from the active platooning control without the need to change traffic infrastructure or vehicle equipment.

It is shown in this thesis that the capacity reduction at a merging bottleneck is primarily contributed by the deactivation of the CACC system in the mainline to provide sufficient gaps for merging vehicles. Based on this finding, coordination and cooperation between the merging vehicles and vehicles in the mainline are highly desired to increase the capacity at a merging bottleneck. Future research may focus on cooperative merging control to facilitate vehicle merging.

Bibliography

Arnaout, G. and S. Bowling. (2011). Towards reducing traffic congestion using cooperative adaptive cruise control on a freeway with a ramp. *Journal of industrial Engineering and Management, vol. 4*, no. 4, pp. 699-717

Arnaout, G. M. and J. P. Arnaout. (2014). Exploring the effects of cooperative adaptive cruise control on highway traffic flow using microscopic traffic simulation. *Transportation Planning and Technology, vol. 37*, no. 2, pp. 186-199

Arnaout, G. M. and S. Bowling. (2015). A progressive deployment strategy for cooperative adaptive cruise control to improve traffic dynamics. *International Journal of Automation and Computing, vol. 11*, no. 1, pp. 10-18

Banks, J. H. (1991). The two-capacity phenomenon: Some theoretical issues. *Transportation Research Record: Journal of the Transportation Research Board*, no. 1320, pp. 234-241

Baskar, L. D., B. De Schutter and H. Hellendoorn. (2012). Traffic management for automated highway systems using model-based predictive control. *IEEE Transactions on Intelligent Transportation Systems, vol. 13*, no. 2, pp. 838-847

Bose, A. and P. Ioannou. (2003). Mixed manual/semi-automated traffic: a macroscopic analysis. *Transportation Research Part C: Emerging Technologies, vol. 11*, no. 6, pp. 439-462

Bu, F. P., H. S. Tan and J. H. Huang. (2010). *Design and field testing of a cooperative adaptive cruise control system*. Paper presented at the American Control Conference, Baltimore

Calvert, S. C., T. H. A. v. d. Broek and M. v. Noort. (2011). Modelling cooperative driving in congestion shockwaves on a freeway network. In *proceedings of 14th International IEEE Conference on Intelligent Transportation Systems*, Washington, DC. pp. 614-619

Chen, D. J., S. Ahn, M. Chitturi and D. A. Noyce. (2017). Towards vehicle automation: Roadway capacity formulation for traffic mixed with regular and automated vehicles. *Transportation Research Part B-Methodological, vol. 100*, pp. 196-221

Chen, Z. B., F. He, L. H. Zhang and Y. F. Yin. (2016). Optimal deployment of autonomous vehicle lanes with endogenous market penetration. *Transportation Research Part C-Emerging Technologies, vol. 72*, pp. 143-156

De Winter, J. C. F., Stanton, N. A., Price, J. S., & Mistry, H. (2016). The effects of driving with different levels of unreliable automation on self-reported workload and secondary task performance. *International Journal of Vehicle Design, vol.* 70, pp. 297–324.

Delis, A. I., I. K. Nikolos and M. Papageorgiou. (2016). *Simulation of the penetration rate effects of ACC and CACC on macroscopic traffic dynamics*. Paper presented at the 19th International Conference on Intelligent Transportation Systems (ITSC), Rio de Janeiro

Deng, Q. (2016). A general simulation framework for modeling and analysis of heavy-duty vehicle platooning. *IEEE Transactions on Intelligent Transportation Systems, vol. 17*, no. 11, pp. 3252-3262

Ge, J. I. and G. Orosz. (2017). Optimal control of connected vehicle systems with communication delay and driver reaction time. *IEEE Transactions on Intelligent Transportation Systems, vol. 18*, no. 8, pp. 2056-2070

Ghiasi, A., O. Hussain, Z. Qian and X. Li. (2017). A mixed traffic capacity analysis and lane management model for connected automated vehicles: A Markov chain method. *Transportation Research Part B: Methodological, vol. 106*, pp. 266-292

Guériau, M., R. Billot, N.-E. El Faouzi, J. Monteil, F. Armetta and S. Hassas. (2016). How to assess the benefits of connected vehicles? A simulation framework for the design of cooperative traffic management strategies. *Transportation Research Part C: Emerging Technologies, vol. 67*, pp. 266-279

Guin, A., M. Hunter and R. Guensler. (2008). Analysis of reduction in effective capacities of high-occupancy vehicle lanes related to traffic behavior. *Transportation Research Record: Journal of the Transportation Research Board*, no. 2065, pp. 47-53

Hall, R. W. and C. Li. (1999). Lane capacity for an automated highway with mixed vehicle classes. *ITS Journal - Intelligent Transportation Systems Journal, vol. 5*, no. 3, pp. 217-240

Hartmann, M., N. Motamedidehkordi, S. Krause, S. Hoffmann, P. Vortisch and F. Busch. (2017). *Impact of automated vehicles on capacity of the German freeway network*. Paper presented at the ITS World Congress 2017 Montreal

HCM. (2000). *Highway Capacital Manual*. Washington, D.C: Transportation Research Board.

Hoogendoorn, R., B. van Arem and S. Hoogendoorn. (2014). Automated driving, traffic flow efficiency, and human factors. *Transportation Research Record: Journal of the Transportation Research Board, vol. 2422*, pp. 113-120

INRIX. (2020a). *2019 Global Traffic Scorecard.* Retrieved from https://inrix.com/scorecard

INRIX. (2020b). Congestion costs each American nearly 100 hours, $1,400 A Year [Press release]. Retrieved from http://inrix.com/press-releases/

INRIX. (2020c). Congestion costs U.K. economy £6.9 billion in 2019 [Press release]. Retrieved from http://inrix.com/press-releases

Ioannou, P. A. (1997). *Automated highway systems*. New York: Springer US.

Ioannou, P. A. and M. Stefanovic. (2005). Evaluation of ACC vehicles in mixed traffic: Lane change effects and sensitivity analysis. *IEEE Transactions on Intelligent Transportation Systems, vol. 6*, no. 1, pp. 79-89

Jia, D. and D. Ngoduy. (2016). Platoon based cooperative driving model with consideration of realistic inter-vehicle communication. *Transportation Research Part C: Emerging Technologies, vol. 68*, pp. 245-264

Kan, X., L. Xiao, H. Liu, M. Wang, W. J. Schakel, X.-Y. Lu, et al. (2019). Cross-comparison and calibration of two microscopic traffic simulation models for complex freeway corridors with dedicated lanes. *Journal of Advanced Transportation, vol. 2019*, pp. 1-14

Kanaris, A., P. Ioannou and F. S. Ho. (1997). Spacing and capacity evaluations for different AHS concepts. *Proceedings of the 1997 American Control Conference, vols 1-6*, pp. 2036-2040

Kesting, A., M. Treiber and D. Helbing. (2010). Enhanced intelligent driver model to access the impact of driving strategies on traffic capacity. *Philosophical Transactions: Mathematical, Physical and Engineering Sciences, vol. 368*, no. 1928, pp. 4585-4605

Kesting, A., M. Treiber, M. Schönhof and D. Helbing. (2008). Adaptive cruise control design for active congestion avoidance. *Transportation Research Part C: Emerging Technologies, vol. 16*, no. 6, pp. 668-683

Kiefer, R. J., D. J. LeBlanc and C. A. Flannagan. (2005). Developing an inverse time-to-collision crash alert timing approach based on drivers' last-second braking and steering judgments. *Accident Analysis and Prevention, vol. 37*, no. 2, pp. 295-303

Klunder, G., M. Li and M. Minderhoud. (2009). Traffic flow impacts of adaptive cruise control deactivation and (re)activation with cooperative driver behavior. *Transportation Research Record: Journal of the Transportation Research Board*, no. 2129, pp. 145-151

Levin, M. W. and S. D. Boyles. (2016). A multiclass cell transmission model for shared human and autonomous vehicle roads. *Transportation Research Part C-Emerging Technologies, vol. 62*, pp. 103-116

Liu, H., X. Kan, S. E. Shladover, X.-Y. Lu and R. E. Ferlis. (2018a). Impact of cooperative adaptive cruise control on multilane freeway merge capacity. *Journal of Intelligent Transportation Systems, vol. 22*, no. 3, pp. 263-275

Liu, H., X. Kan, S. E. Shladover, X.-Y. Lu and R. E. Ferlis. (2018b). Modeling impacts of cooperative adaptive cruise control on mixed traffic flow in multi-lane freeway facilities. *Transportation Research Part C: Emerging Technologies, vol. 95*, pp. 261-279

Makridis, M., K. Mattas, B. Ciuffo, M. A. Raposo and C. Thiel. (2017). Assessing the impact of connected and automated vehicles. A freeway scenario. In *Zachäus C., Müller B., Meyer G. (eds) Advanced Microsystems for Automotive Applications 2017. Lecture Notes in Mobility.* (pp. 213-225): Springer, Cham.

Michael, J. B., D. N. Godbole, J. Lygeros and R. Sengupta. (1998). Capacity analysis of traffic flow over a single-lane automated highway system. *ITS Journal - Intelligent Transportation Systems Journal, vol. 4*, no. 1-2, pp. 49-80

Milanés, V. and S. E. Shladover. (2014). Modeling cooperative and autonomous adaptive cruise control dynamic responses using experimental data. *Transportation Research Part C-Emerging Technologies, vol. 48*, pp. 285-300

Milanés, V. and S. E. Shladover. (2015). Handling cut-in vehicles in strings of cooperative adaptive cruise control vehicles. *Journal of Intelligent Transportation Systems, vol. 20*, no. 2, pp. 178-191

Milanés, V., S. E. Shladover, J. Spring, C. Nowakowski, H. Kawazoe and M. Nakamura. (2014). Cooperative adaptive cruise control in real traffic situations. *IEEE Transactions on Intelligent Transportation Systems, vol. 15*, no. 1, pp. 296-305

Minderhoud, M. and P. H. L. Bovy. (1999). Impact of intelligent cruise control on motorway capacity. *Transportation Research Record: Journal of the Transportation Research Board, vol.* 1679, no 1, pp. 47-57

Ngoduy, D. (2013). Instability of cooperative adaptive cruise control traffic flow: A macroscopic approach. *Communications in Nonlinear Science and Numerical Simulation, vol. 18*, no. 10, pp. 2838-2851

Nowakowski, C., S. E. Shladover, D. Cody, F. Bu, J. O'Connell, J. Spring, et al. (2011). Cooperative adaptive cruise control: Testing drivers' choices of following distances. *California PATH Research Report, UCB-ITS-PRR-2009-23.* Retrieved from https://merritt.cdlib.org/d/ark:%2F13030%2Fm5h70d3r/2/producer%2F775593226.pdf

Pauwelussen, J. and P. J. Feenstra. (2010). Driver behavior analysis during ACC activation and deactivation in a real traffic environment. *IEEE Transactions on Intelligent Transportation Systems, vol. 11*, no. 2, pp. 329-338

Pauwelussen, J. and M. Minderhoud. (2008). *The effects of deactivation and (re)activation of ACC on driver behaviour analyzed in real traffic.* Paper presented at the IEEE Intelligent Vehicles Symposium, Eindhoven, The Netherlands.

Ploeg, J., A. F. A. Serrarens and G. J. Heijenk. (2011). Connect & Drive: Design and evaluation of cooperative adaptive cruise control for congestion reduction. *Journal of Modern Transportation, vol. 19*, no. 3, pp. 207-213

Qom, S. F., Y. Xiao and M. Hadi. (2016). *Evaluation of cooperative adaptive cruise control (CACC) vehicles on managed lanes utilizing macroscopic and mesoscopic simulation.* Paper presented at the Transportation Research Board 95th Annual Meeting, Washington, DC.

Raboy, K., J. Ma, J. Stark and F. Zhou. (2017). *Cooperative control for lane-change maneuvers with connected automated vehicles: Field Experiment* Paper presented at the Transportation Research Board 96th Annual Meeting.

Rajamani, R., S. B. Choi, B. K. Law, J. K. Hedrick, R. Prohaska and P. Kretz. (2000). Design and experimental implementation of longitudinal control for a platoon of automated vehicles. *Journal of Dynamic Systems Measurement and Control-Transactions of the Asme, vol. 122*, no. 3, pp. 470-476

Roncoli, C., I. Papamichail and M. Papageorgiou. (2016). Hierarchical model predictive control for multi-lane motorways in presence of Vehicle Automation and Communication Systems. *Transportation Research Part C: Emerging Technologies, vol. 62*, pp. 117-132

SAE. (2018). Taxonomy and definitions for terms related to driving automation systems for on-road motor vehicles. J3016.

Schakel, W. J. MOTUS. Retrieved from http://homepage.tudelft.nl/05a3n/

Schakel, W. J., V. L. Knoop and B. van Arem. (2012). Integrated lane change model with relaxation and synchronization. *Transportation Research Record: Journal of the Transportation Research Board,* no. 2316, pp. 47-57

Schakel, W. J., B. van Arem and B. D. Netten. (2010). *Effects of cooperative adaptive cruise control on traffic flow stability.* Paper presented at the 13th International IEEE Annual Conference on Intelligent Transportation Systems, Madeira Island, Portugal.

Shladover, S. E. (1995). Review of the state of development of advanced vehicle control systems (AVCS). *Vehicle System Dynamics, vol. 24*, no. 6-7, pp. 551-595

Shladover, S. E., C. Nowakowski, X. Y. Lu and R. Ferlis. (2015). Cooperative adaptive cruise control: Definitions and operating concepts. *Transportation Research Record,* no. 2489, pp. 145-152

Shladover, S. E., D. Su and X.-Y. Lu. (2012). Impacts of cooperative adaptive cruise control on freeway traffic flow. *Transportation Research Record: Journal of the Transportation Research Board,* no. 2324, pp. 63-70

Swaroop, D., J. K. Hedrick, C. C. Chien and P. Ioannou. (1994). A comparision of spacing and headway control laws for automatically controlled vehicles. *Vehicle System Dynamics, vol. 23*, no. 1, pp. 597-625

Swaroop, D., J. K. Hedrick and S. B. Choi. (2001). Direct adaptive longitudinal control of vehicle platoons. *IEEE Transactions on Vehicular Technology, vol. 50*, no. 1, pp. 150-161

Talebpour, A. and H. S. Mahmassani. (2016). Influence of connected and autonomous vehicles on traffic flow stability and throughput. *Transportation Research Part C-Emerging Technologies, vol. 71*, pp. 143-163

Talebpour, A., H. S. Mahmassani and A. Elfar. (2017). Investigating the effects of reserved lanes for autonomous vehicles on congestion and travel time reliability. *Transportation Research Record,* no. 2622, pp. 1-12

Tientrakool, P., Y. C. Ho and N. F. Maxemchuk. (2011). Highway capacity benefits from using vehicle-to-vehicle communication and sensors for collision avoidance. *Proceedings of the IEEE Vehicular Technology Conference, pp. 1-5*.

Tilg, G., K. Yang and M. Menendez. (2018). Evaluating the effects of automated vehicle technology on the capacity of freeway weaving sections. *Transportation Research Part C: Emerging Technologies, vol. 96*, pp. 3-21

Treiber, M., A. Hennecke and D. Helbing. (2000). Congested traffic states in empirical observations and microscopic simulations. *Physical Review E, vol. 62*, no. 2, pp. 1805-1824

Treiber, M., A. Kesting and D. Helbing. (2006). Understanding widely scattered traffic flows, the capacity drop, and platoons as effects of variance-driven time gaps. *Phys Rev E Stat Nonlin Soft Matter Phys, vol. 74*, no. 1, pp. 016123

van Arem, B., A. P. de Vos and M. J. W. A. Vanderschuren. (1997). *The microscopic traffic simulation model MIXIC 1.3*. (INRO-VVG 1997-02b).

van Arem, B., J. H. Hogema and S. A. Smulders. (1996). *The Impact of autonomous intelligent cruise control on traffic flow.* Paper presented at the Third World Congress on Intelligent Transport Systems, Orlando, Florida.

van Arem, B., C. J. G. van Driel and R. Visser. (2006). The impact of cooperative adaptive cruise control on traffic-Flow characteristics. *IEEE Transactions on Intelligent Transportation Systems, vol. 7*, no. 4, pp. 429-436

VanderWerf, J., S. E. Shladover, N. Kourjanskaia, M. Miller and H. Krishnan. (2001). Modeling effects of driver control assistance systems on Traffic. *Transportation*

Research Record: Journal of the Transportation Research Board, no. 1748, pp. 167-174

VanderWerf, J., S. E. Shladover, M. A. Miller and N. Kourjanskaia. (2002). Effects of adaptive cruise control systems on highway traffic flow capacity. *Transportation Research Record: Journal of the Transportation Research Board,* no. 1800, pp. 78-84

Varotto, S. F., H. Farah, T. Toledo, B. van Arem and S. P. Hoogendoorn. (2018). Modelling decisions of control transitions and target speed regulations in full-range adaptive cruise control based on risk allostasis theory. *Transportation Research Part B: Methodological, vol. 117*, pp. 318-341

Varotto, S. F., R. G. Hoogendoorn, B. van Arem and S. P. Hoogendoorn. (2015). Empirical longitudinal driving behavior in authority transitions between adaptive cruise control and manual driving. *Transportation Research Record: Journal of the Transportation Research Board, vol. 2489*, pp. 105-114

Viti, F., S. P. Hoogendoorn, T. P. Alkim and G. Bootsma. (2008). Driving behavior interaction with ACC: results from a field operational test in the Netherlands. *2008 IEEE Intelligent Vehicles Symposium, vols 1-3,* pp. 444-449

Vugts, R. P. A. (2009). *String-stable CACC design and experimental validation.* (Master Thesis), Technische Universiteit Eindhoven,

Wang, M., W. Daamen, S. P. Hoogendoorn and B. van Arem. (2016a). Connected variable speed limits control and car-following control with vehicle-infrastructure communication to resolve stop-and-go waves. *Journal of Intelligent Transportation Systems, vol. 20*, no. 6, pp. 559-572

Wang, M., W. Daamen, S. P. Hoogendoorn and B. van Arem. (2016b). Cooperative car-following control: Distributed algorithm and impact on moving jam features. *IEEE Transactions on Intelligent Transportation Systems, vol. 17*, no. 5, pp. 1459-1471

Wang, M., S. P. Hoogendoorn, W. Daamen, B. van Arem and R. Happee. (2015). Game theoretic approach for predictive lane-changing and car-following control. *Transportation Research Part C: Emerging Technologies, vol. 58*, pp. 73-92

Wang, X., R. Jiang, L. Li, Y. Lin, X. Zheng and F.-Y. Wang. (2018). Capturing car-following behaviors by deep learning. *IEEE Transactions on Intelligent Transportation Systems, vol. 19*, no. 3, pp. 910-920

Wilmink, I. R., G. A. Klunder and B. van Arem. (2007). *Traffic flow effects of integrated full-range speed assistance (IRSA).* Paper presented at the IEEE Intelligent Vehicles Symposium, Istanbul.

Wu, N. (2002). A new approach for modeling of fundamental diagrams. *Transportation Research Part a-Policy and Practice, vol. 36*, no. 10, pp. 867-884

Xiao, L., M. Wang, W. Schakel and B. van Arem. (2018). Unravelling effects of cooperative adaptive cruise control deactivation on traffic flow characteristics at merging bottlenecks. *Transportation Research Part C: Emerging Technologies, vol. 96*, pp. 380-397

Xiao, L., M. Wang, W. J. Schakel, S. E. Shladover and B. van Arem. (2017). *Modeling lane change behavior on a highway with a high occupancy vehicle lane with continuous access and egress*. Paper presented at the Transportation Research Board, Washington, D.C

Xiao, L., M. Wang and B. van Arem. (2017). Realistic car-following models for microscopic simulation of adaptive and cooperative adaptive cruise control vehicles. *Transportation Research Record: Journal of the Transportation Research Board, no. 2623*, pp. 1-9

Yi, J. and R. Horowitz. (2006). Macroscopic traffic flow propagation stability for adaptive cruise controlled vehicles. *Transportation Research Part C: Emerging Technologies, vol. 14*, no. 2, pp. 81-95

Yuan, K., V. L. Knoop and S. P. Hoogendoorn. (2015). Capacity drop relationship between speed in congestion and the queue discharge rate. *Transportation Research Record: Journal of the Transportation Research Board,* no. 2491, pp. 72-80

Yuan, K., V. L. Knoop and S. P. Hoogendoorn. (2017). A microscopic investigation into the capacity drop: Impacts of longitudinal behavior on the queue discharge rate. *Transportation Science, vol. 51*, no. 3, pp. 852-862

Zhang B. de Winter J, Varotto S, Happee R, Martens MH. (2019). Determinants of take-over time from automated driving: A meta-analysis of 129 studies. *Transportation Research Part F: Psychology and Behaviour, vol. 64*, pp. 285-307.

Zhao, L. and J. Sun. (2013). Simulation framework for vehicle platooning and car-following behaviors under connected-vehicle environment. *Intelligent and Integrated Sustainable Multimodal Transportation Systems Proceedings from the 13th Cota International Conference of Transportation Professionals (Cictp2013), vol. 96*, pp. 914-924

Zhou, M., X. Qu and X. Li. (2017). A recurrent neural network based microscopic car following model to predict traffic oscillation. *Transportation Research Part C: Emerging Technologies, vol. 84*, pp. 245-264

Summary

Traffic congestion causes detrimental effects on economy and society in terms of travel time delay, increased vehicle collision risk and increased air pollution. To tackle that, new intelligent transportation systems are being developed. One of these emerging technologies comprise automated driving systems. Adaptive Cruise Control (ACC), enabling a vehicle to follow its leader automatically, is an automated driving system which has been available in the vehicle market. Literature shows that traffic flow performance may not significantly benefit from ACC due to traffic instability and large headways. As an extension of ACC, Cooperative ACC is designed to improve traffic stability and throughput by using Vehicle-to-Vehicle (V2V) communication. Thanks to the anticipation of the downstream traffic, a short following gap can be realized by CACC which is highly expected to considerably increase road capacities. Before CACC vehicle is allowed and promoted in the market, it is crucial for policy makers and road operators to gain insights into the traffic flow impacts of CACC systems. Existing studies show that CACC can increase traffic throughput at high vehicle market penetration. However, the realistic effects of CACC on traffic flow have not been adequately revealed because the behaviour of CACC vehicles has not been realistically modelled. The multiple CACC driving modes, the degraded operation to ACC and the human driver take-over control when it is out of the CACC operational design domain, have not yet been explicitly included in existing CACC impact studies. A scientific gap prevails in modelling the complex CACC behaviour and investigating its actual influence on traffic flow especially at realistic networks with a single bottleneck and interacting bottlenecks.

This thesis aims to develop realistic behavioural models for CACC vehicles and apply them to traffic simulations for a better understanding of CACC vehicles' impact on traffic flow characteristics. In particular, the influence of CACC market penetration rates (MPRs) in improving roadway capacity and traffic flow homogeneity is investigated and the combined

impacts of CACC vehicles with a dedicated lane are evaluated. This thesis consists of four publications corresponding to the chapter 2-5. Chapter 2 and Chapter 4 are the modelling of CACC vehicles' car-following and lane change behaviour, providing useful tools for the bottleneck impact evaluation in Chapter 3 and CACC lane evaluation in Chapter 5.

Chapter 2 proposes a multi-regime model to represent the realistic car-following response of CACC vehicles. It integrates the CACC system control and driver control in parallel where the control authority transition under specific situations can be captured in simulation. Within CACC, a gap-closing mode is designed especially for the approaching scenario and the ACC car-following response is included as the degraded operation of CACC. This model is collision free in a wide range of simulated scenarios and can generate realistic CACC vehicle response in microscopic simulations, providing an effective tool for traffic impact evaluation of CACC vehicles.

Chapter 3 investigates the roadway capacity characteristics regarding CACC MPRs, based on the developed CACC car-following model in Chapter 2 and a lane change model with synchronization and relaxation (LMRS). We pay attention to both pre-queue capacity, queue-discharge rate, and data scatters in the flow-density diagram of a highway merging bottleneck. It is found that increasing CACC MPRs can increase roadway capacities during congestion. The capacity drop, as the difference between the pre-queue capacity and queue discharge rate, is found to pertain at all CACC MPRs and is highly correlated to the authority transitions from CACC to manual driving. The relations between the CACC deactivation and capacity reduction indicate the main application limitations of current CACC system and call for a high level of vehicle coordination and cooperation at highway bottlenecks.

The CACC benefits on traffic flows at low MPRs are not substantial due to the low time usage of the CACC system. To increase CACC usage, a CACC dedicated lane clustering these vehicles in one lane, is considered as an optional lane-management strategy. In order to assess the effectiveness of a CACC lane, the lane change model with synchronization and relaxation used in Chapter 3 is extended for a dedicated lane scenario in Chapter 4. The lane change incentive is modified for eligible and ineligible users of dedicated lanes and the model is systematically calibrated using detector data from the SR-99 corridor in California where an existing high occupancy vehicle lane is in operation. The extended and calibrated lane change model can reproduce congestion pattern along the corridor, as well as section-based fundamental diagrams and lane-based flow distribution, with plausible face-validated lane change behaviour.

Based on the CACC car-following model in Chapter 2 and the extended lane change model in Chapter 4, Chapter 5 conducts simulations at 10-50% CACC MPRs to explore the effectiveness of a CACC lane at low MPRs. Taking the California SR99 corridor as the use case, it is revealed that traffic flow performance is sensitive to CACC MPRs when a CACC lane is present. The traffic congestion is severe when the CACC MPR is below 20 % and it is considerably alleviated only when CACC vehicles reach 40% of the traffic. At the same demand level of the reference case with 100% conventional vehicles, the CACC lane is not oversaturated at all MPRs between 10% to 50% but speed reduction still takes place in the CACC lane due to the friction effects between the CACC lane and the adjacent general-purpose lane, which results in

safety concerns. This implies that deploying a CACC lane is not an effective strategy in improving overall traffic performance at low MPRs. Road operators should therefore deploy a CACC lane only when the CACC vehicle demand is sufficient.

Future research directions include examining and validating model assumptions in authority transitions, extending the simulation experiment to lane drop or weaving bottleneck, or developing new traffic management measures to mitigate the negative impacts of CACC deactivation and its degradation to ACC found in this thesis.

Samenvatting

Files hebben schadelijke gevolgen voor de economie en de samenleving in termen van reistijdvertraging, een verhoogd risico op ongevallen en meer luchtvervuiling. Om dat aan te pakken worden nieuwe intelligente verkeers- en vervoerssystemen ontwikkeld. Een van deze opkomende technologieën is automatisch rijden. Adaptive Cruise Control (ACC), waarmee een voertuig het voertuig voor hem automatisch kan volgen, is een systeem voor automatisch rijden dat op de voertuigmarkt beschikbaar is. Uit de literatuur blijkt dat de toepassing van ACC de doorstroming van het verkeer mogelijk niet significant verbetert, vanwege instabiliteit van het verkeer en grote volgafstanden. Een uitbreiding van ACC is Cooperative Adaptive Cruise Control (CACC), ontworpen om de stabiliteit van het verkeer en de doorstroming te verbeteren door gebruik te maken van voertuig-voertuig communicatie (V2V). Dankzij de anticipatie op het verkeer stroomafwaarts kan door CACC een korte volgtijd worden gerealiseerd, die naar verwachting de capaciteit van de wegen aanzienlijk kan doen toenemen. Voordat CACC in voertuigen op de markt kan worden toegelaten en gepromoot zal worden, is het voor beleidsmakers en wegbeheerders van cruciaal belang om inzicht te krijgen in de gevolgen van CACC systemen voor de doorstroming van het verkeer. Bestaande studies tonen aan dat CACC de doorstroming van het verkeer kan verhogen indien een hoog percentage voertuigen is uitgerust met het systeem. De realistische effecten van CACC op de verkeersdoorstroming zijn echter niet voldoende aangetoond, omdat het gedrag van voertuigen met CACC niet realistisch is gemodelleerd. Bestaande CACC effectstudies houden nog niet expliciet rekening met meerdere CACC modi, de terugval van CACC naar het minder efficiënte ACC als er geen CACC voorligger is en de overname van de controle door de bestuurder wanneer het voertuig buiten het operationele CACC domein komt. Hierdoor is er een wetenschappelijke kloof in het modelleren van het complexe gedrag van CACC en het onderzoeken van de daadwerkelijke invloed ervan op de verkeersstroom, met name op realistische netwerken met een bottleneck en bij interactie tussen meerdere bottlenecks.
Deze dissertatie heeft tot doel realistische gedragsmodellen te ontwikkelen voor CACC voertuigen, en deze toe te passen op verkeerssimulaties om een beter begrip van de impact van CACC voertuigen op de verkeersdoorstroming te krijgen. In het bijzonder wordt de invloed van

de marktpenetratiegraad (MPR) onderzocht op de verbetering van de wegcapaciteit en de homogeniteit van de doorstroming, en worden de gecombineerde effecten van CACC voertuigen met een speciale rijstrook geëvalueerd. Dit proefschrift is gebaseerd op vier publicaties die overeenkomen met hoofdstuk 2-5. Hoofdstuk 2 en hoofdstuk 4 zijn de modellering van het volg- en rijstrookwisselgedrag van CACC voertuigen, wat nuttige hulpmiddelen biedt voor de evaluatie van de impact van knelpunten in hoofdstuk 3 en de evaluatie van de CACC strook in hoofdstuk 5.

In hoofdstuk 2 wordt een multi-regime model voorgesteld om de realistische voertuig-volg respons van CACC voertuigen weer te geven. Het integreert de systeembesturing van de CACC en de besturing door de bestuurder op parallelle wijze in het model, waarbij de overgang van de controle door het systeem of de bestuurder (autoriteitstransities) in specifieke situaties in de simulatie kan worden gemodelleerd. In de CACC modellering is een "gap-closing" modus ontworpen, speciaal om het hiaat te verkleinen in naderingsscenario’s en is het ACC volggedrag opgenomen als een gedegradeerde werking van CACC. Dit model is vrij van botsingen in een groot aantal gesimuleerde scenario's en kan een realistisch CACC voertuiggedrag genereren in microscopische simulaties, zodat het een effectief instrument is voor de evaluatie van CACC voertuigen in het verkeer.

Hoofdstuk 3 onderzoekt de capaciteit van de weg met betrekking tot de penetratiegraad van CACC, op basis van het ontwikkelde CACC voertuigvolgmodel in hoofdstuk 2 en een rijstrookwisselmodel met synchronisatie en relaxatie (LMRS). We besteden zowel aandacht aan de vrije capaciteit, de afrijcapaciteit, en aan het intensiteits-dichtheidsdiagram van een invoeging op de snelweg. Er is geconstateerd dat het verhogen van de penetratiegraad van CACC de wegcapaciteit kan verhogen bij congestie. De capaciteitsval, bepaald als het verschil tussen de vrije capaciteit en de afrijcapaciteit, blijkt bij alle CACC penetratiegraden voor te komen en is sterk gecorreleerd met de overgang van CACC naar handmatig rijden. De relatie tussen de CACC deactivering en de capaciteitsvermindering geeft de belangrijkste beperking voor toepassing van het huidige CACC systeem aan en vraagt om een hoge mate van coördinatie en samenwerking tussen voertuigen bij knelpunten op de snelweg.

De voordelen voor de verkeersstroom bij een lage penetratiegraad van CACC zijn beperkt, omdat het CACC systeem dan maar weinig gebruikt kan worden. Om het CACC gebruik te verhogen, beschouwen we een specifieke rijstrookclustering van CACC voertuigen in één rijstrook als een optionele rijstrookmanagementstrategie. Om de doeltreffendheid van een CACC strook te beoordelen, wordt het in hoofdstuk 3 gebruikte rijstrookwisselmodel met synchronisatie en relaxatie uitgebreid voor een specifiek rijstrookscenario in hoofdstuk 4. De stimulans om van rijstrook te wisselen is aangepast voor in aanmerking komende en niet in aanmerking komende gebruikers van de speciale rijstrook, en het model is systematisch gekalibreerd met behulp van detectorgegevens van de SR-99-corridor in Californië, waar een bestaande carpoolstrook in gebruik is. Het uitgebreide en gekalibreerde rijstrookwisselmodel is in staat het congestiepatroon langs de corridor te reproduceren, evenals fundamentele diagrammen op doorsnedes en de intensiteitsverdeling over de rijstroken, met een aannemelijk op zicht gevalideerd rijstrookwisselgedrag.

Op basis van het CACC voertuigvolgmodel uit hoofdstuk 2 en het uitgebreide rijstrookwisselmodel uit hoofdstuk 4, zijn in hoofdstuk 5 simulaties uitgevoerd bij 10-50% penetratiegraad van CACC, om de effectiviteit van een CACC strook bij lage penetratiegraden te onderzoeken. Door de SR99-corridor in Californië als use case te nemen, blijkt dat bij de aanwezigheid van een CACC strook de verkeersafwikkeling gevoelig is voor de penetratiegraad van CACC. Er zijn ernstige files wanneer de CACC penetratiegraad lager is dan 20% en deze files worden pas aanzienlijk verlicht wanneer de penetratiegraad 40% van het verkeer bereikt. Bij dezelfde verkeersvraag als in de referentie met 100% conventionele voertuigen, is de CACC strook bij alle penetratiegraden tussen 10% en 50% niet oververzadigd, maar er vindt toch een

snelheidsvermindering plaats op de CACC strook als gevolg van de wrijving tussen de CACC strook en de aangrenzende algemene rijstrook, wat aanleiding geeft tot veiligheidsproblemen. Dit betekent dat het gebruik van een CACC strook bij lage penetratiegraden geen effectieve strategie is om de algemene verkeersprestaties te verbeteren. Wegbeheerders zouden daarom alleen een CACC strook moeten inzetten wanneer de vraag naar CACC voertuigen voldoende groot is.

Toekomstige onderzoeksrichtingen zijn onder meer het onderzoeken en valideren van modelaannames bij autoriteitstransities, het uitbreiden van het simulatie-experiment met afvallende rijstroken of weefvakken, of het ontwikkelen van nieuwe verkeersmanagementmaatregelen om de negatieve effecten van CACC deactivering en hem degradatie aan ACC die in dit proefschrift zijn gevonden, te verminderen.

About the author

Lin Xiao was born on October 26th 1986 in Xiamen (China). She received her Bachelor of Engineering degree in Traffic Engineering at the Beijing Institute of Technology in 2009 and is graduated with honour. In 2013, she received her Master of Engineering degree at Tongji University, with specialisation in Transportation Planning and Management.

In April 2014, she joined the Transport and Planning Department at Delft University of Technology as a PhD candidate. She worked in the project "Using cooperative adaptive cruise control to for high-performance vehicle streams" funded by a Federal Highway Administration Exploratory Advanced Research Program Grant, in collaboration with California PATH. Her PhD research focused on modelling the behaviour of operative adaptive cruise control (CACC) vehicles in microscopic simulations and traffic flow impact assessments of CACC vehicles at various vehicle market penetration rates. During her doctoral studies, she assisted in the master course Intelligent Vehicles and served as referees for international journals and conferences.

Since April 2019, she has been working at the Department of Sustainable Urban Mobility and Safety in TNO as a researcher. Her research interests are behaviour modelling and impact analysis of automated vehicles in coordination and cooperation with intelligent traffic infrastructures.

Journal publications

Xiao, L., M. Wang and B. van Arem. (2017). Realistic car-Following models for microscopic simulation of adaptive and cooperative adaptive cruise control vehicles. *Transportation Research Record: Journal of the Transportation Research Board, vol. 2623*, pp. 1-9

Xiao, L., M. Wang, W. Schakel and B. van Arem. (2018). Unravelling effects of cooperative adaptive cruise control deactivation on traffic flow characteristics at merging bottlenecks. *Transportation Research Part C: Emerging Technologies, vol. 96*, pp. 380-397

Xiao, L., M. Wang and B. Van Arem. (2020). Traffic flow impacts of converting an HOV lane into a dedicated CACC lane on a freeway corridor. *IEEE Intelligent Transportation Systems Magazine, vol 12(1), pp. 60 -73.*

Kan, X., L. Xiao, H. Liu, M. Wang, W. J. Schakel, X.-Y. Lu, et al. (2019). Cross-comparison and calibration of two microscopic traffic simulation models for complex freeway corridors with dedicated lanes. *Journal of Advanced Transportation, vol. 2019*, pp. 1-14

Peer-reviewed conference articles

Xiao, L., M. Wang, W. J. Schakel, S. E. Shladover and B. van Arem. (2017). *Modeling lane change behavior on a highway with a high occupancy vehicle lane with continuous access and egress*. In proceedings of the 96th Annual Meeting of Transportation Research Board, Washington, D.C.

Xiao, L., M. Wang and B. van Arem. (2017). *Realistic car-Following models for microscopic simulation of adaptive and cooperative adaptive cruise control vehicles*. In proceedings of the 96th Annual Meeting of Transportation Research Board, Washington, D.C.

Report

Liu, H., L. Xiao, X. Kan, S. E. Shladover, X. -Y. Lu, M. Wang, W. Schakel and B. van Arem. (2018). Using cooperative adaptive cruise control to for high-performance vehicle streams. No. DTFH61-13-H-00013

Conference presentations

Xiao, L., M. Wang and B. van Arem. (2017). Realistic car-Following models for microscopic simulation of adaptive and cooperative adaptive cruise control vehicles. Oral presentation at *the 96th Annual Meeting of Transportation Research Board*, Washington, D.C.

Xiao, L., M. Wang, W. J. Schakel, S. E. Shladover and B. van Arem. (2017). *Modeling lane change behavior on a highway with a high occupancy vehicle lane with continuous access and egress*. Poster presentation at *the 96th Annual Meeting of Transportation Research Board*, Washington, D.C.

Xiao, L., M. Wang and B. van Arem. (2015). String strategies of cooperative adapative cruise control for high-performance streams. Poster presentation at *Automated Vehcile Symposium*, San Francisco, CA.

Xiao, L., M. Wang and B. van Arem. (2015) Modelling cooperative adpative cruise control vehicles in traffic simulations. Oral presentation at *the 2nd TRAIL-BETA congress*, Utrecht, The Netherlands.

Xiao, L., R. Hoogendoorn and B. van Arem. (2014). Destination Celled platooning. Poster presentation at *Automated Vehcile Symposium*, San Francisco, CA.

TRAIL Thesis Series

The following list contains the most recent dissertations in the TRAIL Thesis Series. For a complete overview of more than 250 titles see the TRAIL website: www.rsTRAIL.nl.

The TRAIL Thesis Series is a series of the Netherlands TRAIL Research School on transport, infrastructure and logistics.

Xiao, L., *Cooperative Adaptive Cruise Control Vehicles on Highways: Modelling and Traffic Flow Characteristics*, T2020/19, December 2020, TRAIL Thesis Series, the Netherlands

Polinder, G.J., *New Models and Applications for Railway Timetabling*, T2020/18, December 2020, TRAIL Thesis Series, the Netherlands

Scharpff, J.C.D., Collective Decision Making trough Self-regulation, T2020/17, November 2020, TRAIL Thesis Series, the Netherlands

Guo, W. *Optimization of Synchromodal Matching Platforms under Uncertainties,* T2020/16, November 2020, TRAIL Thesis Series, the Netherlands

Narayan, J., *Design and Analysis of On-Demand Mobility Systems,* T2020/15, October 2020, TRAIL Thesis Series, the Netherlands

Gong, X., *Using Social Media to Characterise Crowds in City Events for Crowd Management,* T2020/14, September 2020, TRAIL Thesis Series, the Netherlands

Rijal, A., *Managing External Temporal Constraints in Manual Warehouses,* T2020/13, September 2020, TRAIL Thesis Series, the Netherlands

Alonso González, M.J., *Demand for Urban Pooled On-Demand Services: Attitudes, preferences and usage*, T2020/12, July 2020, TRAIL Thesis Series, the Netherlands

Alwosheel, A.S.A., *Trustworthy and Explainable Artificial Neural Networks for choice Behaviour Analysis,* T2020/11, July 2020, TRAIL Thesis Series, the Netherlands

Zeng, Q., *A New Composite Indicator of Company Performance Measurement from Economic and Environmental Perspectives for Motor Vehicle Manufacturers,* T2020/10, May 2020, TRAIL Thesis Series, the Netherlands

Mirzaei, M., *Advanced Storage and Retrieval Policies in Automated Warehouses,* T2020/9, April 2020, TRAIL Thesis Series, the Netherlands

Nordhoff, S., *User Acceptance of Automated Vehicles in Public Transport,* T2020/8, April 2020, TRAIL Thesis Series, the Netherlands

Winter, M.K.E., *Providing Public Transport by Self-Driving Vehicles: User preferences, fleet operation, and parking management,* T2020/7, April 2020, TRAIL Thesis Series, the Netherlands

Mullakkal-Babu, F.A., *Modelling Safety Impacts of Automated Driving Systems in Multi-Lane Traffic*, T2020/6, March 2020, TRAIL Thesis Series, the Netherlands

Krishnakumari, P.K., *Multiscale Pattern Recognition of Transport Network Dynamics and its Applications: A bird's eye view on transport,* T2020/5, February 2020, TRAIL Thesis Series, the Netherlands

Wolbertus, *Evaluating Electric Vehicle Charging Infrastructure Policies*, T2020/4, February 2020, TRAIL Thesis Series, the Netherlands

Yap, M.D., *Measuring, Predicting and Controlling Disruption Impacts for Urban Public Transport,* T2020/3, February 2020, TRAIL Thesis Series, the Netherlands

Luo, D., *Data-driven Analysis and Modeling of Passenger Flows and Service Networks for Public Transport Systems*, T2020/2, February 2020, TRAIL Thesis Series, the Netherlands

Erp, P.B.C. van, *Relative Flow Data: New opportunities for traffic state estimation,* T2020/1, February 2020, TRAIL Thesis Series, the Netherlands

Zhu, Y., *Passenger-Oriented Timetable Rescheduling in Railway Disruption Management*, T2019/16, December 2019, TRAIL Thesis Series, the Netherlands

Chen, L., *Cooperative Multi-Vessel Systems for Waterborne Transport*, T2019/15, November 2019, TRAIL Thesis Series, the Netherlands

Kerkman, K.E., *Spatial Dependence in Travel Demand Models: Causes, implications, and solutions*, T2019/14, October 2019, TRAIL Thesis Series, the Netherlands

Liang, X., *Planning and Operation of Automated Taxi Systems,* T2019/13, September 2019, TRAIL Thesis Series, the Netherlands

Ton, D., *Unravelling Mode and Route Choice Behaviour of Active Mode Users*, T2019/12, September 2019, TRAIL Thesis Series, the Netherlands

Shu, Y., *Vessel Route Choice Model and Operational Model Based on Optimal Control,* T2019/11, September 2019, TRAIL Thesis Series, the Netherlands

Luan, X., *Traffic Management Optimization of Railway Networks,* T2019/10, July 2019, TRAIL Thesis Series, the Netherlands

Hu, Q., *Container Transport inside the Port Area and to the Hinterland,* T2019/9, July 2019, TRAIL Thesis Series, the Netherlands

Andani, I.G.A., *Toll Roads in Indonesia: transport system, accessibility, spatial and equity impacts,* T2019/8, June 2019, TRAIL Thesis Series, the Netherlands

Ma, W., *Sustainability of Deep Sea Mining Transport Plans*, T2019/7, June 2019, TRAIL Thesis Series, the Netherlands